Helsinki University of Technology
Laboratory of Computational Engineering
Espoo 2006 REPORT B53

STUDIES OF SURFACE DIFFUSION AND DISSIPATIVE PARTICLE DYNAMICS

Petri Nikunen

Dissertation for the degree of Doctor of Science in Technology to be presented with due permission of the Department of Electrical and Communications Engineering, Helsinki University of Technology, for public examination and debate in Auditorium S4 at Helsinki University of Technology (Espoo, Finland) on the 18th of March, 2006, at 12 o'clock noon.

Helsinki University of Technology
Department of Electrical and Communications Engineering
Laboratory of Computational Engineering

Teknillinen korkeakoulu
Sähkö- ja tietoliikennetekniikan osasto
Laskennallisen tekniikan laboratorio

Distribution:
Helsinki University of Technology
Laboratory of Computational Engineering
P.O. Box 9203
FI-02015 TKK
FINLAND
Tel. +358-9-451 4826
Fax. +358-9-451 4830
http://www.lce.hut.fi/

Online in PDF format: http://lib.tkk.fi/Diss/2006/isbn9512280590/

E-mail: Petri.Nikunen@tkk.fi

ISBN 951-22-8058-2 (printed)
ISBN 951-22-8059-0 (PDF)
ISSN 1455-0474
PicaSet Oy
Espoo 2006

Abstract

In the first part of this thesis, we study diffusion of atoms on solid surfaces. To this end, we carry out Monte Carlo simulations for a lattice-gas model of O/W(110), first on clean surfaces and then on surfaces containing small concentrations of quenched (immobile) impurities. In both cases, we examine how thermodynamic non-equilibrium affects tracer diffusion and collective diffusion of atoms on a surface. We find that non-equilibrium effects can play an important role when there are strong interactions in the system. These effects persist even when there are only slight deviations from equilibrium. We also find that even minute impurity concentrations can lead to major changes in the diffusion coefficients. The combined effect is not, however, additive. Indeed, we find that the non-equilibrium effects are most pronounced on clean surfaces, while on surfaces covered by impurities the role of non-equilibrium conditions is weaker. This is essentially due to the similarity between disorder as induced either by the non-equilibrium condition or by the presence of impurities on the surface.

In the second part of the thesis, we consider methodological aspects of the dissipative particle dynamics (DPD) technique. First, we address the question: "How to integrate the equations of motion in DPD simulations?" We test and analyze several novel DPD integration schemes on an equal footing through DPD simulations of different model systems. By monitoring a number of physical observables including temperature, radial distribution function, radius of gyration for polymers, and tracer diffusion, we find that the methods by Lowe and Shardlow give the best overall performance and are superior also to the integrators tested in previous studies.

Second, we study the dynamics of polymer melts. In standard DPD, as well as in other coarse-grained soft potential models, there is a problem that polymers can penetrate through themselves. This is a clear artifact, and has direct consequences on polymer dynamics. To correct this problem, we tune the conservative forces within the polymer chain so strong that chains cannot cut through each other. Indeed, if a certain geometric criterion is met, it is impossible for polymer chains to cross. Through DPD simulations, we show that our approach is able to reproduce the Rouse-like dynamics for short chains and reptational dynamics for longer chains. The results are in good agreement with polymer theories and experiments.

Tiivistelmä

Tämän väitöskirjan ensimmäisessä osassa tutkitaan atomien diffuusiota kiinteillä pinnoilla. Tarkoitusta varten suoritetaan Monte Carlo -simulaatioita O/W(110)-systeemin hilakaasumallilla; ensin puhtailla pinnoilla ja sen jälkeen pinnoilla, joihin on lisätty sammutettuja (liikkumattomia) epäpuhtauksia. Kummassakin tapauksessa tarkastellaan, kuinka termodynaaminen epätasapaino vaikuttaa atomien diffuusioon pinnalla. Tulokseksi saadaan, että epätasapainoilmiöillä on tärkeä rooli, jos systeemin sisäiset vuorovaikutukset ovat voimakkaita. Vaikka systeemi olisi hyvin lähelläkin tasapainoa, epätasapainoilmiöiden vaikutus voi tällöin olla merkittävä. Toinen tulos on, että hyvin pienet epäpuhtauskonsentraatiot voivat johtaa suuriin muutoksiin diffuusiotekijöissä. Yhteisvaikutus ei kuitenkaan ole additiivinen: epätasapainoilmiöt ovat voimakkaimpia puhtailla pinnoilla, kun taas epäpuhtailla pinnoilla niiden vaikutus on vähäisempi. Tämä johtuu oleellisesti siitä, että epäjärjestys, joka systeemiin aiheutetaan, on hyvin samankaltainen, johtuipa se termodynaamisesta epätasapainosta tai pinnalla olevista epäpuhtauksista.

Väitöskirjan toisessa osassa tarkastellaan dissipatiivinen partikkelidynamiikka (DPD) -menetelmän ominaisuuksia. Ensin pohditaan, kuinka liikeyhtälöitä olisi parasta integroida DPD-simulaatioissa. Muutamia uusia integrointialgoritmeja testataan ja analysoidaan suorittamalla DPD-simulaatioita eri mallisysteemeille. Tarkastelemalla tiettyjä fysikaalisia suureita kuten lämpötilaa, radiaalista jakaumafunktiota, polymeerien gyraatiosädettä ja merkkipartikkelin diffuusiota päädytään tulokseen, että tutkituista algoritmeista Lowen ja Shardlowin ehdottamat toimivat yleisesti ottaen parhaiten ja ovat myös parempia kuin aiemmin tutkitut algoritmit.

Väitöskirjassa tutkitaan myös polymeerisulan dynamiikkaa. Normaalissa DPD:ssä, kuten muissakin karkeistetuissa pehmeän potentiaalin malleissa, ongelmana on, että polymeerit voivat tunkeutua toistensa läpi. Tämä on virheellistä ja voi johtaa vääränlaiseen polymeeridynamiikkaan. Ongelman korjaamiseksi konservatiiviset voimat säädetään niin vahvoiksi, että polymeeriketjut eivät pysty leikkaamaan toisiaan. Voidaan osoittaa, että jos tietty geometrinen kriteeri täyttyy, polymeerit eivät yksinkertaisesti pysty leikkaamaan toisiaan. Suorittamalla DPD-simulaatioita osoitetaan, että käytettävä lähestymistapa tuottaa Rouse-tyyppisen dynamiikan lyhyille ketjuille ja reptaatiodynamiikan pidemmille ketjuille. Saadut tulokset ovat sopusoinnussa vallitsevien polymeeriteorioiden ja kokeiden kanssa.

Preface

This thesis has been done in the Laboratory of Computational Engineering at the Helsinki University of Technology during the years 2000–2006 and in the Laboratory of Physics at the Helsinki University of Technology during the years 1999–2000. I first wish to thank Prof. Mikko Karttunen, Prof. Ilpo Vattulainen, and Prof. Tapio Ala-Nissilä for their guidance and encouragement. Working with them has been a great experience. I also want to thank Acad. Prof. Kimmo Kaski for his supervision and for providing extremely good computer resources. Many thanks belong also to Prof. Roland Faller and Prof. Kai Nordlund for the pre-examination of this thesis.

I have been fortunate to meet many nice and interesting people during these years. Especially I wish to thank Markus Miettinen, Sebastian von Alfthan, and Teemu Leppänen for long and interesting discussions we have had on various scientific and non-scientific topics.

Finally, I would like to thank my parents Tarja and Markku their support and understanding. I also want to thank my sister Riikka and brother Risto for many nice moments during these years. Last but not least, I wish to thank my wife Kati for her continuous love and support.

Espoo, March 2006

Petri Nikunen

List of publications

This thesis consists of an introduction and the following publications.

[1] P. Nikunen, I. Vattulainen, and T. Ala-Nissila, *Non-Equilibrium Effects in Profile Evolution Measurements of Surface Diffusion*, Surf. Sci. **447**, L162 (2000).

[2] P. Nikunen, I. Vattulainen, and T. Ala-Nissila, *Density Profile Evolution and Nonequilibrium Effects in Partial and Full Spreading Measurements of Surface Diffusion*, J. Chem. Phys. **114**, 6335 (2001).

[3] P. Nikunen, I. Vattulainen, and T. Ala-Nissila, *Effects of Quenched Impurities on Surface Diffusion, Spreading, and Ordering of O/W(110)*, J. Chem. Phys. **117**, 6757 (2002).

[4] P. Nikunen, M. Karttunen, and I. Vattulainen, *How would you integrate the equations of motion in dissipative particle dynamics simulations?*, Comp. Phys. Comm. **153**, 407 (2003).

[5] P. Nikunen, I. Vattulainen, and M. Karttunen, *Reptational dynamics in dissipative particle dynamics simulations of polymer melts*, submitted to Phys. Rev. E (December, 2005); Helsinki Institute of Physics preprint HIP–2005–54/Th.

The author has played an active role in all stages of the work reported in this thesis. He has been involved in planning the research work, designing the numerical simulations, and interpreting the results. He has developed all the necessary computer programs, performed all numerical simulations, and analyzed all results. The author has written the first drafts of publications [4, 5] and contributed actively to the writing of the others.

Contents

Chapter 1

Introduction

Physics is a science that attempts to find the fundamental laws governing the motion of matter and energy in the universe. The fundamental principles of physics control everything from quarks to galaxies. By its very nature, physics is an experimental science, and as such the experimental basis for any physical theory is extremely important.

Physical problems are in general very difficult to solve exactly. Consider for example the well-known three-body problem, i.e., three objects interacting through known forces. Although the problem seems very simple, it cannot be solved analytically [6]. If the number of interacting bodies is further increased, the problem becomes even more complicated. In such a case, one has to either make approximations or use numerical methods. The solutions obtained by both of these approaches differ from the true solution. When using approximations, one reduces the original problem to a new, simpler one. When using numerical approaches, the solution is not fully exact because of finite numerical accuracy and related numerical errors. Nevertheless, both issues can be controlled and accounted for when calculations are done with sufficient care.

Numerical methods usually make use of thousands of repetitive calculations. In this task computers are invaluable. Today, computational methods are the standard tools in almost every field of physics including particle physics, materials science, and cosmology.

In relation to theory and experiments, computational physics lies somewhere in between the two. If compared to theories, computational methods are typically able to avoid the often necessary and sometimes even crude approximations that may be needed in building theories. If compared to experiments, computational methods can address questions that are beyond the limits and resolution of experimental techniques. Nevertheless, computational methods should not be considered as an alternative to theories or

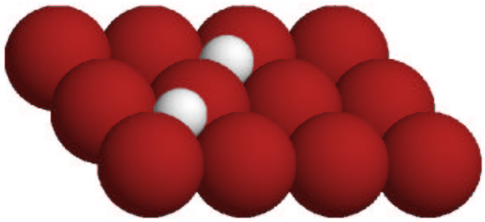

Figure 1.1: Two atoms adsorbed on a surface. The adsorbed atoms tend to sit at the high-symmetry sites of the underlying solid.

experiments, but these three approaches complement each other.

Although the computing power is constantly increasing, current methods are restricted to rather limited length and time scales. For example, *ab initio* approaches based on quantum mechanics are restricted to a few hundreds of atoms and picoseconds; one cannot study everything from quarks to galaxies with a single method. To fill the gaps between different computational methods, various coarse-graining procedures have been developed to link them. One example of methods based on coarse-graining is the dissipative particle dynamics technique [7, 8], which attempts to fill the gap between atomistic and continuum methods.

In the future, the role of computational physics will certainly keep growing. The increase in computing power and algorithmic development has enabled studies of more complicated and interesting systems than ever before.

1.1 Surface Diffusion

In the first part of this thesis, we study the diffusion of atoms on solid surfaces. When atoms are adsorbed onto a surface, they tend to sit at the potential energy minima of the underlying solid (Fig. 1.1). These minima correspond to potential adsorption sites for the adsorbed atoms and are typically high-symmetry sites of the solid surface. Because adsorbed atoms are most probably located at their adsorption sites, it is convenient to model the system as a two-dimensional lattice gas. The problem seems quite simple, but it is analytically solvable in special cases only. Computational methods are therefore needed.

The technological importance of surface diffusion is apparent. Indeed,

surface diffusion plays a key role in various important applications such as the growth of semiconductor structures for electronic devices, the purification of exhaust gases in the automotive industry, and the wetting of solid materials by liquids to reduce friction in mechanical devices [9–11]. Importantly, in many cases surface diffusion may even constitute the rate limiting step in the process [1–3]. Therefore, more and more effort has been directed toward understanding the physical laws that govern the diffusion of atoms and more complex molecules on solid surfaces.

In this respect, the last few decades have been very successful. Thanks to a wide range of experimental techniques [11–15] such as scanning tunneling microscopy and field ion microscopy, the basic knowledge of surface structures and related diffusion mechanisms [15–18] is nowadays reasonably good. Experimental studies have been complemented by theoretical investigations [19–21], which in turn have provided plenty of insight into our understanding of the microscopic details of diffusion processes on solid surfaces. Due to all these activities, it is fair to say that many of the key features of surface diffusion under ideal conditions in thermodynamic equilibrium are now well understood.

The situation becomes much more complicated, however, when the system is no longer in equilibrium or, for example, contains impurities, steps, or other defects that are typical under realistic conditions [12]. Indeed, there is ample evidence that non-equilibrium or impurities (and other defects) can, and often do, play a major role in diffusion processes. Several experimental and theoretical studies have shown [13,22–31] that non-equilibrium measurements may yield results that are distinctly different from the equilibrium ones. As for impurities, experiments have shown that they can strongly affect surface diffusion processes. For example, impurities can adsorb preferentially to step edges [10, 11, 32–34], where they may block diffusion and initiate non-smooth growth. This is undesirable in growing semiconductor structures. Certain surfactants, on the other hand, have been noticed to have an opposite effect in stabilizing smooth, layer-by-layer growth [35, 36]. Similarly, some impurities "poison" surfaces as they block possible reaction sites and thus inhibit the reaction processes, while others can promote reactions [32, 33, 37, 38]. Hydrogen, in turn, has been found to either promote or inhibit surface diffusion of other particles in various systems [39–41]. The objective of the present work is to shed some light on the above issues.

Table 1.1: Different length and time scales and typical methods to study them.

Scale	Example	Length/m	Time/s	Experiment	Simulation
Macroscale	Grain of sand	10^{-3}	10^{-3}	Naked eyd	Phase field models, finite element method
Mesoscale	Transistors	10^{-6}	10^{-9}	Light microscope	Dissipative particle dynamics, lattice–Boltzmann
	Molecules	10^{-9}			
Atomistic	Atoms		10^{-15}	Electron microscope	Monte Carlo, molecular dynamics

1.2 Dissipative particle dynamics

In the second part of the thesis, we consider the dissipative particle dynamics (DPD) technique. Before going into to the details of the DPD method, let us consider different length and time scales that are present in materials (Table 1.1). In experimental work, the most important length scales are the sample size and the resolution of the experimental technique. The ratio of these lengths determines the number of details that can be seen. Of course, the work required for sample preparation and analysis grows accordingly, and therefore the number of details cannot be increased without limit. The same problem is also faced in computer simulations: the CPU time required for a simulation grows with the number of details.

In soft materials [42–44], such as liquid crystals, colloids, and biomembranes, the range of different length and time scales is huge. For example, in protein folding all scales starting from the atomistic scale and ending to the macroscopic scale are important. All these scales cannot be studied with a single experimental technique or modeled using a single simulation approach. Multiscale modeling aims to unite different methods in a systematic way and is one of the hottest topics in materials modeling. We will discuss multiscale modeling more in Sec. 3.4.1.

To systematically bridge and link different methods, various coarse-graining procedures have been developed. One example of such a method is the inverse Monte Carlo technique [45], which attempts to link atomistic and mesoscale methods.

Typically, the coarse-graining of microscopic interactions results in coarse-grained "particles" that represent a collection of molecules or molecular groups rather than individual atoms. These particles interact with each other through soft forces, which arise directly from coarse-graining of microscopic interactions. The DPD technique, in particular in its most typical formulation [46], deals with this kind of particles.

Although coarse-graining might also be considered implicit in Brownian and Langevin dynamics simulations, the DPD technique offers the explicit advantage of a proper description of hydrodynamic modes significant in the physical approach toward a system's equilibrium. These issues are discussed in detail in Chapter 3. This is achieved in DPD by implementing a thermostat in terms of pairwise random and dissipative forces such that the total momentum of the system is conserved. Due to these reasons, DPD has been used in studies covering a wide range of aspects in soft matter systems, including the structure of lipid bilayers [47, 48], self-assembly [49], and the formation of polymer-surfactant complexes [50].

In this thesis, we will mainly consider methodological aspects of the DPD technique. DPD is a relatively new method and despite its potential there are still fundamental and methodological problems related to it. In relation to the DPD technique, the first topic in this thesis is related to the integration of the equations of motion. Due to the pairwise coupling of particles through random and dissipative forces, the integration of the equations of motion is a nontrivial task. The main difficulty arises from the dissipative force, which depends explicitly on the relative velocities of the particles, while the velocities in turn depend on the dissipative forces. An accurate description of the dynamics requires, at least in principle, a self-consistent solution.

The considerable computational load associated with this task has motivated the development of integration schemes [46, 51–57] which account for the velocity dependence of dissipative forces in some approximate manner allowing the integration to be carried out to a sufficient degree of computational efficiency. The search for a satisfactory integration scheme is ongoing, since many of the recent proposals have been found to exhibit non-physical behavior, such as systematic drift in temperature, and artificial structures in the radial distribution function [53–55].

In order to overcome these problems, a number of new integration schemes for DPD simulations have been developed in the past few years. Self-consistent determination schemes exist on the one hand [53–55], but these are rather elaborate and do not necessarily lead to improvements. Alternative proposals include (i) a parameterization of the integrator based on the specific application being modeled by den Otter and Clarke [56], (ii) operator splitting by Shardlow [57], and (iii) an elegant Monte Carlo-based approach

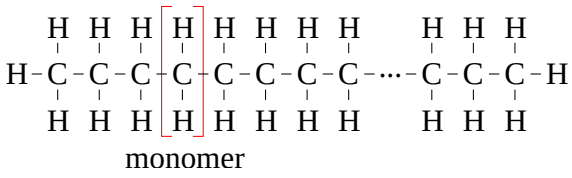

Figure 1.2: Polymers are long chain-like molecules composed of many repeating structural units called monomers.

due to Lowe [58] which completely avoids the problems arising from random and dissipative forces as it does not use random or dissipative forces at all. In the present work, we apply these schemes respectively to specific model systems, with the objective of assessing their relative performance.

The second topic in the studies concerning the DPD method focuses on the dynamics of polymeric liquids. Polymers are long chainlike molecules composed of many repeating structural units called monomers (Fig. 1.2). The dynamic properties of polymer solutions and melts are affected by topological constraints. The origin of these constraints is easy to understand: polymers can slide past, but not penetrate through each other. This is the physical origin of the reptation model pioneered by P.-G. de Gennes, M. Doi, and S. F. Edwards [59–61], which is the most successful theory in describing the behavior of entangled polymers. Despite active research in the field, entangled polymeric liquids keep posing many challenges to theorists [62–64], experimentalists [65–67] and computational modelers [68–74]. The importance of understanding the fundamentals of polymeric liquids can hardly be overemphasized as they are one of the key issues in novel (bio)materials science [75, 76].

The dynamics of polymer melts is typically described in terms of the Rouse and reptation models [61]. Short chains are able to move to any direction and are not entangled. This is the physical origin of the Rouse model [61, 77]. For longer chains, entanglements and uncrossability of chains cannot be ignored, and the chains become constrained to move in the direction of the chain backbone. The motion resembles that of a reptating snake; hence the name reptation model [59–61].

Computer simulations offer a detailed look into polymers and their dynamics. As was mentioned earlier, coarse-grained methods, such as DPD, allow access to much greater length and time scales than atomistic simulation methods do. This is due to the soft potentials and, like everything in life, they do not come without a price to pay: the softness of the conservative potentials allows the chains to slide through each other thus strongly affecting the dynamics of the system. Indeed, the scaling laws obtained from

DPD simulations of polymer melts [78,79] are not able to describe entangled liquids. This is a direct consequence of the fact that in DPD simulations, polymers can penetrate through themselves. Whereas this is not a problem in studying the equilibrium properties of polymeric liquids, reptation cannot be studied using the basic DPD model.

To preserve the advantages of coarse-grained models and to take into account the entanglement effects, there are currently two off-lattice methods for this purpose. J. T. Padding and W. J. Briels [71] recently introduced an algorithm that explicitly detects and prevents bond crossings. They consider bonds as elastic bands that become entangled and use energy minimization to determine the entanglement positions. This approach is general and very promising but it is complicated to implement and computationally intensive. Another promising approach was put forward by G. Pan and C. W. Manke [80]. They reduce the frequency of bond crossings by introducing segmental repulsive forces between the points of nearest contact between neighboring chains. This approach is simple to implement but the introduction of a new force and a related cutoff increases the computational load, and adds a new length scale whose physical determination is somewhat ambiguous. In the present work, we introduce a third alternative.

1.3 Structure of this thesis

This thesis is written in the style of a compilation of several scientific publications. In the first part of this thesis (Papers [1–3]) we study the diffusion of atoms on solid surfaces. To this end, we carry out Monte Carlo simulations for a lattice-gas model of O/W(110), first on clean surfaces and then on surfaces containing small concentrations of immobile, site-blocking impurities. In both cases, we examine how non-equilibrium condition affects tracer diffusion and collective diffusion of atoms on a surface.

In the second part, we consider methodological aspects of the dissipative particle dynamics (DPD) technique. DPD is a relatively new method and despite its potential there are still fundamental and methodological problems related to it. First, in Paper [4] we address the question: "How to integrate the equations of motion in DPD simulations?" To this end, we test several novel DPD integration schemes on an equal footing through DPD simulations of three different model systems, with the objective of assessing their relative performance.

Second, we study the dynamics of polymer melts. Melt is the liquid state of a polymeric system, from which it is processed into plastics, rubbers, and many other polymeric materials. The understanding of the dynamics of

melts is important. In standard DPD, as well as in other coarse-grained soft-potential models, there is a problem that polymers can penetrate through themselves. This is possible because with soft potentials it can happen that two particles are in the same place at the same time. This is a clear artifact, and has direct consequences on the polymer dynamics. To correct this problem, in Paper [5] we tune the conservative forces within the polymer chain so strong that chains cannot cut through each other. Our objective is to demonstrate that if a certain geometric criterion is met, it is impossible for polymer chains to cross.

The first three chapters of this thesis give background information on the research topics. Chapter 2 gives a brief introduction to the essential physics, including statistical mechanics, hydrodynamics, diffusion, and polymer physics. In Chapter 3 we discuss the simulation methods and models. We focus on the Monte Carlo and dissipative particle dynamics techniques, which are the main numerical methods used in this thesis. Finally, in Chapter 4 we summarize the work and draw conclusions.

Chapter 2

Physical Background

2.1 Statistical Mechanics

Statistical mechanics is a framework for relating the microscopic laws governing individual atoms and molecules to the macroscopic properties of materials that can be observed in everyday life, therefore explaining thermodynamics as a natural result of the statistical properties of a very large number ($\sim 10^{24}$) of microscopic particles. In particular, it can be used to calculate the macroscopic thermodynamic properties of bulk materials from the microscopic data of individual particles. For a comprehensive approach to statistical mechanics see the books by L. D. Landau and E. M. Lifshitz [81], R. K. Pathria [82], or K. Huang [83], for example.

2.1.1 Thermodynamic equilibrium

When two systems are put in contact with each other, there will be a net exchange of energy and/or matter between them unless they are in *thermodynamic equilibrium*. Qualitatively speaking, two systems are in thermodynamic equilibrium with each other if they remain the same after being put in contact. More precisely, thermodynamic equilibrium requires thermal equilibrium (associated to heat exchange), mechanical equilibrium (associated to work exchange), and chemical equilibrium (associated to matter exchange).

The definition of equilibrium is that forces $\vec{F}_i$ and torques $\vec{\tau}_i$ must sum to zero,

$$\sum_i \vec{F}_i = 0 \tag{2.1}$$

$$\sum_i \vec{\tau}_i = 0, \tag{2.2}$$

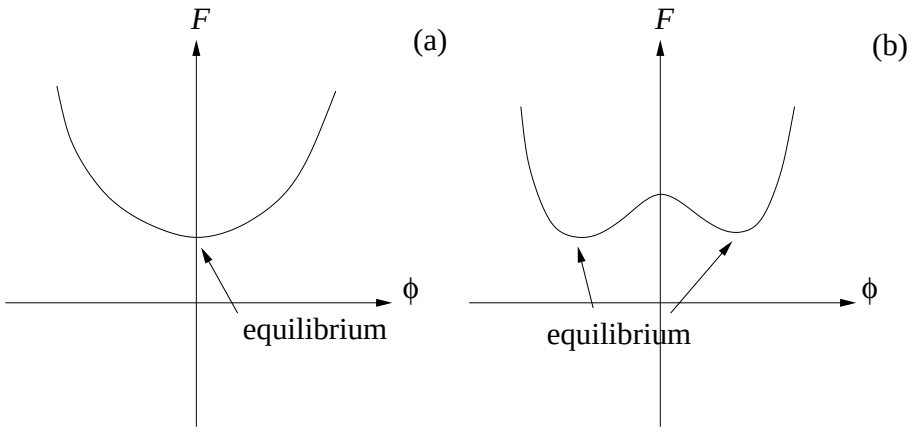

Figure 2.1: Free energy F as a function of the order parameter ϕ. In thermodynamic equilibrium, F is minimized.

chemical potentials of system components i are constant, i.e.,

$$\mu_i = \text{const}, \tag{2.3}$$

and that the thermodynamic potentials are minimized (Fig. 2.1). In equilibrium all macroscopic variables (such as pressure and temperature) remain constant in time.

Non-equilibrium thermodynamics [84] concerns situations where the system under study is not in thermodynamic equilibrium. One important class of non-equilibrium problems is the *steady state*, where a system is subject to external forces or torques. If the forces do not vary with time, the system quickly approaches steady state, where all macroscopic variables remain constant in time. Some systems, in turn, are in non-equilibrium because of the initial condition. These systems approach the thermodynamic equilibrium as time goes on. If the system is sufficiently close to equilibrium, it can be divided into small partitions that are much closer to the equilibrium than the whole system. In addition, if these partitions are large enough such that thermodynamics is applicable to them, the system is said to be in *local equilibrium*.

2.1.2 Ensemble theory

A microstate of a given classical system may be defined by specifying the instantaneous positions and momenta of all the particles of the system. Thus, the definition of a microstate requires the specification of $3N$ positions $q_1, q_2, \ldots, q_{3N}$ and $3N$ momenta $p_1, p_2, \ldots, p_{3N}$, where N is the number of particles in the system. The set of coordinates $(\{q_i\}, \{p_i\})$, where

$i = 1, 2, \ldots, 3N$, may be regarded as a point in a space of $6N$ dimensions. This space is referred to as the *phase space*.

Of course, the coordinates $q = \{q_i\}$ and $p = \{p_i\}$ are functions of time t. The time evolution of these coordinates is determined by the canonical equations of motion,

$$\frac{dq_i}{dt} = \frac{\partial \mathcal{H}(q,p)}{\partial p_i} \tag{2.4}$$

$$\frac{dp_i}{dt} = -\frac{\partial \mathcal{H}(q,p)}{\partial q_i}, \tag{2.5}$$

where $\mathcal{H}(q,p)$ is the Hamiltonian of the system. During the time evolution of the system, one can evaluate the *time average* $\langle A \rangle_{\text{time}}$ of a desired physical quantity A. This is what is done in a molecular dynamics simulation, see Sec. 3.3.

Instead of considering a single system at many instants of time, one can consider a large number of system replicas at a single instant of time. In a molecular dynamics simulation, this is achieved by starting the simulation of the system at hand from different initial configurations. The replicas of the system are chosen in such a way that they represent the same macrostate, but are in distinctly different microstates. This kind of collection of microstates is called an *ensemble*. The average over all microstates forming an ensemble is called the *ensemble average* $\langle A \rangle_{\text{ens}}$. Under certain conditions, i.e., if the system is ergodic, the time average and the ensemble average are equal,

$$\langle A \rangle_{\text{time}} = \langle A \rangle_{\text{ens}}. \tag{2.6}$$

In general, the microstates are not equally distributed. This feature is best described in terms of the *distribution function* $\rho(q,p;t)$, which tells how the microstates forming an ensemble are distributed at different instants of time. In thermodynamic equilibrium, the distribution function is stationary,

$$\frac{\partial}{\partial t}\rho(q,p;t) = 0. \tag{2.7}$$

The most common equilibrium distribution functions are the canonical and microcanonical distributions.

In a *microcanonical ensemble*, the macrostate of the system is defined by the number of particles N, volume V, energy E, linear momentum $\vec{p}$, and the angular momentum $\vec{l}$. This ensemble describes the statistical properties of a completely isolated system, i.e., there is no exchange of heat or particles with the environment. The microcanonical distribution function is given by

$$\rho(q,p) = \frac{1}{\Omega}\delta(\mathcal{H}(q,p) - E), \tag{2.8}$$

where the normalization constant Ω is called the microcanonical partition function. The conservation of linear and angular momenta can also be incorporated.

In a *canonical ensemble*, the macrostate of the system is defined by the number of particles N, volume V, and the temperature T. This ensemble, also called the NVT ensemble, describes the statistical properties of a closed system connected to a heat bath. The canonical distribution function is given by

$$\rho(q,p) = \frac{1}{Z}\exp[-\mathcal{H}(q,p)/k_BT], \tag{2.9}$$

where k_B is Boltzmann's constant, T is the temperature of the heat bath, and Z is the canonical partition function.

2.1.3 Ergodicity

In the previous subsection, we stated that for an ergodic system the time average equals the ensemble average if the system is ergodic [Eq. (2.6)]. To clarify the concept of ergodicity, consider the time-averaging process of a given physical quantity. If the given quantity is averaged only over a short period of time, the result is biased because it is taken from a non-representative set of microstates. However, if instead we average over a sufficiently long period of time, the system may be expected to pass through all its possible microstates. In this case, the result of the averaging process would depend only on the macrostate of the system, not on any particular subset of microstates. A direct consequence of this would be that the time average is equal to the ensemble average.

The above hypothesis, which states that the system passes through all its possible microstates in the course of time, is called the *ergodic theorem*. According to this theorem, the phase space trajectory of an ergodic system passes through each and every point of the relevant region of the phase space, if one only waits long enough. In a strict sense, only very simple systems can be considered as truly ergodic. One example of a truly ergodic system is the simple harmonic oscillator (Fig. 2.2a). In a broader sense, it is sufficient that the phase space trajectory passes through any neighborhood of any point of the relevant region of the phase space. In this sense, almost all real systems can be considered as ergodic.

There are, however, systems that are not ergodic even in the broader sense. They may be either truly non-ergodic or non-ergodic in practice. For example, a system of N coupled harmonic oscillators will never reach equilibrium but stays with whatever normal modes it started with [85]. Glass

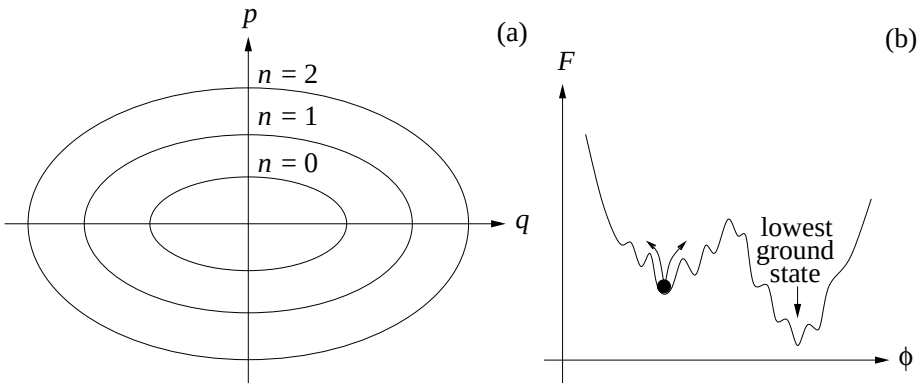

Figure 2.2: (a) Eigenstates of a simple harmonic oscillator. (b) Free energy curve $F(\phi)$ of a glass. Variable ϕ is the order parameter.

(Fig. 2.2b), in turn, is a famous example of a system that is non-ergodic in practice (i.e., trapped for indefinitely long time).

2.2 Phase transitions

Consider a physical system of N particles at constant pressure P and temperature T. At high temperatures the system is disordered, uncorrelated, uniform, and isotropic. Assume that this high-temperature state has the full rotational and translational symmetry of space, as, e.g., in a gas. As temperature is lowered, at some particular temperature, called the transition temperature $T_{\rm tr}$, a new thermodynamic state emerges. This low-temperature state is more ordered and correlated than the high-temperature state. The transition between the disordered high-temperature state and the ordered low-temperature state is called a *phase transition*. Examples of phase transitions are: (i) solid–liquid–gas transitions (melting, boiling, etc.), (ii) ferromagnetic–paramagnetic transition in magnetic systems, (iii) conductor–superconductor transition in metals, (iv) superfluid transition in liquid helium, and (v) separation of fundamental forces in the early universe. For a comprehensive approach to phase transitions, see the books by J. J. Binney, N. J. Dowrick, A. J. Fisher, and M. E. J. Newman [86], N. Goldenfeld [87], or P. M. Chaikin and T. C. Lubensky [88], for example.

2.2.1 First-order phase transitions

As a concrete example, let us consider the liquid–gas transition of water. At high temperatures, water is in the gas phase. Its kinetic energy dominates

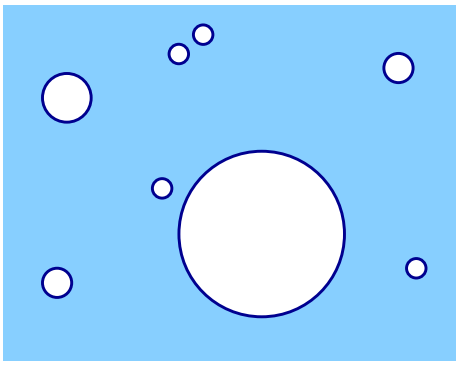

Figure 2.3: A first-order phase transition proceeds by nucleation of small bubbles of the new phase (white) in the old phase (colored).

its potential energy, and, as a result, it exists in a state that is disordered, uncorrelated, uniform, and isotropic. Now, let us lower the temperature, i.e., the average kinetic energy. As the potential energy becomes more important, specific intermolecular interactions come into play. For water molecules, the relevant interactions are the dipole–dipole interaction and hydrogen bonding, both of which are attractive for a particular configuration. Attraction tends to enhance density fluctuations: each molecule wants to spend most of its time in a region where there are other molecules rather than in a region where there are none. This clustering grow in amplitude and persists for longer times. Density is still uniform but only when averaged over large regions of space or over long intervals of time. The end result of these attractive interactions is the formation of the liquid phase, whose density is greater than that of the gas phase.

Under ordinary circumstances the phase transitions of water are *first-order* phase transitions. First-order transitions are those that involve latent heat: when a substance makes a first-order transition from a high-temperature phase to the low-temperature phase, a non-zero quantity of heat is released as the temperature passes the transition temperature T_{tr}. The latent heat is given out as the substance cools through an infinitesimally small temperature range around the transition temperature T_{tr}. The emission of heat at the transition tells us that the structure of the substance is being radically changed at T_{tr}. For example, the latent heat $L = 2300$ kJ/kg is released when H_2O molecules condense into liquid.

A first-order phase transition proceeds by nucleation of small bubbles of the new phase in the old phase (Fig. 2.3). These small bubbles grow in size and coalesce with other bubbles until the old phase has disappeared. This phenomenon is familiar to anyone who has boiled water in a kettle: the

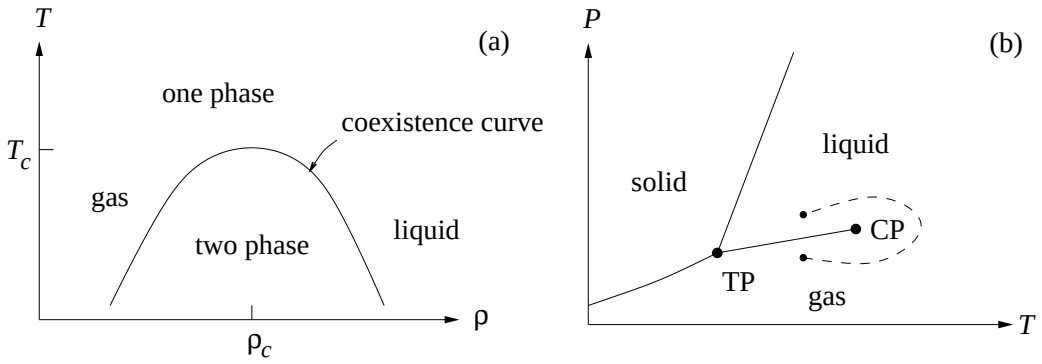

Figure 2.4: (a) Phase diagram of a typical substance at fixed pressure. (b) Phase diagram of a typical substance at fixed density. (CP = critical point, TP = triple point)

water does not instantly turn to vapor but forms a mixture of water and vapor bubbles. The reason for this behavior is the latent heat. Because of the latent heat, it takes a long time to accumulate the required energy.

Fig. 2.4a shows a portion of the phase diagram of a typical substance. Below the critical temperature T_c, there is a coexistence curve, which separates the one-phase region from the two-phase regions. Above T_c it is possible to pass continuously from liquid to gas by increasing density ρ. In this case, there is no density at which a liquid and a gas coexist. Note that even starting below T_c it is possible to pass from a liquid to gas without passing through the two-phase region: simply raise the temperature above T_c, reduce the density, and then lower the temperature below T_c. Fig. 2.4b shows the similar process in the temperature–pressure (T–P) plane. The solid phase, however, is completely separated by the phase boundary, which means that there is no way to turn solid to liquid (or gas) continuously.

2.2.2 Continuous phase transitions

The previous section demonstrated that a liquid can be transformed into a gas continuously if one first raises the temperature above the critical point T_c, reduces the density, and then lowers the temperature below T_c. What happens if we pass exactly through the critical point? This situation can be produced by heating water in a sealed container. As the container is heated, water steadily turns to vapor, raising the vapor density in the container. Meanwhile the water expands slightly, so that the density difference between the water and vapor becomes steadily smaller. If the volume of the container is just right, the density difference between the water and vapor eventually

vanishes. At this point the latent heat becomes zero, because it reflects the different intermolecular binding energies of H_2O molecules in liquid and vapor. The temperature and pressure of water at this point are $T_c = 647.4$ K and $P_c = 22.1$ MPa. These values define the *critical point* of the liquid–vapor transition.

First-order phase transitions are generally defined to be those that involve a non-zero latent heat, all other phase transition being considered as continuous. The name "first order" refers to the fact that in the first order phase transition the first derivative of the free energy is discontinuous. In the continuous phase transition, in turn, the first derivative is continuous; hence the name "continuous". The vanishing of the latent heat at the critical point does not ensure that the specific heat of a sample is a smooth function of temperature, or even finite. In fact the specific heat c_p often diverges in the neighborhood of T_c as

$$c_p \sim |T - T_c|^{-\alpha}. \tag{2.10}$$

where α is the *critical exponent* related to the specific heat. Typically, $0 < \alpha \leq 0.2$. Several thermodynamic quantities other than the specific heat c_p usually diverge at a continuous phase transition. For example, the isothermal compressibility κ_T of a container filled with fluid at the critical density diverges near T_c as

$$\kappa_T \sim |T - T_c|^{-\gamma}, \tag{2.11}$$

where γ is the critical exponent related to the isothermal compressibility. Typically, $1 \leq \gamma \leq 2$. In addition to α and γ, there are four more critical exponents related to other observables [86–88].

The large value of the isothermal compressibility κ_T near T_c gives rise to large fluctuations in the density of the material. In fact, the relation between the isothermal compressibility and the particle number fluctuations is given by

$$\frac{\langle (\delta N)^2 \rangle}{\langle N \rangle} = \rho k_B T \kappa_T, \tag{2.12}$$

where N is the number of particles, δN is the particle number fluctuation, ρ is density, and k_B is Boltzmann's constant. As the system approaches the critical point, the system will no longer be homogeneous: there are regions with greater and lesser density. As the size of these regions approaches the wavelength of visible light, scattering increases dramatically. This gives the fluid a cloudy appearance. This phenomenon is known as *critical opalescence*.

The state of a system is usually characterized by a physical quantity called the *order parameter*. The order parameter is used to distinguish between different phases, such that above T_c the order parameter is zero and below

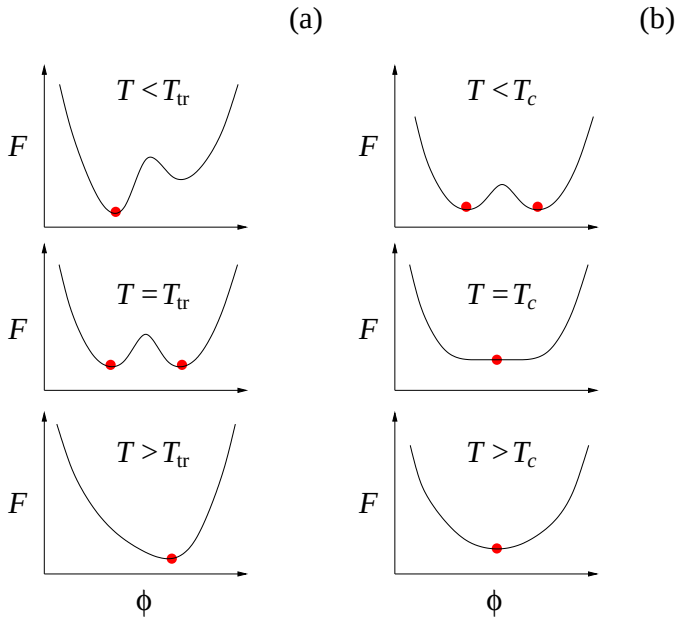

Figure 2.5: Free energy F as a function of the order parameter ϕ. (a) First-order phase transition. (b) Continuous phase transition

T_c it has a small but finite value. We will denote the order parameter by the symbol ϕ. For example, a suitable order parameter for the liquid–gas phase transition is $\phi = \rho - \rho_c$, where ρ_c is the density of a fluid at the critical point.

The equilibrium state of the system corresponds to the minimum of the free energy. Fig. 2.5a shows a schematic free energy curve $F(\phi)$ for the first-order phase transition. In the first-order transition, the free energy has two wells, the left one representing the low-temperature phase and the right one representing the high-temperature phase. When the system approaches the transition temperature from below ($T < T_{\rm tr}$), the system stays in the left minimum until the transition temperature $T_{\rm tr}$ is reached. At $T_{\rm tr}$ the system suddenly jumps to the right minimum.

In the continuous phase transition (Fig. 2.5b), there is no barrier between different phases. For this reason, the system can stay at all times at the lowest possible value of $F(\phi)$, moving continuously from the high-temperature phase to the low-temperature phase and vice versa. Near the critical temperature $T = T_c$, the free energy $F(\phi)$ is very flat around the minimum so that small fluctuations in F correspond to large fluctuations in ϕ. This is the cause of critical opalescence observed in liquid–gas phase transitions.

In the case of a first-order transition, $F(\phi)$ is never flat so the fluctuations in ϕ are never particularly large. As a result there are no critical phenomena.

What can happen, however, is that the system can become trapped in a local minimum for long times, and then suddenly jump to the true global minimum.

To understand the critical behavior in Eqs. (2.10) and (2.11), we introduce the concept of the *correlation length*, usually denoted by ξ. The correlation length sets the scale over which each domain has a significant probability of finding like domains in excess of the average domain. One can alternatively interpret ξ as a measure of the average linear size of the domains containing the minority phase. For example, in a gas, there will be density fluctuations in thermal equilibrium. In a particular region of the sample, the density may be higher than the average density. We can choose to think of such a region as a droplet of near-liquid density floating in the gas. In thermal equilibrium, there is a distribution of droplet sizes, of course, but it turns out that there is a well-defined average size, at least away from the critical point itself. This characteristic size is, roughly speaking, what we mean by the term correlation length. A more precise definition of this important quantity is given in Refs. [86–88].

The system fluctuates in all sizes up to size ξ, but fluctuations that are significantly larger are exceedingly rare. As T_c is approached from either above or below, ξ grows without limit. In fact, one finds empirically that near T_c, ξ diverges as

$$\xi \sim |T - T_c|^{-\nu} \quad (|T - T_c|/T_c \ll 1), \tag{2.13}$$

where ν is the critical exponent related to the correlation length. Typically, $0.5 \leq \nu \leq 1$. The physical picture of this divergence is that of huge droplets of one phase containing smaller droplets of other phase containing still smaller droplets of the first phase and so on. This suggests that the system is self-similar for a large range of different length scales: if we zoomed in on part of the system at the phase transition, we would notice that the resulting picture is essentially indistinguishable from the one presented by the system as a whole: differences appear only at scales comparable to atomistic lengths, which set a natural limit, often called the ultraviolet cutoff. This scale invariance is exploited in renormalization theory, which has led to a qualitative and quantitative understanding of critical phenomena and continuous transitions.

It is remarkable that continuous phase transitions arising in different systems often have the same set of critical exponents. This phenomenon is known as *universality*. As a matter of fact, there is only a limited number of universality classes. Physically this can be explained the following way: as the correlation length ξ increases, microscopic properties become less and

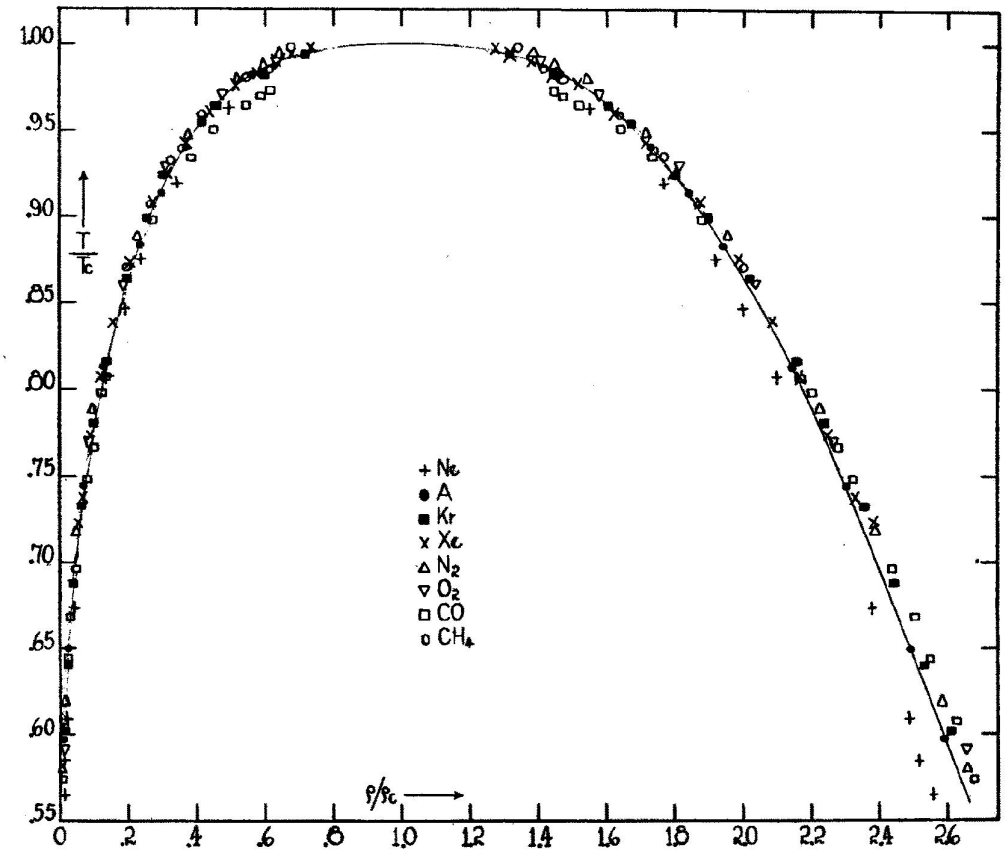

Figure 2.6: Temperature T/T_c as a function of density ρ/ρ_c for several fluids. The data collapse implies that the critical exponent $\beta \approx 1/3$ for all fluids. Figure taken from the article by E. A. Guggenheim [89].

less important. Instead, as ξ becomes large, *generic* properties such as the symmetry group of the Hamiltonian, the dimensionality of the system, and whether or not the forces are short-ranged determine the behavior of the system. For example, the critical exponents at the liquid–gas phase critical point have been found to be independent of the chemical composition of the fluid (Fig. 2.6). More surprisingly, the critical exponents of such very different transitions as the liquid–gas transition and the separation of a mixture of two organic chemicals have been found to be equal within experimental accuracy, which can be understood in terms of the above arguments. Systems exhibiting same critical exponents are said to be in the same *universality class*.

2.3 Hydrodynamics

Hydrodynamics concerns the macroscopic motion of liquids and gases. At the macroscopic level, fluids (i.e., liquids and gases) can be considered as a continuous medium. This means that, instead of individual molecules, fluids are described with field variables such as mass density, momentum density, and energy density. Although hydrodynamics is most often applied to fluids, it can be used to study internal motions in any system including crystalline solids and spin systems. For a comprehensive approach to hydrodynamics, see the books by L. D. Landau and E. M. Lifshitz [90], or P. M. Chaikin and T. C. Lubensky [88], for example.

2.3.1 Continuity equation

The state of a moving fluid can be described in terms of the fluid velocity $\vec{v}(\vec{r},t)$, pressure $P(\vec{r},t)$, and the density $\rho(\vec{r},t)$. Together with the equation of state, these three quantities define the state of the moving fluid completely. All these quantities are functions of position $\vec{r}$ and time t. We emphasize that $\vec{v}(\vec{r},t)$ is the velocity of the fluid at a given point $\vec{r}$ in space at a given time t, i.e., it refers to fixed points in space and not to specific particles of the fluid. In the course of time, the latter move about in space. The same remarks apply to $P(\vec{r},t)$ and $\rho(\vec{r},t)$.

The conservation of the total energy, total momentum, and the total mass leads to three conservation equations. Let us begin with the equation that expresses the conservation of mass. Consider some volume V_0 of space. The mass of fluid in this volume is $\int \rho dV$, where ρ is the fluid density, and the integration is taken over the volume V_0. The mass of fluid flowing in unit time through an element $d\vec{S}$ of the surface bounding this volume is $\rho\vec{v}\cdot d\vec{S}$, where the magnitude of the vector $d\vec{S}$ is equal to the area of the surface element, and its direction is along the normal. By convention, we take $d\vec{S}$ along the outward normal. Then $\rho\vec{v}\cdot d\vec{S}$ is positive if the fluid is flowing out of the volume, and negative if the flow is into the volume. The total mass of fluid flowing out of the volume V_0 in unit time is therefore

$$\oint \rho\vec{v}\cdot d\vec{S}, \tag{2.14}$$

where the integration is taken over the whole closed surface surrounding the volume in question.

Next, the decrease per unit time in the mass of fluid in the volume V_0 can be written

$$-\frac{\partial}{\partial t}\int \rho dV. \tag{2.15}$$

Equating the two expressions, we get

$$\frac{\partial}{\partial t}\int \rho dV = -\oint \rho\vec{v}\cdot d\vec{S}. \tag{2.16}$$

The surface integral can be transformed by Green's formula to a volume integral. Thus

$$\frac{\partial}{\partial t}\int \rho dV = -\int \nabla\cdot(\rho\vec{v})dV \tag{2.17}$$

$$\int\left[\frac{\partial\rho}{\partial t}+\nabla\cdot(\rho\vec{v})\right]dV = 0. \tag{2.18}$$

Since this equation must hold for any volume, the integrand must vanish, i.e.,

$$\partial\rho/\partial t+\nabla\cdot\vec{j}=0. \tag{2.19}$$

This equation is called the *continuity equation*. It states that in a fluid, the total mass is conserved. The vector

$$\vec{j}=\rho\vec{v} \tag{2.20}$$

is called the *mass flux density*. Its direction is that of the motion of the fluid, while its magnitude equals the mass of fluid flowing in unit time through unit area perpendicular to the velocity.

2.3.2 Euler's equation

Next we derive the equation that expresses the conservation of momentum. Consider some volume in the fluid. The total force acting on this volume is equal to the integral of the pressure,

$$-\oint P d\vec{S}, \tag{2.21}$$

taken over the surface bounding the volume. Transforming it to a volume integral, we get

$$-\oint P d\vec{S} = -\int \nabla P dV. \tag{2.22}$$

Hence we see that the fluid surrounding any volume element dV exerts on that element a force $-\nabla P dV$. In other words, we can say that a force $-\nabla P$ acts on unit volume of the fluid.

We can now write down the equation of motion of a volume element in the fluid by equating the force $-\nabla P$ to the product of the mass per unit volume (i.e., density ρ) and the acceleration $d\vec{v}/dt$:

$$\rho d\vec{v}/dt = -\nabla P. \tag{2.23}$$

The derivative $d\vec{v}/dt$ which appears here denotes not the rate of change of the fluid velocity at a fixed point in space, but the rate of change of the velocity of a given fluid particle as it moves about in space. This derivative has to be expressed in terms of quantities referring to points fixed in space. To do so, we expand $d\vec{v}$ in terms of the partial derivatives with respect to $\vec{r}$ and t:

$$d\vec{v} = dt\frac{\partial\vec{v}}{\partial t} + dr_x\frac{\partial\vec{v}}{\partial r_x} + dr_y\frac{\partial\vec{v}}{\partial r_y} + dr_z\frac{\partial\vec{v}}{\partial r_z} \tag{2.24}$$

$$= dt\frac{\partial\vec{v}}{\partial t} + (d\vec{r}\cdot\nabla)\vec{v}. \tag{2.25}$$

Dividing both sides by dt, we get

$$\frac{d\vec{v}}{dt} = \frac{\partial\vec{v}}{\partial t} + (\vec{v}\cdot\nabla)\vec{v}, \tag{2.26}$$

and substituting this in Eq. (2.23), we find

$$\frac{\partial\vec{v}}{\partial t} + (\vec{v}\cdot\nabla)\vec{v} = -\frac{1}{\rho}\nabla P. \tag{2.27}$$

This equation is called *Euler's equation*. It states that in a fluid the total momentum is conserved. By combining Euler's equation with the continuity equation [Eq. (2.19)] we get

$$\partial(\rho\vec{v})/\partial t + \nabla\cdot\mathbf{\Pi} = 0, \tag{2.28}$$

where the tensor Π_{ik} is called the *momentum flux density tensor*,

$$\Pi_{ik} = P\delta_{ik} + \rho v_i v_k. \tag{2.29}$$

Equation (2.28) is often referred to as the *momentum continuity equation*.

2.3.3 Navier–Stokes equation

The momentum flux given in Eq. (2.29) represents a completely reversible transfer of momentum, due to the mechanical transport of the different particles of fluid from place to place and to the pressure forces acting in the fluid. The viscosity causes another transfer of momentum from points where the velocity is large to those where it is small. This process is the result of the thermodynamic irreversibility of the motion, which always occurs to some extent, and is due to internal friction and thermal conduction.

In order to obtain the equations describing the motion of a viscous fluid, we have to include some additional terms in the "ideal" momentum flux given

in Eq. (2.29). Thus we write the momentum flux density tensor of a viscous fluid in the form

$$\Pi_{ik} = P\delta_{ik} + \rho v_i v_k - \sigma'_{ik} \tag{2.30}$$
$$= -\sigma_{ik} + \rho v_i v_k. \tag{2.31}$$

The tensor $\sigma_{ik} = -P\delta_{ik} + \sigma'_{ik}$ is called the *stress tensor* and σ'_{ik} is the *viscous stress tensor*. The viscous stress tensor σ'_{ik} is due to the irreversible "viscous" transfer of momentum in the fluid.

The general form of the tensor σ'_{ik} is given by

$$\sigma'_{ik} = \eta\left(\frac{\partial v_i}{\partial r_k} + \frac{\partial v_k}{\partial r_i} - \frac{2}{3}\delta_{ik}\nabla\cdot\vec{v}\right) + \zeta\delta_{ik}\nabla\cdot\vec{v}, \tag{2.32}$$

where the constant η is called the *shear viscosity* and ζ is the *bulk viscosity*. Eq. (2.32) is based on following assumptions: (i) the fluid is isotropic, (ii) velocity gradients in the fluid are small, (iii) pressure and density gradients are small, (iv) σ'_{ik} vanishes when the whole fluid moves with uniform velocity, and (v) σ'_{ik} vanishes when the whole fluid is in uniform rotation.

The equations of motion of a viscous fluid can now be obtained by simply adding the expressions $\nabla\sigma'$ to Euler's equation [Eq. (2.27)]. Thus we have

$$\rho\left[\frac{\partial\vec{v}}{\partial t} + (\vec{v}\cdot\nabla)\vec{v}\right] = -\nabla P + \eta\Delta\vec{v} + (\zeta + \frac{1}{3}\eta)\nabla\nabla\cdot\vec{v}. \tag{2.33}$$

This equation is called the *Navier–Stokes equation*. It becomes considerably simpler if the fluid may be regarded as incompressible. In this case $\nabla\cdot\vec{v} = 0$, as follows from Eq. (2.19). Hence,

$$\frac{\partial\vec{v}}{\partial t} + (\vec{v}\cdot\nabla)\vec{v} = -\frac{1}{\rho}\nabla P + \frac{\eta}{\rho}\Delta\vec{v}. \tag{2.34}$$

When combined with the continuity equation [Eq. (2.19)], the Navier–Stokes equations yield four equations with four unknowns, i.e., density ρ and three components of velocity $\vec{v}$. These equations are very often treated in a discretized form on a computer. This field of research is called computational fluid dynamics [91].

2.4 Diffusion

Consider a drop of ink in water. In the beginning, ink is highly concentrated at the point where it is inserted. As time goes on, ink steadily spreads, until

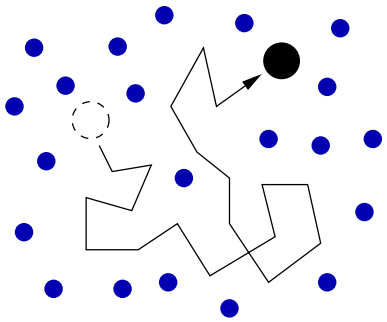

Figure 2.7: Brownian motion. In a pure diffusion process, particles move in a completely random manner.

the ink is evenly distributed throughout the water. This process is called *diffusion* (Fig. 2.7). In a pure diffusion process, there is no systematic force driving the particles; they move in a completely random manner. The macroscopic motion of particles from concentrated regions to non-concentrated regions is a consequence of the second law of thermodynamics: because there are more microstates available with (nearly) uniform distribution than with non-uniform distributions, the diffusion process proceeds toward the uniform concentration. For a comprehensive approach to diffusion, see the book by J. P. Hansen and I. R. McDonald [92], or the article by R. Gomer [13], for example.

2.4.1 Fick's laws of diffusion

Consider a small amount of particles of type A distributed among particles of type B. If the particles of each type are not evenly distributed, there will be a net flux of particles from regions of higher concentration toward regions of lower concentration. The driving force for such a mass transport is the concentration gradient—the steeper the concentration gradient, the greater the diffusion. This proportionality is described by the equation

$$\vec{j}(\vec{r},t) = -D_C \nabla\theta(\vec{r},t), \tag{2.35}$$

called *Fick's first law*, which states that the net flow of particles $\vec{j}$ is proportional to the concentration gradient $\nabla\theta$. The proportionality constant D_C in Eq. (2.35) is called the *collective diffusion coefficient*. Sometimes D_C is called the inter-diffusion coefficient or the chemical diffusion coefficient. Eq. (2.35) is sufficient to define D_C but for practical purposes it is useful to combine Eq. (2.35) with the continuity equation [Eq. (2.19)]:

$$\frac{\partial\theta}{\partial t} + \nabla\cdot\vec{j} = 0, \tag{2.36}$$

to obtain

$$\frac{\partial\theta}{\partial t} = \nabla\cdot(D_C\nabla\theta), \tag{2.37}$$

This equation is called *Fick's second law* or the *diffusion equation*. Typically, D_C is a function of $\vec{r}$, t, or θ. Therefore D_C cannot be taken outside the gradient operator. For example, in Sec. 2.4.6 we consider a situation where D_C is a function of θ.

2.4.2 Tracer diffusion

Let us next focus on the motion of a single particle. Its position vector is given by $\vec{r}_i(t)$. As a result of collisions with other particles, the particle will slowly move away from its starting position $\vec{r}_i(0)$. The displacement vector $\vec{r}_i(t) - \vec{r}_i(0)$ can be used to measure diffusion. Because the particle has the equal probability to move in any direction,

$$\langle\vec{r}_i(t) - \vec{r}_i(0)\rangle = 0. \tag{2.38}$$

The mean square displacement $\langle[\vec{r}_i(t) - \vec{r}_i(0)]^2\rangle$ in turn is not zero. To make this clear, we divide time t into M intervals of equal length τ_0 and the coordinate $\vec{r}_i$ correspondingly at times $t_m = m\tau_0$ with $m = 0, 1, \ldots, M$. Then $\vec{r}_i(t) = \vec{r}_i(M\tau_0) = \sum_{m=1}^{M}\delta\vec{r}_i(t_m) + \vec{r}_i(0)$, where $\delta\vec{r}_i(t_m) = \vec{r}_i(t_m) - \vec{r}_i(t_{m-1})$ is the change in the position of the particle between two consecutive observations at times t_m and t_{m-1}. This leads to

$$\begin{aligned}\langle[\vec{r}_i(t) - \vec{r}_i(0)]^2\rangle &= \left\langle\left[\sum_{m=1}^{M}\delta\vec{r}_i(t_m)\right]^2\right\rangle &(2.39)\\ &= \sum_{n=1}^{M}\sum_{m=1}^{M}\langle\delta\vec{r}_i(t_n)\cdot\delta\vec{r}_i(t_m)\rangle. &(2.40)\end{aligned}$$

At long times displacements $\delta\vec{r}_i(t_m)$, $m = 1, 2, \ldots, M$, are uncorrelated. Therefore, in the limit $|t_m - t_n| \to \infty$, $\langle\delta\vec{r}_i(t_n)\cdot\delta\vec{r}_i(t_m)\rangle = \langle\delta\vec{r}_i(t_n)\rangle\cdot\langle\delta\vec{r}_i(t_m)\rangle = 0$. The last equality results from the fact that the particle has the same probability to move to any direction [cf. Eq. (2.38)]. Thus we obtain

$$\begin{aligned}\langle[\vec{r}_i(t) - \vec{r}_i(0)]^2\rangle &= \sum_{m=1}^{M}\langle[\delta\vec{r}_i(t_m)]^2\rangle &(2.41)\\ &= M\langle(\delta\vec{r}_i)^2\rangle &(2.42)\\ &= (t/\tau_0)\langle(\delta\vec{r}_i)^2\rangle. &(2.43)\end{aligned}$$

In Eq. (2.42) we assume that $\langle(\delta\vec{r}_i)^2\rangle = \langle[\delta\vec{r}_i(t_m)]^2\rangle$ for all $m = 1, 2, \ldots, M$, which states that the mean square displacement depends on time difference, not on time origin.

From Eq. (2.43) we see that the mean square displacement is proportional to t if t is large. This proportionality is related to the *tracer diffusion coefficient* D_T:

$$D_T = \lim_{t\to\infty} \frac{1}{2dt} \langle [\vec{r}_i(t) - \vec{r}_i(0)]^2 \rangle, \tag{2.44}$$

where d is the dimension of the space. Sometimes D_T is called the self-diffusion coefficient. We can use Eq. (2.44) to estimate the distance r traveled by a single particle. When t is sufficiently large,

$$r^2 = 2dD_T t. \tag{2.45}$$

The relations like Eq. (2.44) between a transport coefficient and a infinite-time limit of a mean square quantity are called the *Einstein relations*. Einstein relations are derived for many transport coefficients such as the shear viscosity, thermal conductivity, and electrical conductivity. For example, the Einstein relation for D_C is given by

$$D_C = \lim_{t\to\infty} \frac{\xi N}{2dt} \langle [\vec{R}_{\mathrm{cm}}(t) - \vec{R}_{\mathrm{cm}}(0)]^2 \rangle. \tag{2.46}$$

Here $\vec{R}_{\mathrm{cm}} = \frac{1}{N}\sum_{i=1}^{N} \vec{r}_i(t)$ is the center of mass of the diffusing material and $\xi = \langle N \rangle / \langle (\delta N)^2 \rangle$ is the so-called thermodynamic factor describing the particle number fluctuations. The thermodynamic factor is inversely proportional to the isothermal compressibility $\kappa_T = 1/k_B T \theta \xi$ of the diffusing material [cf. Eq. (2.12)].

2.4.3 Green–Kubo relations

In the previous section, we related the diffusion coefficient D_T to the mean square displacement of the particle. One can also use particle velocities $\vec{v}_i(t)$ to measure diffusion. If we write $\vec{r}_i(t)$ as the time integral of the velocity, the mean square displacement becomes

$$\begin{aligned}
\langle [\vec{r}_i(t) - \vec{r}_i(0)]^2 \rangle &= \left\langle \left[\int_0^t dt_1 \vec{v}_i(t_1) \right]^2 \right\rangle && (2.47)\\
&= \int_0^t dt_1 \int_0^t dt_2 \langle \vec{v}_i(t_1) \cdot \vec{v}_i(t_2) \rangle && (2.48)\\
&= 2\int_0^t dt_1 \int_0^{t_1} dt_2 \langle \vec{v}_i(t_1) \cdot \vec{v}_i(t_2) \rangle && (2.49)\\
&= 2\int_0^t dt' (t - t') \langle \vec{v}_i(t') \cdot \vec{v}_i(0) \rangle. && (2.50)
\end{aligned}$$

In the last equation we have defined a new variable $t' = t_1 - t_2$ and used the property

$$\langle \vec{v}_i(t_1) \cdot \vec{v}_i(t_2) \rangle = \langle \vec{v}_i(t_1 - t_2) \cdot \vec{v}_i(0) \rangle, \tag{2.51}$$

which states that the correlations in velocity depend on time difference, not on time origin. Inserting Eq. (2.50) into the definition of tracer diffusion [Eq. (2.44)] gives

$$\begin{aligned} D_T &= \lim_{t\to\infty} \frac{1}{2dt} \langle [\vec{r}_i(t) - \vec{r}_i(0)]^2 \rangle & (2.52)\\ &= \lim_{t\to\infty} \frac{1}{dt} \int_0^t dt' (t - t') \langle \vec{v}_i(t') \cdot \vec{v}_i(0) \rangle & (2.53)\\ &= \frac{1}{d} \int_0^\infty dt' \langle \vec{v}_i(t') \cdot \vec{v}_i(0) \rangle. & (2.54) \end{aligned}$$

Often this quantity is averaged over all particles in the system, summing i from 1 to N and dividing by N:

$$D_T = \frac{1}{dN} \sum_{i=1}^{N} \int_0^\infty dt' \langle \vec{v}_i(t') \cdot \vec{v}_i(0) \rangle. \tag{2.55}$$

The diffusion coefficients D_T and D_C give two views to the diffusion processes: microscopic and macroscopic. The relation between D_C and D_T is derived in Sec. 2.4.4.

In Eqs. (2.54) and (2.55) the integrand $\langle \vec{v}_i(t') \cdot \vec{v}_i(0) \rangle$ is called the velocity autocorrelation function. Such relations between a transport coefficient and an integral over a time-correlation function are called *Green–Kubo relations*. Green–Kubo relations have been derived for many transport coefficients, such as the shear viscosity, thermal conductivity, and electrical conductivity. For example, the Green–Kubo relation for collective diffusion is given by

$$D_C = \frac{\xi}{dN} \int_0^\infty dt' \langle \vec{J}(t') \cdot \vec{J}(0) \rangle. \tag{2.56}$$

Here $\vec{J}(t) = \sum_{i=1}^{N} \vec{v}_i(t)$ is the total flux of particles and ξ is the thermodynamic factor defined in Sec. 2.4.2.

2.4.4 Relation between D_C and D_T

The relation between D_C and D_T is obtained by dividing D_C in Eq. (2.56) with the averaged D_T in Eq. (2.54). The result is

$$\begin{aligned} \frac{D_C}{D_T} &= \xi \frac{\sum_{ij} \int_0^\infty dt' \langle \vec{v}_i(t') \cdot \vec{v}_j(0) \rangle}{\sum_i \int_0^\infty dt' \langle \vec{v}_i(t') \cdot \vec{v}_i(0) \rangle} & (2.57)\\ &= \xi \left[1 + \frac{\sum_{i\neq j} \int_0^\infty dt' \langle \vec{v}_i(t') \cdot \vec{v}_j(0) \rangle}{\sum_i \int_0^\infty dt' \langle \vec{v}_i(t') \cdot \vec{v}_i(0) \rangle} \right]. & (2.58) \end{aligned}$$

If the concentration is very low ($\theta \to 0$) the diffusing particles do not interact with each other. In this case $\xi = 1$ and $\langle \vec{v}_i(t') \cdot \vec{v}_j(0) \rangle = 0$ for all $i \neq j$. Therefore, in the limit $\theta \to 0$ we have

$$D_C = D_T, \tag{2.59}$$

The result $\xi = 1$ is obtained by inserting the equation of state of an ideal gas, $pV = Nk_BT$, into the definition $\kappa_T = -(1/V)(\partial V/\partial p)_T$, and then relating $\kappa_T = 1/k_BT\theta\xi$.

2.4.5 Memory expansion

In Secs. 2.4.2 and 2.4.3 we introduced two different ways to measure diffusion coefficients. There is yet another possible way to measure D_T (and D_C). Let us focus on the motion of a single particle. Instead of directly evaluating D_T from the long-time limit of Eq. (2.44), we consider the motion of the particle at short time scales. The time t is divided into M time intervals of equal length τ_0 and the coordinate $\vec{r}_i$ is discretized correspondingly at times $t_m = m\tau_0$ with $m = 0, 1, \ldots, M$. Then $\vec{r}_i(t) = \vec{r}_i(M\tau_0) = \sum_{m=1}^{M} \delta\vec{r}_i(t_m) + \vec{r}_i(0)$, where $\delta\vec{r}_i(t_m) = \vec{r}_i(t_m) - \vec{r}_i(t_{m-1})$ is the change in the position of the particle between two consecutive observations at times t_m and t_{m-1}. This leads to the expression [93]

$$\begin{aligned} D_T &= \lim_{M\to\infty} \frac{1}{2dM\tau_0} \langle [\vec{r}_i(M\tau_0) - \vec{r}_i(0)]^2 \rangle & (2.60)\\ &= \lim_{M\to\infty} \frac{1}{2dM\tau_0} \sum_{n=1}^{M} \sum_{m=1}^{M} \langle \delta\vec{r}_i(t_n) \cdot \delta\vec{r}_i(t_m) \rangle & (2.61)\\ &= \lim_{M\to\infty} \frac{1}{2dM\tau_0} \left[M\langle [\delta\vec{r}_i(0)]^2 \rangle + 2 \sum_{k=1}^{M-1} (M-k) \langle \delta\vec{r}_i(t_k) \cdot \delta\vec{r}_i(0) \rangle \right]. & (2.62) \end{aligned}$$

In the last equation we have defined a new variable $k = n - m$ and used the property

$$\langle \delta\vec{r}_i(t_n) \cdot \delta\vec{r}_i(t_m) \rangle = \langle \delta\vec{r}_i(t_n - t_m) \cdot \delta\vec{r}_i(0) \rangle. \tag{2.63}$$

This equation states that displacement correlations depend on time difference, not on time origin. By denoting $C_T(t_k) = \langle \delta\vec{r}_i(t_k) \cdot \delta\vec{r}_i(0) \rangle$, we obtain the expansion

$$D_T = \frac{1}{2d\tau_0} \left[C_T(0) + 2 \sum_{k=1}^{\infty} C_T(k\tau_0) \right]. \tag{2.64}$$

The application of this equation is called the *memory expansion*. S. C. Ying *et al.* [93] generalized this method to the case of collective diffusion, where

the memory expansion reads as

$$D_C = \frac{\xi N}{2d\tau_0}\left[C_C(0) + 2\sum_{k=1}^{\infty} C_C(k\tau_0)\right]. \tag{2.65}$$

In this equation, one considers correlation terms $C_C(t_k) = \langle \delta\vec{R}_{\rm cm}(t_k)\cdot\delta\vec{R}_{\rm cm}(0)\rangle$, where $\vec{R}_{\rm cm} = \frac{1}{N}\sum_{i=1}^{N}\vec{r}_i(t)$ is the center of mass of the diffusing material and $\delta\vec{R}_{\rm cm}(t_k) = \vec{R}_{\rm cm}(t_k) - \vec{R}_{\rm cm}(t_{k-1})$ is the change in the position of the center of mass between two consecutive observations at times t_k and t_{k-1}.

The advantage of the memory expansion method with respect to corresponding Green–Kubo relations is that memory expansions such as Eqs. (2.64) and (2.65) do not involve continuous functions. This is beneficial because the data to be analyzed is usually given as a set of consecutive observations, not as a continuous function.

2.4.6 Boltzmann–Matano analysis

One of the most common approaches for studying collective diffusion is to form a highly non-equilibrated concentration distribution, and then to let it broaden diffusively with time. To determine the collective diffusion coefficient $D_C(\theta)$ as a function of concentration θ, one usually applies the *Boltzmann–Matano* method, developed by C. Matano in 1933 [94]. The basis of this method is to start with a step-like initial concentration profile,

$$\theta(\vec{r}, t=0) = \begin{cases} 1 & \text{if } r_x < 0; \\ 0 & \text{otherwise,} \end{cases} \tag{2.66}$$

and then to let it evolve with time. With this initial condition, provided D_C is a function of θ only, the diffusion equation becomes one-dimensional:

$$\frac{\partial\theta}{\partial t} = \frac{\partial}{\partial r_x}\left(D_C(\theta)\frac{\partial\theta}{\partial r_x}\right). \tag{2.67}$$

L. Boltzmann showed that in this case, θ may be expressed in terms of a single variable $r_x/\sqrt{t}$, so that the diffusion equation may be reduced to an ordinary differential equation. Let us define a new variable

$$\eta = \frac{r_x}{\sqrt{t}}. \tag{2.68}$$

Thus we can write

$$\frac{\partial\theta}{\partial t} = \frac{d\theta}{d\eta}\frac{d\eta}{dt} = -\frac{r_x}{2\sqrt{t^3}}\frac{d\theta}{d\eta}, \tag{2.69}$$

$$\frac{\partial\theta}{\partial r_x} = \frac{d\theta}{d\eta}\frac{d\eta}{dr_x} = \frac{1}{\sqrt{t}}\frac{d\theta}{d\eta}, \tag{2.70}$$

and

$$\frac{\partial}{\partial r_x}\left(D_C\frac{\partial\theta}{\partial r_x}\right) = \frac{d}{d\eta}\left(D_C\frac{\partial\theta}{\partial r_x}\right)\frac{d\eta}{dr_x} = \frac{1}{\sqrt{t}}\frac{d}{d\eta}\left(D_C\frac{\partial\theta}{\partial r_x}\right). \tag{2.71}$$

Inserting Eqs. (2.69), (2.70), and (2.71) into Eq. (2.67) gives

$$-\frac{\eta}{2}\frac{d\theta}{d\eta} = \frac{d}{d\eta}\left(D_C(\theta)\frac{d\theta}{d\eta}\right). \tag{2.72}$$

This equation is an ordinary differential equation with respect to the variable η.

By integrating with respect to η, we obtain the following expression for $D_C(\theta)$:

$$D_C(\theta) = -\frac{1}{2}\left(\frac{d\eta}{d\theta'}\right)_\theta \int_0^\theta \eta d\theta'. \tag{2.73}$$

Applying this expression to analyze concentration profiles is called the *Boltzmann–Matano analysis*. It enables one to calculate the concentration dependence of the collective diffusion coefficient D_C over the whole concentration range even from a single concentration profile. This is a great advantage in experimental work. However, due to the fact that the law $r_x \propto \sqrt{t}$ [cf. Eq. (2.45)] holds true only for long times and distances, great care must be taken when the Boltzmann–Matano method is used.

2.4.7 Surface diffusion

Consider a gas–solid interface in the vicinity of a solid surface. The motion of an atom (or molecule) is characterized by four different dynamical processes. First, an atom in a gas may stick (*adsorb*) to the surface and find a thermodynamically stable site, where it may *vibrate* and interact with substrate excitations such as phonon modes and electron–hole pair excitations, until diffusion to another location on a surface takes place. After several such *diffusion* events have occurred, the atom may finally detach (*desorb*) from the surface. Atoms adsorbed on a surface are called adatoms (Fig. 2.8a).

When an atom adsorbs (chemisorbs) onto a surface, it tends to sit at the bottom of the potential well of the underlying solid. These minima correspond to potential *adsorption sites* for the adatom and are typically high-symmetry sites of the solid surface. Examples of possible adsorption sites include a bridge site between two surface atoms and a hollow site in

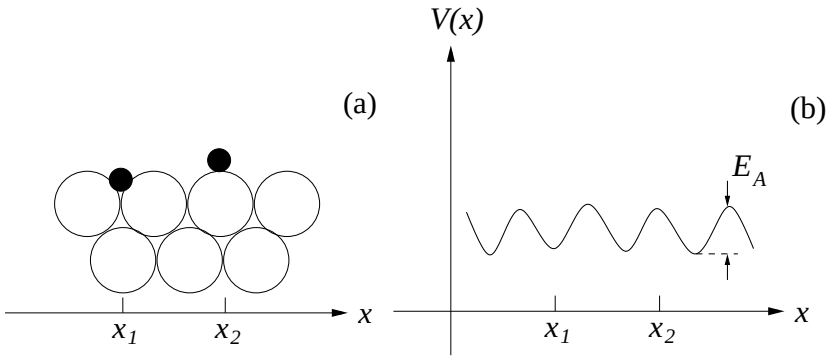

Figure 2.8: (a) A substrate (open circles) and two adatoms. (b) Potential energy curve for an adatom moving parallel to the surface.

the middle of three or four surface atoms. The possible adsorption sites vary from one adsorption system to another and their precise location is of no importance for the present discussion.

At low temperatures, adsorbed atoms will remain almost indefinitely on the surface. This is because the energy required to desorb an adatom is much greater than the thermal energy at that temperature. The energy barrier E_A (Fig. 2.8b) for surface diffusion is typically much lower, and thus the adatoms are able to diffuse on the surface even at relatively low temperatures.

When an atom is adsorbed on a surface, it vibrates in the adsorption well until it tries to jump to the neighboring adsorption site by crossing a saddle point of the surface potential. Under this condition, diffusion takes place by thermally activated jumps from one adsorption site to another. It is found that the diffusion coefficients obey (at least approximately) *Arrhenius laws*:

$$D_T(T) = D_{T,0} \exp(-E_A^T/k_BT) \tag{2.74}$$

and

$$D_C(T) = D_{C,0} \exp(-E_A^C/k_BT), \tag{2.75}$$

where E_A^T and E_A^C are the activation energies for tracer and collective diffusion, respectively. The effective activation energies are usually determined from so-called *Arrhenius plots* (i.e., $\ln D$ vs. $1/k_BT$) by the equations

$$E_A^T = -\frac{\partial \ln D_T}{\partial(1/k_BT)} \tag{2.76}$$

and

$$E_A^C = -\frac{\partial \ln D_C}{\partial(1/k_BT)}. \tag{2.77}$$

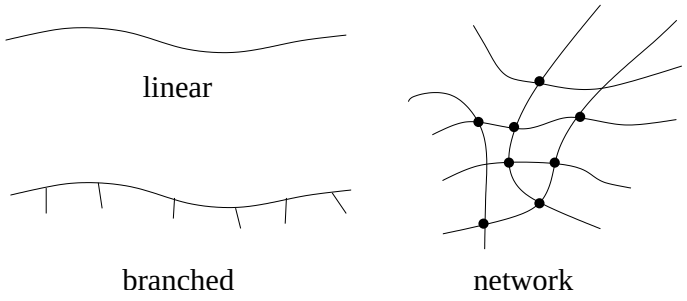

Figure 2.9: Several different polymer structures: linear, branched, and network.

In the case of tracer diffusion, it was shown by T. Ala-Nissila and S. C. Ying [20] that the Arrhenius form of Eq. (2.74) arises from a microscopic theory at low temperatures in the so-called high friction limit. In the many-particle case, similar proofs for Eq. (2.75) do not exist, and thus there is no theoretical reason why the Arrhenius analysis should still work. Still, mostly because of its simplicity, the Arrhenius analysis is frequently used to analyze and interpret experimental diffusion data.

2.5 Polymer physics

Polymers are long chainlike molecules composed of many repeating structural units called monomers (Fig. 1.2). A single polymer molecule may consist of hundreds to millions of monomers and may have a linear, branched, or network structure (Fig. 2.9). Covalent bonds hold the atoms in the polymer molecules together and secondary bonds then hold groups of polymer chains together to form the polymeric material.

Polymers include natural materials such as rubber and synthetic materials such as plastics and elastomers. Polymers are very useful materials because their structures can be altered and tailored to produce materials with a range of mechanical properties, in a wide spectrum of colors, and with different transparent properties. For a comprehensive approach to polymer physics, see the books by M. Doi [95], A. Y. Grosberg and A. R. Khokhlov [96, 97], or M. Doi and S. F. Edwards [61], for example.

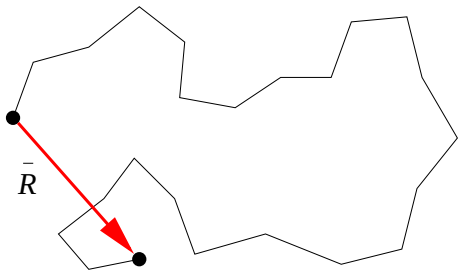

Figure 2.10: End-to-end vector.

2.5.1 Static properties of polymers

Freely jointed chain model

Polymer molecules can take up an enormous number of configurations by the rotation of chemical bonds. The shape of polymers is therefore usually described statistically. Let us begin with a very simple polymer model composed of a sequence of N rigid segments, each of length ℓ and able to point in any direction independently of each other. In this case, the configuration of the polymer will be the same as a random flight and so the calculation we are about to perform can also be applied to the statistical properties of random walks. Such a model is called the freely jointed chain.

To characterize the size of a polymer, we consider the end-to-end vector $\vec{R}$ of the chain (Fig. 2.10). We denote the radius vector of the beginning of the ith segment by $\vec{r}_i$ and that of its end by $\vec{r}_{i+1}$. Additionally, we introduce the bond vectors $\delta\vec{r}_i = \vec{r}_{i+1} - \vec{r}_i$. Therefore, the end-to-end vector $\vec{R}$ can be written as

$$\vec{R} = \sum_{i=1}^{N} \delta\vec{r}_i, \tag{2.78}$$

Clearly, the average value $\langle\vec{R}\rangle$ of $\vec{R}$ is zero, because the end-to-end vector has the equal probability to point in any direction. Therefore we will calculate $\langle\vec{R}^2\rangle$, the average of the square of $\vec{R}$, and express the size of the polymer by taking the square root of this quantity. From Eq. (2.78),

$$\langle\vec{R}^2\rangle = \left\langle \left(\sum_{i=1}^{N} \delta\vec{r}_i \right)^2 \right\rangle = \sum_{i=1}^{N}\sum_{j=1}^{N} \langle \delta\vec{r}_i \cdot \delta\vec{r}_j \rangle. \tag{2.79}$$

Because there is no correlation between the directions of different bond vectors, $\langle \delta\vec{r}_i \cdot \delta\vec{r}_j \rangle = \langle\delta\vec{r}_i\rangle\langle\delta\vec{r}_j\rangle = 0$ if $i \neq j$. In addition, $\langle(\delta\vec{r}_i)^2\rangle = \ell^2$, and thus

$$\langle\vec{R}^2\rangle = N\ell^2. \tag{2.80}$$

We see that the size of the polymer is proportional to $N^{1/2}$, while the total length measured along the contour of a polymer chain is proportional to N. This significant conclusion implies that in the set of conformations that a freely jointed chain takes, stretched or nearly straight conformations constitute a minor fraction; the majority of chain conformations are strongly coiled in space.

Distribution of the end-to-end vector

Let us calculate the probability distribution of $\vec{R}$. For the freely jointed chain, the vector $\vec{R}$ equals the sum of N independent, randomly oriented contributions $\delta\vec{r}_i$. According to the central limit theorem of probability theory, such a quantity has the Gaussian distribution:

$$P_N(\vec{R}) = \left(\frac{3}{2\pi N\ell^2}\right)^{3/2} \exp\left(-\frac{3\vec{R}^2}{2N\ell^2}\right), \tag{2.81}$$

when $N \gg 1$. The factor $(3/2\pi N\ell^2)^{3/2}$ is found from the normalization condition $\int d\vec{r} P_N(\vec{R}) = 1$. The Gaussian function in Eq. (2.81) decays at the distance of order $R \approx N^{1/2}\ell$, which agrees with Eq. (2.80) defining the size of the freely jointed chain. Indeed, an accurate calculation of the mean square using the general formula $\langle\vec{R}^2\rangle = \int d\vec{r}\,\vec{r}^2 P_N(\vec{R})$ would yield precisely the result of Eq. (2.80).

Short-range interactions

In the freely jointed chain model described earlier, we assumed that the orientation of each bond is random and completely independent of the orientation of the previous bonds. This means that the polymer is able to fold back on to itself at certain locations, which is physically impossible because two portions of the polymer cannot occupy the same region in space. In polymer physics two common modifications to the freely jointed approach are so-called *short-range* and *long-range* interactions. Short-range interactions involve chain units close to each other in terms of the path of the random flight. Long-range interactions involve interactions which are spatially close but which involve chain units separated by long distances along the chain path. Both short-range and long-range interactions involve chain units that are spatially close to each other.

For both modifications, $\langle\delta\vec{r}_i \cdot \delta\vec{r}_j\rangle$ does not vanish for $i \neq j$. However, if the interactions are short ranged, $\langle\delta\vec{r}_i \cdot \delta\vec{r}_j\rangle$ decreases rapidly as $|i-j|$ increases. Therefore there is no change in the fundamental result that $\langle\vec{R}^2\rangle$ is proportional to N for large N.

Radius of gyration

The end-to-end vector [Eq. (2.78)] is a useful quantity for describing the size of the polymer coil. Another measure for the size of the coil is the *radius of gyration* R_g, defined as

$$R_g^2 = \frac{1}{N}\sum_{i=1}^{N}\langle(\vec{r}_i - \vec{r}_{\rm cm})^2\rangle, \tag{2.82}$$

where

$$\vec{r}_{\rm cm} = \frac{1}{N}\sum_{i=1}^{N}\vec{r}_i \tag{2.83}$$

is the center of mass of the coil. The radius of gyration is closely related to the moment of inertia of the object. Substituting Eq. (2.83) into Eq. (2.82) gives

$$R_g^2 = \frac{1}{2N^2}\sum_{i=1}^{N}\sum_{j=1}^{N}\langle(\vec{r}_i - \vec{r}_j)^2\rangle. \tag{2.84}$$

Let us calculate the radius of gyration for an ideal chain, i.e., for a freely jointed chain model. When $|i-j|$ is large, $\vec{r}_i - \vec{r}_j$ of an ideal chain has a Gaussian distribution with variance $|i-j|\ell^2$, which means that

$$\langle(\vec{r}_i - \vec{r}_j)^2\rangle = |i-j|\ell^2. \tag{2.85}$$

Therefore

$$R_g^2 = \frac{1}{2N^2}\sum_{i=1}^{N}\sum_{j=1}^{N}|i-j|\ell^2. \tag{2.86}$$

For large N the summation can be replaced by an integration:

$$R_g^2 = \frac{\ell^2}{2N^2}\int_0^N dx\int_0^N dy|x-y| = \frac{1}{6}N\ell^2 \tag{2.87}$$

Therefore, for an ideal chain the ratio of R_g^2 to $\langle\vec{R}^2\rangle$ is 1/6.

There are several advantages to use the radius of gyration R_g rather than the end-to-end vector $\vec{R}$. First, because $\vec{R}$ describes mainly the behavior of the chain ends, it contains very little information about the distribution of the rest of the monomers. Second, polymers are often studied with scattering experiments, where R_g is a natural measure for polymer size. Third, for branched, ring, or star chains $\vec{R}$ has no meaning while R_g is still meaningful.

Long-range interactions

In the polymers considered earlier, the interaction between the polymer segments is limited to within a several neighbors in the chain. In reality, however, segments distant along the chain do interact if they come close to each other in space. An obvious interaction is the steric effect: because the segment has finite volume, other segments cannot come into its region. This interaction swells the polymer; the size of a chain with such an interaction is larger than that which does not have such an interaction. Even when there are attractive forces, as long as the repulsive force dominates, the polymer will swell. This effect is called the excluded volume effect.

The excluded volume effect was first discussed by W. Kuhn [98], and the modern development was initiated by P. J. Flory [99]. It had been recognized by these pioneers that the long-range interaction changes the statistical properties of the chain entirely. For example, in the case of a single polymer in a "good" solvent (discussed below in more detail) R_g is no longer proportional to $N^{1/2}$ but to a higher power of N

$$R_g \propto N^{\nu}. \tag{2.88}$$

The exponent ν is about 0.588 [61], so that the excluded volume effect is very important for long chains. One interesting point about ν is that it is essentially of universal nature: in good solvents in three dimensions polymers prefer open coil-like conformations characterized by $\nu = 0.588$. Thus, chemical details such as polymer sequence are not important. This result is by no means self-evident from a chemical perspective. Overall, the chain scaling follows Eq. (2.88), and the value of the exponent depends only on a few matters such as the dimension of the system and the quality of the solvent.

In the case of a chain in vacuum one may intuitively understand why $\nu > 1/2$. Consider building the chain by consecutively adding monomers. At every step there are on average more monomers in the back than in front of the last monomer. Therefore the chain can gain entropy by going out, and being larger than a chain in which the new monomer does not feel its predecessors.

Effect of solvent

The models of polymers discussed above do not explicitly take into account the influence of solvent, whereas it is well known that the size of a polymer will strongly depend on the type of liquid in which it is placed. If there is a high affinity with the solvent such that the polymer is easily dissolved, the

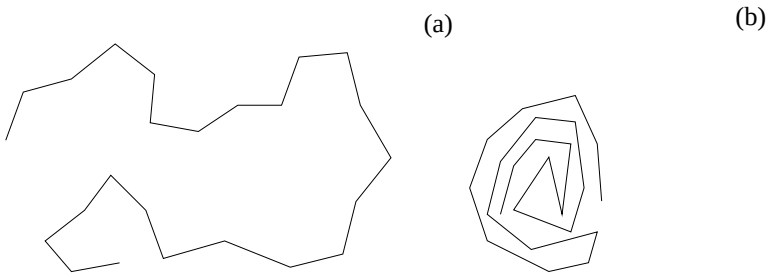

Figure 2.11: A polymer in a solvent. (a) In a good solvent, the polymer is spread out. (b) In a bad solvent, the polymer is shrunken and compact.

polymer configurations will be very spread out. In this case, the solvent is called a *good solvent*. On the other hand, in a solvent which does not dissolve the polymer, the polymer will be shrunken and compact. In this case, the solvent is called a *bad solvent*. To explain this dependence of the polymer size on the type of solvent we must consider the interaction between the polymer and solvent molecules.

W. Stockmayer predicted in 1959 that if the attraction between monomers becomes strong enough, the polymer undergoes a phase transition of the same sort as the transition from gas to liquid. Bits of the polymer "condense on to themselves" and instead of a free coil we end up with a dense "drop", a polymer *globule*. This is called the *coil–globule* transition (Fig. 2.11).

At a very narrow temperature range the coil will not display excluded volume at all. At this unique temperature the coil in dilute solution will be Gaussian. This temperature is called the *theta temperature* (or θ-temperature), which varies from one polymer–solvent pair to another. Sometimes the θ-temperature is called the Flory temperature.

Polymer solutions and melts

As the concentration in a polymer solution is increased, the polymers start to overlap and begin to interact with each other. The critical concentration at which this takes place is called the *overlap concentration*. Let us write c^* for the number of segments per unit volume at this concentration, so that the number of polymers per unit volume is c^*/N. Because the volume of one polymer is of the order R_g^3, we have

$$\frac{c^*}{N} R_g^3 \approx 1. \tag{2.89}$$

As was explained above, R_g is proportional to N^ν, so we have

$$c^* \propto N^{1-3\nu} \approx N^{-0.764} \tag{2.90}$$

for $\nu = 0.588$ [100]. The value of c^* is very small if N is large, because it is proportional to N raised to a negative power. Therefore, polymers with large molecular weight are almost always in the overlapping state, and are interacting with each other.

The limiting state of a polymer solution as a concentration is increased is known as the polymer melt, which is a liquid state composed only of polymers. This is an important state for industrial uses where polymeric liquids are processed into plastics, rubbers, and many other polymeric materials.

A fundamental question of the conformation theory of polymer solutions and melts is: "What is the conformation of a test (or labeled) chain in a dense polymer system?" At first glance, it seems impossible to assert any universal properties about the conformation of an individual polymer. In reality, however, this is not the case. There is a significant statement, first made by P. J. Flory in 1949 called the *Flory theorem*, which states that a test chain in a dense polymer system has the conformation of an ideal Gaussian coil.

The Flory theorem can be understood by the following observation: in a homogeneous polymer melt, every monomer is isotropically surrounded by other monomers, and there is no way to decide whether the surrounding monomers belong to the same chain as the monomer at hand or to a different one. Consequently there will be no preferred direction and therefore the polymer melt will have the ideal chain configuration. This is called screening of the excluded volume interactions.

2.5.2 Polymer dynamics

Until now, we have considered only the static properties of polymer systems. Polymer systems are also known to possess remarkable dynamic properties. For example, polymeric liquids (solutions and melts) are usually very viscous, they "keep memory" of their previous history, and often provide a qualitatively different response to weak and strong action. A fundamental property of polymeric liquids is viscoelasticity: when exposed to sufficiently rapidly changing actions, such liquids behave as elastic rubber-like materials, whereas under slowly varying forces, a flow typical for a viscous liquid sets in. The understanding of molecular motion in polymer solutions enables us to understand many non-equilibrium phenomena, such as diffusion, phase separation, and flow.

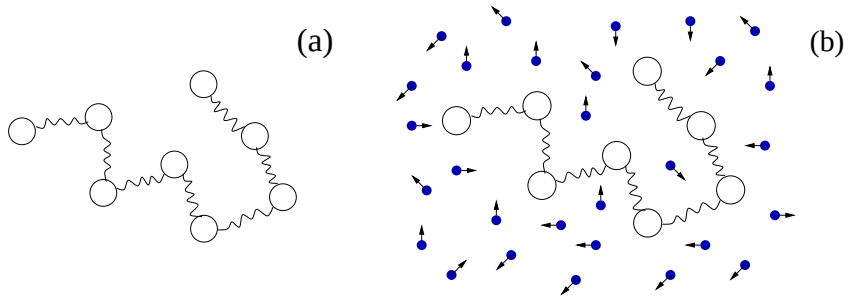

Figure 2.12: (a) Rouse model. (b) Zimm model.

Rouse model

We now need a model that we can use to calculate dynamical properties of polymer systems. Our starting point will not be an equation of motion at the molecular level, because the polymer is such a complex many-bodied system and is also much larger than the solvent molecules. Earlier, we introduced several polymer chain models, of which the standard Gaussian bead model proved to be the most convenient for a theoretical analysis of equilibrium properties. Therefore we adjust the Gaussian chain such that it serves our purposes.

Consider a standard Gaussian chain of N segments (Fig. 2.12a). Let us try to simplify the analysis of such a chain as much as possible. First, we neglect the volume interactions of the segments, i.e., we assume the chain is ideal. Second, we do not take into account the motion of the solvent, i.e., we assume the solvent to be an immobile viscous medium, in which the moving chain segments (beads) experience friction but which is not carried along with their motion. Third, the polymer chain we assume to be phantom, i.e., we neglect topological constraints on possible chain motions and allow chain sections to pass freely through each other.

In this model, each segment is subjected to the conservative forces f^{ch} from the neighboring segments in the chain, to the force f^{fr} of friction against the solvent, and to the random force f^{r}, which appears when the given segment collides with solvent molecules. Therefore, the equation of motion for the ith segment of the polymer chain can be written as

$$m\frac{\partial^2 \vec{r}_i}{\partial t^2} = \vec{f}_i^{\,\mathrm{ch}} + \vec{f}_i^{\,\mathrm{fr}} + \vec{f}_i^{\,\mathrm{r}}, \tag{2.91}$$

where $\vec{r}_i$ is the radius vector of the position of the ith segment, $\partial^2\vec{r}_i/\partial t^2$ is the acceleration of the ith segment, and m its mass. For the motion of the segment in dense solvent, the inertial term is quite insignificant, and the

equation of motion takes the form

$$\vec{f}_i^{\,\mathrm{ch}} + \vec{f}_i^{\,\mathrm{fr}} + \vec{f}_i^{\,\mathrm{r}} = 0. \tag{2.92}$$

The force $\vec{f}_i^{\,\mathrm{ch}}$ exerted on the ith segment by neighboring segments in the chain is

$$\vec{f}_i^{\,\mathrm{ch}} = k(\vec{r}_{i+1} + \vec{r}_{i-1} - 2\vec{r}_i). \tag{2.93}$$

for $i = 2, 3, \ldots, N-1$, and for $i = 0$ and $i = N$,

$$\vec{f}_0^{\,\mathrm{ch}} = k(\vec{r}_1 - \vec{r}_0) \tag{2.94}$$

$$\vec{f}_N^{\,\mathrm{ch}} = k(\vec{r}_{N-1} - \vec{r}_N), \tag{2.95}$$

respectively. If we define $\vec{r}_{-1}$ and $\vec{r}_{N+1}$ as

$$\vec{r}_{-1} = \vec{r}_0, \qquad \vec{r}_{N+1} = \vec{r}_N, \tag{2.96}$$

then Eqs. (2.94) and (2.95) can be included in Eq. (2.93). Here k is the spring constant of the ideal chain.

The friction force $\vec{f}_i^{\,\mathrm{fr}}$ is naturally assumed to be proportional to the velocity,

$$\vec{f}_i^{\,\mathrm{fr}} = -\zeta \frac{\partial \vec{r}_i}{\partial t}, \tag{2.97}$$

where ζ is the friction coefficient of a bead. Inserting Eqs. (2.93) and (2.97) into Eq. (2.92) gives

$$\zeta \frac{\partial \vec{r}_i}{\partial t} = k(\vec{r}_{i+1} + \vec{r}_{i-1} - 2\vec{r}_i) + \vec{f}_i^{\,\mathrm{r}}. \tag{2.98}$$

The model defined in this way is the *Rouse model*.

In order to proceed with our calculations, we assume that the beads are continuously distributed along the polymer chain. Let x be a continuous variable and write $\vec{r}_i(t)$ as $\vec{r}(x,t)$. Then Eq. (2.98) takes the form

$$\zeta \frac{\partial \vec{r}}{\partial t} = k \frac{\partial^2 \vec{r}}{\partial x^2} + \vec{g}(x,t). \tag{2.99}$$

Further, the conditions of Eq. (2.96) become the following boundary conditions at $x = 0$ and $x = N$:

$$\left(\frac{\partial \vec{r}}{\partial x}\right)_{x=0} = 0, \qquad \left(\frac{\partial \vec{r}}{\partial x}\right)_{x=N} = 0. \tag{2.100}$$

Equation (2.99) has the form of a linear harmonic oscillator, and so if we introduce normalized coordinates we can decompose the motion into independent modes. These modes are called the *Rouse modes*, and they can be

used to calculate various quantities, such as the diffusion coefficient of the center of mass of the polymer D_T or the maximum relaxation time τ. The results are

$$D_T = \frac{k_B T}{N\zeta} \tag{2.101}$$

$$\tau = \frac{\zeta N^2 \ell^2}{3\pi^2 k_B T}. \tag{2.102}$$

The Rouse theory may seem to be a very natural way to describe the Brownian motion of a polymer chain, but unfortunately its conclusions do not agree with experiments. As can be seen from Eqs. (2.101) and (2.102), in the Rouse model the diffusion coefficient of the center of mass and the maximum (or rotational) relaxation time depend on the polymer length N as $D_T \propto N^{-1}$ and $\tau \propto N^2$, respectively. However, the following dependencies have been measured experimentally [61, 95, 97]:

$$D_T \propto N^{-1/2}, \qquad \tau \propto N^{3/2}, \tag{2.103}$$

in the θ-state.

The reason for this discrepancy between experiments and the Rouse model is that in the Rouse model we assume the average velocity of a particular bead to be determined only by the external force acting on it, and independent of the motion of the other beads. However, in reality the motion of one bead is influenced by the motion of the surrounding beads through the solvent. For example, if one bead moves, the solvent surrounding it will also move, and as a result other beads will be dragged along. This type of interaction transmitted by the motion of the solvent is of hydrodynamic origin.

When applied to polymer melts, however, the Rouse model is much more appropriate, because in polymer melts friction may be thought of as being caused by the motion of a chain relative to the rest of the material, which to a first approximation may be taken to be at rest; propagation of a velocity field like in a normal liquid is highly improbable, meaning that there is no hydrodynamic interaction. For this reason, the Rouse model is a very useful model to describe polymer melts.

Zimm model

B. H. Zimm modified the bead–spring model of a polymer to include hydrodynamic interaction effects (Fig. 2.12b). In this case, the equation of motion of the bead–spring polymer of Eq. (2.98) becomes

$$\frac{d\vec{r}_i}{dt} = \sum_j \vec{H}_{ij} \cdot [k(\vec{r}_{j+1} + \vec{r}_{j-1} - 2\vec{r}_j) + \vec{f}_i^{\,\mathrm{r}}]. \tag{2.104}$$

Because $\vec{H}_{ij}$ depends on $\vec{r}_i$, Eq. (2.104) is a non-linear in $\vec{r}_i(t)$, and is almost impossible to solve. Zimm's idea was to replace $\vec{H}_{ij}$ (the factor causing the non-linearity) by its equilibrium value $\langle \vec{H}_{ij} \rangle_{\text{eq}}$. This is called the preaveraging approximation. At first this may appear to be a very rough approach, but the preaveraging approximation turns out to be quite good because of the long-range nature of the hydrodynamic interactions. For example, if we calculate the diffusion coefficient using this approximation, the result is within 10 % of the value calculated rigorously.

The results for the diffusion coefficient of the center of mass and the maximum relaxation time are

$$D_T = 0.196 \frac{k_B T}{\eta_s \sqrt{N} \ell} \tag{2.105}$$

$$\tau = 0.325 \frac{\eta_s (\sqrt{N} \ell)^3}{k_B T}, \tag{2.106}$$

where η_s is the viscosity of the solvent. It is clearly seen that D_T and τ depend on the polymer length N as:

$$D_T \propto N^{-1/2}, \qquad \tau \propto N^{3/2}. \tag{2.107}$$

The dependence of these quantities on the polymer length agrees with experiments performed on solutions in the θ-state.

Reptation model

Having considered the basic concepts associated with the dynamic properties of both an individual polymer chain and dilute solutions of chains, we move on to the dynamics of concentrated polymer solutions and polymer melts in which individual polymer coils are strongly overlapped with each other. As mentioned earlier, the concentration of the polymer solution in this case exceeds the overlap concentration c^* of polymer coils.

If the concentration in a polymer solution is well above c^*, the polymer molecules will begin to entangle. In this state, excluded volume interactions, hydrodynamic interactions, and entanglement interactions all strongly affect the molecular motion and the calculations become extremely complicated. A rigorous treatment of the entanglement interactions is particularly difficult, and an analysis from first principles is almost impossible. For these reasons, present theories of the dynamics of concentrated polymer systems are based on very rough models, which manage to capture some features of the motion very well, but cannot describe all aspects of the dynamics.

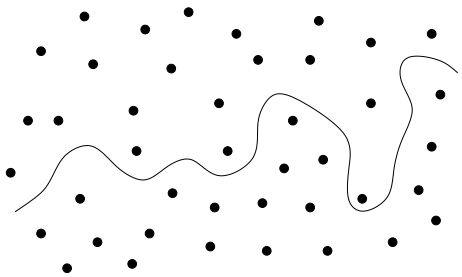

Figure 2.13: A polymer chain in a concentrated system of other chains. The chain under consideration is placed on a plane and the other polymers intersecting the plane are shown by dots.

As a rule, when exceeding the concentration c^*, the dynamic properties of the polymer solution begin to change: the viscosity grows quickly, the diffusion coefficients of polymers decrease, and the effects of memory of previous flow become clearly pronounced. It is easy to realize that these effects are connected with the uncrossability of chains, because in the system of entangled coils, the exclusion of chain crossings dramatically reduces the set of possible motions of polymers. Consequently, the uncrossability of chains is quite significant in most dynamic phenomena taking place in systems of entangled polymer coils. In particular, it defines such important characteristics of a polymer solution as the viscosity η, self-diffusion coefficient of a single chain D_T, the spectrum of relaxation times, and so on.

At the same time, there are some dynamic properties that can be described without taking into account the uncrossability of polymer chains. Concentration fluctuations in a solution of entangled coils belong to this category. These effects result from the simultaneous motion of many polymer chains, and proceed on relatively short times and distances. The uncrossability of chains shows most clearly when the motion of one chain is considered over sufficiently long time intervals, and therefore the entanglement effects are quite insignificant for the fluctuation dynamics in polymer solutions.

However, when we consider the self-diffusion of the polymers, the entanglement effects become very important. If we fix our attention on a single polymer in a concentrated solution, we see that it diffuses through a network made by the surrounding polymers (Fig. 2.13). Therefore the self-diffusion coefficient of a polymer becomes very small due to entanglement effects.

The calculation of the self-diffusion coefficient in concentrated solutions met with very little success for a long time due to the difficulty of treating the entanglement effects theoretically. The application of the tube concept introduced by S. F. Edwards provided the key for solving this problem. P.-

G. de Gennes thought of the problem in the following way. Assume that a polymer molecule is undergoing Brownian motion in a fixed network formed by surrounding polymers.

The fundamental point is that because the chains cannot cross each other, the movement of a chain in a dense polymer system is highly constrained. Due to entanglements with other chains, lateral motions of the chain at many points are highly improbable. Qualitatively we may imagine that the chain is confined in a tube in which it may move with some freedom. In order to move over large distances the chain has to leave the tube by means of longitudinal motions. The concept of a tube clearly has only a statistical meaning. The tube can change by two mechanisms. First, by means of the motion of the central chain itself, by which the chain leaves parts of its original tube, and generates new parts. Second, the tube fluctuates because of the motions of the chains which built up the tube.

The second cause of tube fluctuations, called *tube renewal*, is insignificant in most cases, because it leads to relaxation times much greater than the motions of the chain along the tube [101]. This is why the mechanism based on the concept that the chain moves in a tube, is the basic mechanism of motion for polymers in a concentrated solution or melt.

Polymer motion taking place along a tube is called *reptation*. The corresponding model of the dynamics of polymer solutions and melts is frequently referred to as the *reptation model*. This model was proposed by P.-G. de Gennes in 1971 and developed further in studies of M. Doi and S. F. Edwards.

Let us now look at the mechanism which allows the chain to move along the tube axis, which is also called the primitive path. The primitive path is the main concept in the reptation model. The details of the polymer itself are to a high extent irrelevant. We may therefore choose a polymer model as we wish. Therefore we will use the Rouse-type model to describe the motion of the polymer, and so the self-diffusion coefficient of the polymer should be expressible in terms of the parameters characterizing the Rouse model, which are the number of segments N, the segment length ℓ, and the friction constant of the segment ζ.

Let us discuss in more detail the tube concept in the reptation model. The effective tube is only a model conception. The tube "walls" are by no means formed by direct contacts with other chains. In fact, the effective tube is formed not by all contacts with other chains, but rather by only a small fraction of them, only those that correspond to *entanglements*. To allow for this circumstance, the additional parameter N_e is introduced, which equals the average number of segments in the chain between two consecutive entanglements of the given polymer with other chains.

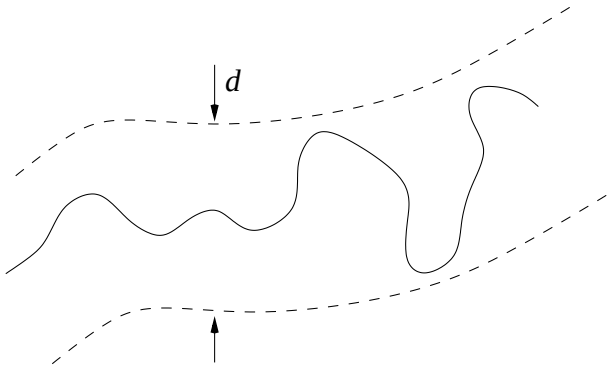

Figure 2.14: Tube model.

A consistent calculation of the parameter N_e is extremely complicated. Therefore in the modern theory of polymer liquids, the parameter N_e appears as a phenomenological one. The parameter N_e characterizes the ability of a polymer chain to become entangled with the other chains and depends, e.g., on chain stiffness, the presence of short side branches, and so on. Because the dynamic characteristics of the melt depend on N_e, the value of this parameter can be found experimentally. Typical values on N_e fall within the interval of 50 to 500.

As the statistics of the polymer chain in the melt is Gaussian on all scales, the statistics of the primitive path is also Gaussian. As long as there exists an average number N_e of segments between two successive entanglements of a given chain, the characteristic scale $d = \ell N_e^{1/2}$ also exists, related to the spatial distance between these entanglements. It can easily be seen that this characteristic scale corresponds to the effective tube diameter, because the tube is formed just by the entanglements (Fig. 2.14).

The total contour length of the primitive path equals

$$L = dN/N_e = \ell N/N_e^{1/2}, \tag{2.108}$$

because the polymer chain in the melt can be considered as a sequence of N/N_e subchains, each of which consists of N_e segments and covers a section of length d along the primitive path.

We now discuss in more detail the reptation mechanism of the motion of a polymer. First, we estimate the friction coefficient for the polymer diffusing along the tube. It can be shown that the hydrodynamic interaction of segments is screened in a concentrated system of polymers, with the screening radius being of the order of the correlation radius ξ. In the melt, the hydrodynamic interaction is totally screened, and the friction forces of each

segment are summed so that the resulting coefficient ζ' of friction of the chain diffusing along the tube is $\zeta' = N\zeta$.

Hence, the self-diffusion coefficient D'_T for reptation along the tube can be calculated using the Einstein relation

$$D'_T = \frac{k_B T}{\zeta'} = \frac{k_B T}{N\zeta}. \tag{2.109}$$

In the process of reptational diffusion along the tube axis, the chain leaves sections of the initial tube and creates new sections. The new sections of the tube are created by the motion of the ends of the polymer chains. Because the motion of the ends leaving the tube is random and uncorrelated with the initial tube conformation, it is natural to expect that the memory of the initial conformation would be lost completely when the chain entirely leaves the initial tube. The average time τ taken by the chain to diffuse out of the initial tube is easy to evaluate on the basis of Eqs. (2.45), (2.108) and (2.109). The result is

$$\tau = \frac{L^2}{6D'_T} = \frac{\ell^2 \zeta}{6N_e k_B T} N^3. \tag{2.110}$$

Because the memory of the initial conformation of each chain and, consequently, of the whole polymer system is erased after the time interval τ, this quantity can be identified as the maximum relaxation time of the polymer solution or melt. The validity of such an identification can be proved by specific calculations of correlation functions [97].

We now determine the self-diffusion coefficient D_T in the polymer melt. To evaluate D_T, note that during the time τ taken by the chain to diffuse entirely out of the initial tube, it is natural to expect that the center of mass of the chain shifts over a distance of the order of the size R of the polymer. On the other hand, displacements of the chain during different time intervals of duration τ are statistically independent. Therefore, for long time intervals, diffusive motion of the center of mass of the chain sets in. According to Eqs. (2.45), (2.80), (2.110), we obtain

$$D_T = \frac{R^2}{6\tau} = \frac{k_B T N_e}{\zeta N^2}. \tag{2.111}$$

The value of D_T decreases with polymer length as N^{-2}. A more rigorous calculation of the diffusion coefficient D_T can be found in Ref. [97].

Near the entanglement molecular weight N_e, there is an abrupt change in the power-law behavior of D_T and τ. The mechanical properties of polymers

differ above and below this molecular weight. For example, strong thermoplastics, such as nylon or polyethylene, become waxy below this molecular weight [102]. Glassy polymers, in turn, become powdery below N_e.

The reptation model predicts that the self-diffusion coefficient scales as $D_T \propto N^{-2}$, which agrees well with experiments. This is not the case, however, for the corresponding dependence $\tau \propto N^3$ for the maximum relaxation time. Usually, the exponent of the experimentally observed dependence is slightly higher: $\tau \propto N^{3.4}$. There are several explanations for this discrepancy. The generally accepted one [95, 103] is associated with fluctuations of the contour length L of the primitive path. The presence of fluctuations reduces the lifetime of the initial tube, i.e., the maximum relaxation time τ. The rigorous calculation carried out by M. Doi in 1981 showed that

$$\tau \propto N^3 \left(1 - \frac{c}{N^{1/2}}\right), \tag{2.112}$$

where c is a positive constant. According to this equation, the apparent scaling exponent is higher than 3 when N is finite. The true asymptotic behavior $\tau \propto N^3$ still holds as $N \to \infty$.

Chapter 3

Methods and models

This chapter presents the simulation methods and model systems used in this thesis.

3.1 Overview

There are essentially two alternatives to performing numerical simulations: stochastic and deterministic. In the field of atomistic and molecular studies, the most popular stochastic approach is the Monte Carlo method [7, 104–106] and the most popular deterministic approach is the molecular dynamics method [7, 104, 105]. The stochastic and deterministic approaches do not exclude each other, but there are hybrid methods [107–109], which combine these two approaches. An example of such a method is the shadow hybrid Monte Carlo [109] used in simulations of large molecules. The hybrid methods is a fast growing area these days. Stochastic and deterministic approaches are also combined in many approaches, such as in Langevin and dissipative particle dynamics, where slow motions are done deterministically and faster motions are taken care by stochastic fluctuations.

The term *Monte Carlo* (MC) [7,104–106] covers a wide range of stochastic methods the common denominator being the repeated use of random numbers. The name Monte Carlo refers to the Monte Carlo casino in Monaco, reflecting the similarities between statistical simulation and gambling. The MC methods provide approximate solutions to a variety of mathematical problems by performing statistical sampling experiments on a computer. A simplistic example of the Monte Carlo method is the estimation of π by direct sampling (Fig. 3.1). In Fig. 3.1, we generate N random points inside a square of side 1, and count how many of them (M) happen to lie in a circle of diameter 1. The π is approximately given by $\pi \approx 4M/N$. In the

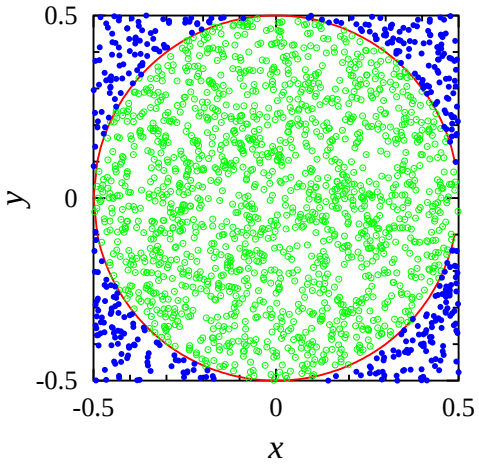

Figure 3.1: Estimating π with the Monte Carlo method. The ratio of the number of points falling inside the circle to the total number of points is $\pi/4$.

field of atomistic and molecular simulations, the MC methods are used to generate system configurations from some probability distribution, usually from a canonical or grand canonical ensemble. In a canonical ensemble, the expectation value of a variable A is given by

$$\begin{aligned} \langle A \rangle &= \frac{1}{Z} \int dr dp A(r) \exp\{-\mathcal{H}(r,p)/k_B T\} && (3.1) \\ &= \frac{1}{Z} \int dr dp A(r) \exp\left\{-\frac{1}{k_B T}\left[\sum_i \frac{p_i^2}{2m_i} + V(r)\right]\right\} && (3.2) \\ &= \frac{1}{Z_r} \int dr A(r) \exp\{-V(r)/k_B T\}, && (3.3) \end{aligned}$$

where $\mathcal{H}$ is the Hamiltonian of the system, V is the conservative potential, k_B is Boltzmann's constant, T is the equilibrium temperature, and Z is the canonical partition function. The function Z_r is the configurational part of the total canonical partition function Z. In general, the integral in Eq. (3.3) cannot be evaluated analytically because $V(r)$ includes all the degrees of freedom and the integral is high-dimensional. On the other hand, common numerical quadrature techniques such as the trapezoidal rule become inefficient when the dimensionality of the integral is large.

The MC method provides a way to solve the above problem. By generating M random configurations r_k, $k = 1, 2, \ldots, M$, from distribution $(1/Z_r)\exp\{-V(r)/k_B T\}$, one can approximate $\langle A \rangle$ by

$$\langle A \rangle \approx \frac{1}{M} \sum_{k=1}^{M} A(r_k). \qquad (3.4)$$

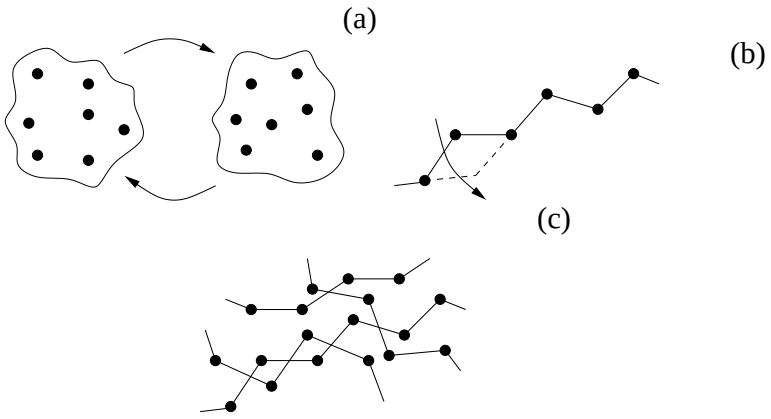

Figure 3.2: (a) Moves between states. (b) A possible MC move in a polymeric system. (c) Moves in dense system become difficult due to the lack of space, which can make MC inefficient.

The most important feature of Monte Carlo integration is that the time requirement to evaluate integrals typically scales as $\mathcal{O}(d)$, whereas numerical quadratures scale worse than $\mathcal{O}[\exp(d)]$ [7, 104, 105]. Here d is the dimension of the integral or, in the case of the integral given in Eq. (3.3), the number of particles in the system. The MC method is not restricted to any particular length or time scale, but it can be successfully used to study various numerical optimization problems, such as the traveling salesman problem [110, 111]. In most MC realizations, random numbers determine the sequence of states through which the system evolves. Due to the stochastic nature of the technique, the MC method does not necessarily offer a true time evolution of the system. The important part in the algorithm are the moves from one state to another. These transitions can be difficult in dense systems, and also in the case of polymers (Fig. 3.2). One appealing feature of the MC method is that it allows sampling from a grand canonical ensemble thus allowing the number of particles to vary. This is important, e.g., in surface growth simulations.

When reformulated properly, the MC method can be used to study dynamic phenomena. In *kinetic Monte Carlo*, the sequence of configurations is created through moves that correspond to real physical events taking place in a system (Fig. 3.3). The simulation model is constructed by identifying all the possible processes which may occur in the system at any stage of the simulation. After this, the moves from one state to another can be constructed. Due to the stochastic nature of the technique, the kinetic MC is subject to the same problem as the regular MC realizations: The MC methods do not necessarily offer true time evolution of the system. However, the kinetic MC correctly describes the dynamics at the limit that all processes are activation

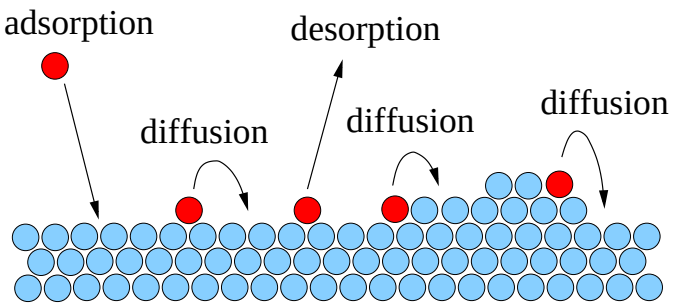

Figure 3.3: Surface growth.

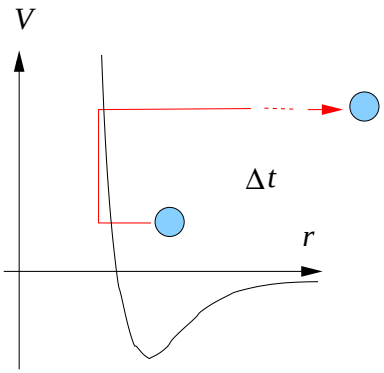

Figure 3.4: Molecular dynamics simulation crashes if it is run with a too large time step Δt.

limited.

In *molecular dynamics* (MD) [7,104,105], the evolution of an atomistic or molecular system is governed by Newton's equations of motion. Equations of motion are integrated in small steps in time Δt. During this time the atoms should not move too much relative to each other—only a small fraction of the atom diameter. The maximum distance an atom moves during Δt has to be restricted to $r \sim 1$ pm. The velocities of atoms, or small molecules, at 300 K are typically $v \sim 100$ m/s. Therefore the time step of integration should not be larger than $\Delta t \sim r/v \sim 10$ fs (Fig. 3.4). If the integration is accurate and the system is purely classical, the MD method offers a true time evolution of the system. The correct dynamics can be very important in some cases. For example, if there are collective motions, e.g., waves or vortices [104], in the system, the time evolution of the system cannot be studied with stochastic methods. In such a case, the MD approach is the method of choice.

The *Langevin dynamics* technique [105] resembles the classical MD technique in many ways. It is based on Newton's equations of motion, but with

the difference that there are two additional forces: random and dissipative. As a consequence, Newton's second law becomes a Langevin equation, which is a stochastic differential equation. The origin of the random and dissipative forces is in coarse-graining (we will discuss this in detail in Sec. 3.4.1). In the usual Langevin description, a system is described in terms of "slow" colloidal particles immersed in a solvent consisting of "fast" fluid particles. Typically, the time scale concerning slow degrees of freedom is of the order of nanoseconds while for the fast degrees of freedom it is few femtoseconds. Due to the large difference in time scales it is possible to coarse-grain, or average over, the fast variables and represent them using their statistical properties. As a result of the coarse-graining, only slow degrees of freedom are kept, fast degrees of freedom being replaced with random noise and dissipation. The random and dissipative forces are coupled through a fluctuation-dissipation relation [88], for which reason the sequence of states generated by Langevin dynamics forms a canonical ensemble. Therefore, Langevin dynamics can be used as a thermostat for any MD simulation—regardless of the level of coarse-graining.

Dissipative particle dynamics (DPD) [7, 8] is a relatively new method based on coarse-graining of microscopic forces. The DPD method was initially developed as a tool for simulating hydrodynamic behavior of colloidal suspensions [112,113]. The equations of motion are otherwise similar to those of the Langevin dynamics, but with the difference that the random and dissipative forces are treated pairwise in the DPD method. For this reason, the DPD method conserves both linear and angular momenta, which is necessary for the emergence of hydrodynamic behavior in macroscopic times and distances.

The usual DPD description differs from that of the Langevin dynamics. In the DPD method, the "particles" do not represent a single atom, molecule, or colloid, but a collection of molecules or molecular groups that move together (Fig. 3.5). The solvent particles, if any, are considered in a similar manner. In the coarse-graining process, the internal degrees of freedom of the particles are coarse-grained out such that the motion of the center of mass only is considered. The particles interact through soft forces, which arise directly from the coarse-graining process. As in the Langevin dynamics technique, the random and dissipative forces in the DPD method are coupled through a fluctuation-dissipation relation. The DPD method can be used as a momentum conserving thermostat for any MD simulation [114, 115].

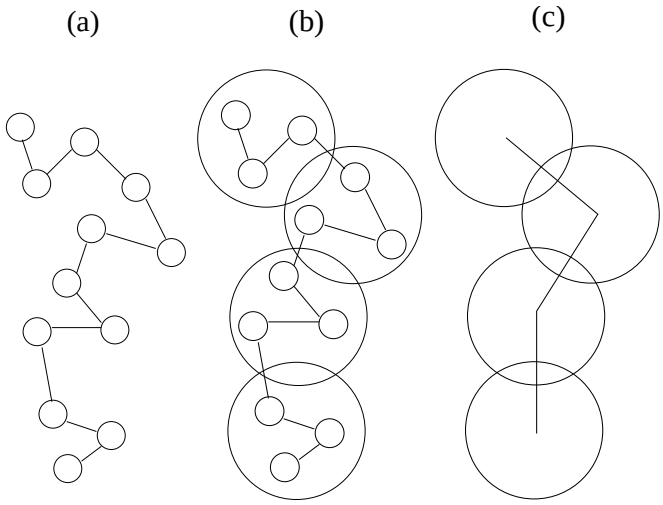

Figure 3.5: Coarse-graining process.

3.2 Monte Carlo (MC)

In this section, we first consider the Monte Carlo (MC) method in detail and discuss some of its popular realizations. After this we present the lattice-gas model of O/W(110), which is used in all of our MC simulation studies (Papers [1–3]). For a comprehensive approach to the MC method see the books by D. Frenkel and B. Smit [7], M. P. Allen and D. J. Tildesley [104], J. M. Thijssen [105], or D. P. Landau and K. Binder [106], for example.

3.2.1 The MC method

In Monte Carlo simulations, random numbers are used to generate physical states with a desired probability distribution. In a canonical ensemble, the probability distribution is given by

$$\pi_i = \frac{1}{Z} e^{-E_i/k_B T}, \tag{3.5}$$

where Z is the normalizing partition function, E_i is the energy of the microstate i, k_B is Boltzmann's constant, and T is temperature. Other commonly used distributions are the microcanonical and the grand canonical distribution. See Sec. 2.1.2 for a detailed discussion of distribution functions.

The approach which first comes to mind for generating configurations with the canonical distribution given in Eq. (3.5) is simply to generate configurations randomly and then accept them with probability $\exp(-E_i/k_B T)$

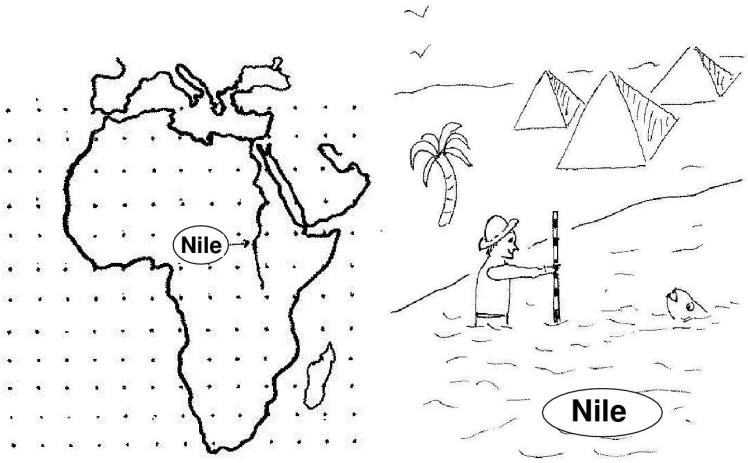

Figure 3.6: Measuring the depth of the river Nile: a comparison of a conventional quadrature (left), with the Metropolis scheme (right). Figure taken from the book by D. Frenkel and B. Smit [7].

where the energy scale should be such that the energy is always positive. However, as the number of configurations with a particular energy increases rapidly with energy, most of the randomly constructed states have a very high energy. Hence, for any finite temperature, states will be accepted with a vanishingly small probability and we spend most of our time generating configurations which are then rejected, which is obviously inefficient.

N. Metropolis *et al.* [116] developed an algorithm that is much more efficient than the approach described above. In this algorithm, the configurations are not constructed statistically independently but through the so-called Markov chain (Appendix A). Each new configuration is still generated with a probability distribution proportional to $\exp(-E_i/k_BT)$, but the new configuration is constructed by making small changes to the present configuration. This approach is called the *Metropolis importance sampling* (Appendix A).

Let us try to clarify the Metropolis importance sampling with a simple example (Fig. 3.6) given by D. Frenkel and B. Smit [7]. In Fig. 3.6, we compare two methods to measure the depth of the river Nile, by conventional quadrature (left) and by Metropolis sampling (right). In the conventional quadrature scheme, the value of the integrand is measured at a predetermined set of points. As the choice of these points does not depend on the value of the integrand, many points may be located in regions where the integrand vanishes.

In contrast, in the Metropolis scheme, a random walk is constructed through that region of space where the integrand is non-negligible (i.e., through the Nile itself). In this random walk, a trial move is rejected if it takes you out of the water, and is accepted otherwise. After every trial move (accepted or not), the depth of the water is measured. The (unweighted) average of all these measurements yields an estimate of the average depth of the Nile.

The above can be summarized in a more algorithmic form. To be precise, the Metropolis simulation algorithm in the canonical ensemble consists of the following steps:

1. Specify an initial configuration i for a system.
2. Generate a new configuration j at random.
3. Compute energy difference $\Delta E = E_j - E_i$.
4. Generate a uniform random number $r \in [0, 1]$.
5. If $r < \min(1, \exp(-\Delta E/k_B T))$, accept the change. Otherwise keep the old configuration.
6. Compute the desired quantities and return to step 2.

In the above algorithm, each new configuration is generated by using some updating scheme. One step in such a scheme is called the Monte Carlo move. In the studies of lattice-gas systems, one typically uses the *Kawasaki dynamics* [106], which proceeds as follows. One particle is selected randomly while the other particles are kept fixed. The new position of the particle is then chosen randomly from its nearest neighbor lattice sites. If the nearest site chosen is full, no jump occurs. If it is empty, a jump occurs with the probability $\min(1, \exp(-\Delta E/k_B T))$. Time is measured in Monte Carlo steps (MCS) per particle, during which every particle attempts to jump once on the average. MCS is not physical time and does not describe dynamics in any way and samples an equilibrium distribution. In constructing the updating scheme, it is important that the transition rate from state i to state j satisfies the detailed balance condition (Appendix A).

The Metropolis Monte Carlo is not the only possible way to do things but there are also more sophisticated approaches available. In *parallel tempering* [7], several independent replicas of a system are simulated simultaneously. Each replica, or a simulation box, is in a different thermodynamic state—usually in different temperature, pressure, or chemical potential—or has a different Hamiltonian [117]. The systems are allowed to interchange configurations from time to time, subject to specific acceptance criteria. These

so-called *swap* moves can improve sampling of configuration space considerably, particularly in systems having free-energy landscapes with many local minima. It should be stressed that the swap moves do not disturb the distribution corresponding to a particular ensemble. One can therefore determine ensemble averages from every individual ensemble, just as we do in a Metropolis Monte Carlo simulation.

Multicanonical simulations [7, 106] use an entirely different strategy to overcome barriers between local free-energy minima. The acceptance criteria for the transition between two states are manipulated in such a way that barriers are artificially made lower. In multicanonical simulations, the conventional Boltzmann weight is replaced by a different, non-Boltzmann weight $\pi(r)$. The expression for $\langle A \rangle$ becomes

$$\langle A \rangle = \frac{1}{Z_r} \int dr A(r) \pi(r) \frac{\exp[-V(r)/k_B T]}{\pi(r)} \tag{3.6}$$

$$= \left\langle A(r) \frac{\exp[-V(r)/k_B T]}{\pi(r)} \right\rangle_\pi , \tag{3.7}$$

where the notation $\langle \cdots \rangle_\pi$ denotes an average over a probability distribution proportional to $\pi(r)$. To ensure that all regions of configuration space are sampled with comparable frequency, functions $\pi(r)$ and $\exp[-V(r)/k_B T]$ should have significant overlap. The multicanonical simulation is also called the *umbrella sampling*, because the distributions $\pi(r)$ and $\exp[-V(r)/k_B T]$ cover each other at the edges. The multicanonical simulations are very useful in free energy calculations.

In complex fluids consisting of chain-like molecules, the conventional Monte Carlo techniques for grand canonical or Gibbs ensemble simulations often fail. The reason is that if a molecule is inserted into the system at random, it will almost certainly overlap with some other molecule or molecules. In the *configurational bias Monte Carlo* (CBMC) technique [7, 106] the sampling efficiency is significantly improved by using "unphysical" MC trial moves which are biased to avoid energetically unfavorable polymer configurations. Biasing an MC trial move means that we are no longer working with a symmetric trial probability matrix a_{ij}. To satisfy detailed balance, the acceptance rules are also changed. In the CBMC technique, a new chain conformation is grown atom by atom. Alternative positions are generated for each atom, and one is chosen with a bias toward avoiding high energy interactions. This bias is removed by the specially constructed acceptance rule after the entire molecule has been grown.

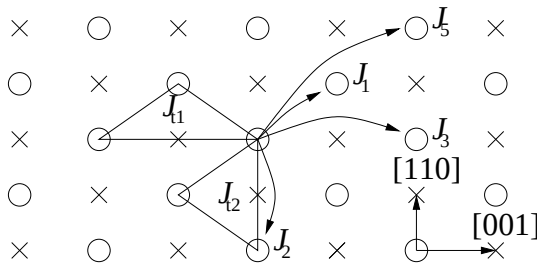

Figure 3.7: Relevant pair and three-body interactions in the O/W(110) system. Substrate atoms are denoted by crosses and possible adsorption sites by open circles.

3.2.2 Lattice-gas model of O/W(110)

In the first part of this thesis (Papers [1–3]), we study the diffusion of atoms on solid surfaces using the Monte Carlo method. The system under study is O/W(110), i.e., oxygen on the tungsten (110) surface (Fig. 3.7). In this system, the W(110) surface provides an array of sites at which it is most probable to find the oxygen atoms localized. Therefore, it is convenient to model the system by a two-dimensional lattice-gas which assumes that the adsorbate atoms can only be found at these sites. The statistical variables in this model are the site occupation numbers n_i which take the value zero or one according to whether the site is empty or filled. Multiple occupation of any site is forbidden.

The lattice-gas model

The O/W(110) system is undoubtedly one of the most studied adsorption systems. Its phase diagram has been determined through experimental studies [24, 118–120] using low energy electron diffraction (LEED) spot profile analysis [121], and scanning tunneling microscopy (STM) [122]. Its main features can be summarized as follows. At temperatures $T > 710$ K, the system is in a disordered phase, while at lower temperatures there is a wide variety of ordered phases at different coverages (surface densities), namely the $p(2 \times 1)$, $p(2 \times 2)$ and $p(1 \times 1)$ phases corresponding to ideal coverages of 1/2, 3/4, and 1, respectively. At intermediate coverages, some coexistence regions also exist. The substrate remains unchanged at all coverages, the oxygen atoms have well-defined adsorption sites on the surface, and desorption of oxygen occurs only at temperatures as high as 1600 K or above. Therefore, this system is a suitable candidate for simulation studies using a lattice-gas description over a wide temperature range.

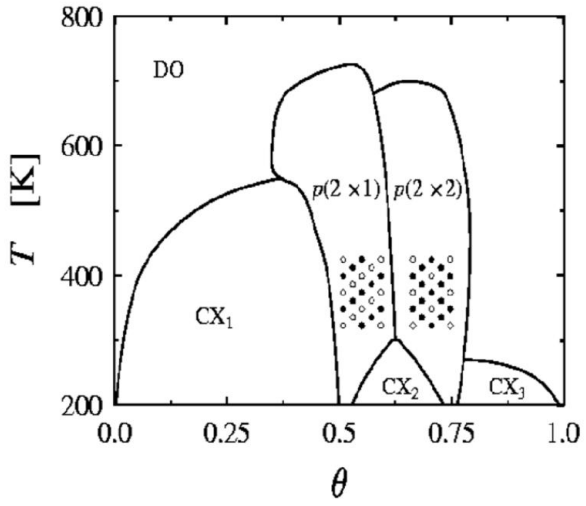

Figure 3.8: Schematic phase diagram of the O/W(110) system in the θ–T plane. The variable θ is the coverage (surface density) and T is temperature.

We shall use the lattice-gas model constructed by D. Sahu, S. C. Ying, and J. M. Kosterlitz [123] to describe the main features of the phase diagram shown in Fig. 3.8. The Hamiltonian includes pair interactions up to fifth nearest neighbors and certain three-body interactions:

$$\mathcal{H} = \sum_{m=1}^{5} \sum_{\langle ij \rangle} J_m n_i n_j + \sum_{m=1}^{2} \sum_{\langle ijk \rangle} J_{tm} n_i n_j n_k - \mu \sum_i n_i. \tag{3.8}$$

Here $n_i = 0, 1$ is the occupation variable of the lattice site i, $\langle ij \rangle$ and $\langle ijk \rangle$ denote that each pair and three-body interaction occurs only once in the summation, and strengths of these interactions are denoted by J_m and J_{tm}. Following Ref. [123] we take $J_2 = J_3 = -0.39 J_1$, $J_4 = 0$, $J_5 = 0.68 J_1$ and $J_{t1} = J_{t2} = -0.72 J_1$. In this work we set the temperature and energy scales by choosing $J_1 = -58.3$ meV, which reproduces the experimental value $T_c \approx 710$ K of a continuous order-disorder phase transition boundary at coverage $\theta = 1/2$. An illustration of the relevant interactions is presented in Fig. 3.7.

In canonical simulations with a constant value of $N = \sum_i n_i$, the term proportional to μ is irrelevant and one may set $\mu = 0$ in the Hamiltonian. The resulting phase diagram in the T–θ plane is presented in Fig. 3.8. The asymmetry about coverage $\theta = 1/2$ is due to the three-body interactions in the Hamiltonian given in Eq. (3.8).

Having introduced the lattice-gas Hamiltonian, we now discuss two un-

derlying simplifications in it. First, in our model the oxygen atoms occupy the hollow sites of the underlying surface. Some STM measurements [119] together with some LEED results [124] have revealed that the true adsorption site is the triply coordinated site instead. However, this alone does not induce serious problems, since the lattice-gas picture is still valid and the sequence of the ordered phases does not change [125]. The second simplification is the absence of interaction between the substrate and the adsorbate in the Hamiltonian. However, since no strong relaxation effects, such as reconstruction, are taking place in this system, we expect this interaction to be reasonably well approximated by a suitable choice of dynamics in the Monte Carlo simulations, which we shall discuss next.

Microscopic dynamics of the model

The lattice-gas Hamiltonian [Eq. (3.8)] alone does not constitute a complete model for surface diffusion, because it does not specify any microscopic dynamics for how the system evolves in time. In the context of lattice-gas models, stochastic methods such as Monte Carlo simulations are widely used for modeling their static and dynamic properties. However, they do not describe time in the usual sense but rather the order of events taking place in the system studied. This may be problematic when dynamic processes involving several time scales, such as diffusion of complex molecules, are studied. A related ambiguity is associated with the choice of the transition probabilities. Namely, the detailed balance condition $\pi_i w_{if} = \pi_f w_{fi}$, where w_{if} is the transition rate from an initial state i to a final state f, and π_i and π_f are the equilibrium probabilities corresponding to the Hamiltonian, does not specify the transition rates uniquely. Nevertheless, Monte Carlo studies [126] suggest that it describes many static and time-dependent properties of simple adsorption systems rather well, and thus its use in the present context is well justified. However, if true quantitative information is needed, methods based on true microscopic dynamics should be used instead.

In the context of diffusion, the fundamental problem with the traditional choices of the transition probability w_{if}, such as the standard Metropolis form, is that they do not take into account the effect of the saddle point of the adiabatic surface potential [127]. One possibility to facilitate a more realistic description is to introduce an intermediate state I and write the transition probability of each jump as a product of two probabilities as

$$w_{if} = w_{iI} w_{If}. \tag{3.9}$$

Within this *transition dynamics algorithm* (TDA) [128], the transition from the initial state with energy E_i to the final state with energy E_f proceeds

by two successive steps via an intermediate state with energy E_I. Here E_I has to be chosen to describe a jump attempt of a particle in the presence of interactions as realistically as possible without violating the detailed balance condition. We use the form [128]

$$E_I = \frac{1}{2}(E_i + E_f) + \Delta, \tag{3.10}$$

where the quantity Δ characterizes the activation barrier in the zero coverage limit due to the substrate–adatom interaction. For the rates w_{iI} and w_{If} any suitable form satisfying the detailed balance condition is applicable, although we have taken them both to be of the Metropolis form [Eq. (A.8)]. The *instantaneous activation barrier* E_a for a jump attempt from a filled to a vacant site is then

$$E_a = \max(E_I - E_i, E_f - E_i, 0). \tag{3.11}$$

This illustrates the main advantage of the TDA method. Namely, for $\Delta > 0$ the rates can be of activated form also for jumps with $E_i > E_f$. Satisfying the detailed balance, the TDA method therefore complements the description of the Hamiltonian given by Eq. (3.8).

For the present study (Papers [1–3]), we chose $\Delta = 0.0437$ eV. This value is believed to be much lower than the true value, which should be closer to the experimentally observed barrier [24] of 0.5 to 0.6 eV in the limit of zero coverage. Our choice is necessitated by the need to speed up the jump rate in the numerical simulations at low temperatures. The effect of changing Δ is estimated in Ref. [125].

3.3 Molecular dynamics (MD)

The molecular dynamics (MD) technique [7, 104, 105] is commonly used to study equilibrium and transport properties of classical many-body systems. The MD technique can also be used in non-equilibrium conditions, such as shear flow, heat flow, or shock waves [104]. In this case the simulations are called non-equilibrium molecular dynamics simulations (NEMD). In the MD technique, the nuclear motions of the constituent particles obey the laws of classical mechanics. The electron motions, in turn, can be treated essentially in two different ways: either through (i) *ab initio* methods or (ii) by using a force-field.

The *ab initio* ("from the beginning") methods are based on the Born–Oppenheimer approximation of the time-dependent Schrödinger equation, which makes the assumption that the motions of electrons and nuclei are

separated form each other. The molecular wave function is expressed as a product of electronic and nuclear wave functions

$$\Psi_T(r, R) = \Psi_e(r, R)\Psi_N(R), \tag{3.12}$$

where the electronic wave function $\Psi_e(r, R)$ depends only parametrically on the nuclear positions R. The Born–Oppenheimer approximation is based on the fact that nuclei are much more massive than the electrons. Thus the time scales involving their motion differ typically by 1000 as the electrons move $v_e \sim 1000$ km/s and nuclei move only $v_N \sim 1$ km/s at 300 K.

The above allows us to make the approximation that the nuclei are nearly fixed with respect to electron motion. Let us consider the total molecular Hamiltonian

$$\hat{H} = \hat{T}_N(R) + \hat{T}_e(r) + \hat{V}_{NN}(R) + \hat{V}_{eN}(r, R) + \hat{V}_{ee}(r), \tag{3.13}$$

where the Hamiltonian $\hat{H}$ consists of the following kinetic energy and potential energy operators: $\hat{T}_N(R)$ is the nuclear kinetic energy as a function of nuclear positions R, $\hat{T}_e(r)$ is the electronic kinetic energy as a function of electron positions r, $\hat{V}_{NN}(R)$ is the potential energy arising from nucleus–nucleus interactions, $\hat{V}_{eN}(r, R)$ is the potential energy arising from electron–nucleus interactions, and $\hat{V}_{ee}(r)$ is the potential energy arising from electron–electron interactions. For a fixed nuclear configuration, we have

$$\hat{H}_e = \hat{T}_e(r) + \hat{V}_{eN}(r, R) + \hat{V}_{ee}(r), \tag{3.14}$$

such that we get the following electronic wave equation

$$\hat{H}_e\Psi_e(r, R) = E_e\Psi_e(r, R). \tag{3.15}$$

If we solve this equation for a range of R, we obtain a potential energy curve. The motions of nuclei are usually treated classically. The Born–Oppenheimer approximation reduces the computational load considerably compared to the direct application of the time-dependent Schrödinger equation. Still, despite the above simplification and reduction in the degrees of freedom, further approximations [105] are often needed to allow studies of reasonable system sizes.

The force-field approach describes systems in a considerably more simplified fashion than the *ab initio* methods. In the force-field approach, the quantum degrees of freedom are integrated over in such a way that their effects are incorporated in the classical intramolecular and intermolecular interactions. A method defined in this way is called the *classical molecular dynamics*. In classical molecular dynamics simulations one typically applies

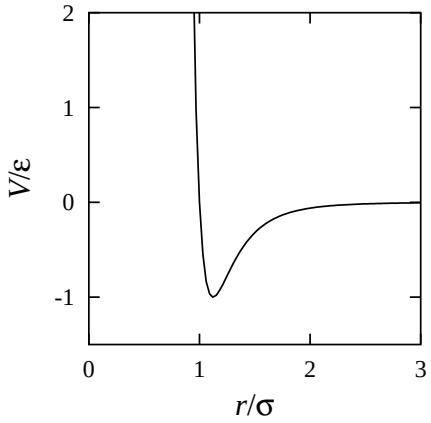

Figure 3.9: Lennard-Jones potential

molecular mechanics force fields. In such force fields, a potential energy describing a molecular system is usually written as [129, 130]

$$V = V_{\rm LJ} + \sum_{\rm bonds} \frac{k_i^{\rm b}}{2}(\ell_i - \ell_i^{\rm ref})^2 + \sum_{\rm angles} \frac{k_i^{\rm a}}{2}(\theta_i - \theta_i^{\rm ref})^2 + \sum_{\rm torsions} \frac{V_{\rm t}}{2}[1 + \cos(n\omega - \gamma)] + \sum_{i<j} \frac{q_i q_j}{4\pi\epsilon_0 r_{ij}}, \tag{3.16}$$

where $V_{\rm LJ}$ is the Lennard-Jones potential (Fig. 3.9)

$$V_{\rm LJ} = \sum_{i<j} 4\epsilon_{ij}\left[\left(\frac{\sigma_{ij}}{r_{ij}}\right)^{12} - \left(\frac{\sigma_{ij}}{r_{ij}}\right)^{6}\right] \tag{3.17}$$

used to describe the steep repulsion caused by the Pauli exclusion principle and the attractive van der Waals interactions resulting from dispersion forces. In typical MD simulations of simple liquids, the only interaction considered is usually the pairwise Lennard-Jones interaction. This is satisfactory in two cases: (i) if the system consists of neutral non-polar atoms or molecules, or (ii) if one is interested in generic properties of simple liquids.

To define a (molecular mechanics) force field, one must specify not only the set of potential energy functions but also the force field parameters ϵ_{ij}, σ_{ij}, $k_i^{\rm b}$, $k_i^{\rm a}$, $V_{\rm t}$, etc. If one of the parameters is changed, the force field is changed. Force field parameters are determined usually from experiments, or in some cases from quantum mechanics calculations. For example, the parameters $k_i^{\rm b}$ and $k_i^{\rm a}$ in bond stretching and bending interactions, can be determined by spectroscopic techniques [129,130], and the parameters ϵ_{ij} and

σ_{ij} in the Lennard-Jones interaction can be obtained by fitting parameters to crystal structures [129, 130]. Even when the parameter fitting process is done carefully, the obtained force field is never perfect in all possible situations. Partly due to this reason there are several different force fields to describe molecular systems, the most popular of them being AMBER [131,132], CHARMM [133, 134], OPLS [135], and GROMOS [136, 137].

In classical and *ab initio* MD methods, the time evolution of atoms (nuclei) is given by Newton's equations of motion

$$\frac{d\vec{r}_i}{dt} = \vec{v}_i \tag{3.18}$$

$$\frac{d\vec{v}_i}{dt} = \frac{\vec{F}_i}{m_i}, \tag{3.19}$$

where $\vec{r}_i$ is position, $\vec{v}_i$ is velocity, and m_i is mass of an atom i. The classical or *ab initio* forces are incorporated into $\vec{F}_i$, which in general is a function of all atom positions. In order to integrate Eqs. (3.18) and (3.19), there are several algorithms available. The most common is the velocity-Verlet algorithm,

$$\vec{r}_i(t+\Delta t) = \vec{r}_i(t) + \Delta t\vec{v}_i(t) + \frac{(\Delta t)^2}{2m_i}\vec{F}_i(t) \tag{3.20}$$

$$\vec{v}_i(t+\Delta t) = \vec{v}_i(t) + \frac{\Delta t}{2m_i}[\vec{F}_i(t) + \vec{F}_i(t+\Delta t)], \tag{3.21}$$

where the trajectories of the N atoms are generated iteratively using Eqs. (3.20) and (3.21). In the algorithm, the most time consuming part of each iteration is to calculate the forces $\vec{F}_i(t)$ from the positions $\vec{r}_i$.

In the MD method, the total energy E and the total momentum $\vec{p}$ are invariant with time. Hence, solving Eqs. (3.18) and (3.19) produces a sequence of states in the microcanonical (NVE) ensemble. However, it is often more convenient to perform simulations in other ensembles, e.g., NVT or NPT ensembles. The reasons for this are [114]: (i) In equilibrium situations, some thermodynamic relations, such as fluctuation relations for the specific heat, are often more straightforward to derive and evaluate for an NVT ensemble than for an NVE ensemble. (ii) The thermostat may remove energy drift, which is unavoidable in long NVE simulations. Small energy drift is present even if the integration scheme is time reversible, because computers make rounding errors in floating point operations. (iii) In non-equilibrium molecular dynamics simulations of steady states, the system is driven by an external force. The external force pumps energy into the system, which is dissipated into heat. The thermostat is needed to remove this heat. There are several *thermostats* and *barostats* to control

temperature and pressure, respectively. The most popular of them are the Berendsen [104,105,138], Andersen [7,104,105,139], Langevin [105,140], and Nosé–Hoover thermostats [7,104,105,141,142].

In the *Berendsen* thermostat [104, 105, 138] the instantaneous temperature is pushed toward the target temperature T_0 by scaling the velocities at each step. All particle velocities are scaled by the same factor $\lambda = [1 + (\Delta t/\tau)(T/T_0 - 1)]^{1/2}$, where Δt is the time step of integration and τ the so-called "rise time" of the thermostat, describing the coupling of the system to the heath bath. This thermostat is very efficient and easy to implement, but strictly speaking it does not give a canonical distribution [104,105]. In fact, the distribution that the Berendsen thermostat gives is distinct from any known statistical ensemble. Typically the Berendsen thermostat is used with a very large value of τ to prevent long-time energy drift. The results obtained in this way are very close to those that would be obtained from an NVE simulation.

The *Andersen* thermostat [7, 104, 105, 139] is a Monte Carlo scheme to sample the equilibrium velocity distribution. The Andersen thermostat works as follows. The velocity of each particle is exchanged for a new velocity drawn from a Maxwell distribution with a probability $\Gamma\Delta t$. The parameter Γ is a "bath collision" frequency, which describes how strongly the system interacts with a heat bath. The Andersen procedure is very efficient and generates a canonical distribution. However, because the Andersen thermostat is a stochastic thermostat, it should be applied with caution if the dynamics is of interest. Another feature of the Andersen thermostat is that it generates rather strong and localized kicks every now and then, for which reason the phase space trajectory is not continuous.

In the *Langevin* thermostat [105,140], the time evolution of atoms is given by Newton's equations of motion [Eqs. (3.18) and (3.19)]. In addition to the conservative force $\vec{F}_i^C$, there is a dissipative force $\vec{F}_i^D$ and a random force $\vec{F}_i^R$ acting on particle i:

$$\vec{F}_i^C = \sum_{i \neq j} \vec{F}_{ij}^{(\mathrm{c})} \tag{3.22}$$

$$\vec{F}_i^D = -\gamma \vec{v}_i \tag{3.23}$$

$$\vec{F}_i^R = \sigma \vec{\zeta}_i(t). \tag{3.24}$$

The variables γ and σ are the strengths of the dissipative and random forces, respectively. The variable $\vec{\zeta}_i(t)$ is a randomly fluctuating function with Gaussian statistics: $\langle \vec{\zeta}_i(t) \rangle = 0$ and $\langle \vec{\zeta}_i(t) \cdot \vec{\zeta}_j(t') \rangle = 3\delta_{ij}\delta(t - t')$. The parameters γ and σ are coupled through the fluctuation-dissipation relation $\sigma^2 = 2\gamma k_B T$ [105]. In actual simulations, the variable $\vec{\zeta}_i(t)$ is replaced by

$\vec{\xi}_i \Delta t^{-1/2}$, where $\vec{\xi}_i = (\xi_{ix}, \xi_{iy}, \xi_{iz})$ are Gaussian random numbers with zero mean and unit variance, taken independently for each time step. If compared to the Andersen thermostat, the Langevin thermostat has the advantage that it gives a continuous phase space trajectory. However, because in the Langevin thermostat all particles are involved, the Langevin thermostat is not as efficient as the Andersen thermostat. Both Andersen and Langevin thermostats are stochastic and do not conserve linear or rotational momenta, for which reason they should be applied with great care, if the dynamics is an issue. The Langevin thermostat is often used in simulations of polymers [115, 143–146].

In the Nosé–Hoover thermostat [7, 104, 105, 141, 142] the system's Hamiltonian is extended by introducing an additional degree of freedom η, representing the coupling to a heat bath. This adds an additional equation to Newton's equations of motion [Eqs. (3.18) and (3.19)], such that the new equations of motion become

$$\frac{d\vec{r}_i}{dt} = \vec{v}_i \tag{3.25}$$

$$\frac{d\vec{v}_i}{dt} = \frac{\vec{F}_i}{m_i} - \eta \vec{v}_i \tag{3.26}$$

$$\frac{d\eta}{dt} = \frac{1}{Q}(T - T_0). \tag{3.27}$$

Here T_0 is a target temperature and Q is a mass-like parameter which sets the rate of how strongly the system is thermostatted. The greatest advantage of the Nosé–Hoover thermostat is that, in most cases, it gives a canonical distribution without affecting the system's dynamics too much. The situations where the Nosé–Hoover thermostat fail are quite exceptional, such as a single harmonic oscillator or a free particle coupled to the Nosé–Hoover thermostat [147, 148]. In such cases, the Nosé–Hoover thermostat does not generate a canonical distribution [147, 148]. The solution to this problem is to use the method called the Nosé–Hoover chain [149], in which one introduces a sequence of Nosé–Hoover thermostats each coupled to the previous one, resulting in a chain. Another problem in the Nosé–Hoover thermostat is that it is not symplectic. To correct this, S. D. Bond, B. J. Leimkuhler, and B. B. Laird introduced recently a modified version of the Nosé–Hoover thermostat called the *Nosé–Poincaré* method [150].

An MD simulation for larger molecules or systems in which solvent molecules are explicitly taken into account is a computationally intensive task. Therefore, approximations are frequently made. The most popular ones are the SHAKE [7, 104, 105, 151], RATTLE [104, 152], and LINCS [153] methods

which in effect freeze vibrations along covalent bonds. These method are also applied sometimes to valence angles. The reason why these methods are used and physically justified is that the characteristic time scales associated with intramolecular motions are typically a factor 10–50 shorter than the other time scales in the system. Therefore, by eliminating these motions, we are allowed to increase the time step of integration from $\Delta t \sim 1$ fs up to $\Delta t \sim 10$ fs. The total simulation time grows respectively.

Another approximation typically made in biomolecular simulations is the *united-atom* approach [129], where the hydrogen atoms are lumped into a heavier atom to form an "atom" of larger size and mass (e.g., a CH_3 group). This approximation is typically justified as long as hydrogen atoms are not polarizable. In such a case, intermolecular potentials are nearly correct at long distances but not close to the molecules. When small molecules are considered, potentials must be reasonably correct also close to molecules. In such a case, the united atom approach cannot be used. An example of a case in which a simple united-atom model is not adequate is the sphingosine chain in a sphingomyelin molecule, where it is appropriate to describe the hydrogens close to the head group explicitly, rather than in a united-atom manner [154].

3.4 Dissipative particle dynamics (DPD)

In this section, we discuss the dissipative particle dynamics (DPD) method, which is the second subject of this thesis (Papers [4,5]). Before going into the details of the DPD method, we briefly discuss the concept of coarse-graining. For an in depth depth discussion of analytical and conceptual aspects of coarse-graining, see the article by P. Español in Ref. [155]. Comprehensive approaches to the DPD method can be found from the book by D. Frenkel and B. Smit [7], or from the article by R. D. Groot [8].

3.4.1 Coarse-graining

Most computer simulation techniques used in these days are based on the use of effective interaction potentials as described above. These effective potentials are less detailed and possibly also less reliable than the *ab initio* potentials used in quantum mechanics calculations, but they are far more efficient. Indeed, classical molecular dynamics can deal with hundreds of thousands of atoms over a timescale of the order of 100 ns, while the *ab initio* approaches are restricted to few hundreds of atoms and a timescale of picoseconds. In many physical phenomena, there is a need for even more

simplified models.

This implies that a given system of many degrees of freedom may be described at different spatial or temporal resolutions (Fig. 3.10). Each level is characterized by a set of relevant variables that specify the state of the system at that level. The word "level" suggests a hierarchical structure and, in fact, the levels of description for a given system order themselves in terms of the amount of information included in the relevant variables.

In any system, among all the possible levels of description two of them are particularly important because they set the extremes of the hierarchy. They are the atomistic and macroscopic levels (Fig. 3.11). The atomistic level has the positions and momenta of all atoms of the system as a set of relevant variables, the dynamic equations are Hamilton's equations, and the time scale is a typical collision or vibration time. The macroscopic level is the level of thermodynamics where the relevant variables are mass, momentum, and energy densities. Any other level of description is in between these two levels and could be named mesoscopic.

To study mesoscopic phenomena, we have to simplify, or *coarse-grain*, the classical atomic-scale models. This is usually done by the use of physical intuition and reasoning. The validity of such coarse-grained model is examined afterwards—by comparing its predictions with experiments. However, molecular specificity is usually lost in these phenomenological approaches, and for this reason such models can only be used to study generic properties of materials. Only by incorporating atomistic details in the coarse-grained model, one can expect to relate a coarse-grained model with the underlying molecular system. Inverse mapping, called *fine-graining* [156], is also important. In the fine-graining process, coarse-grained configurations are used to reproduce sets of atomistic configurations.

The primary aim in coarse-graining is to bridge different length and time scales. This is called *multiscale modeling* and it is often referred to as the Holy Grail of modeling. For example, one may represent a group of atoms with one interaction center (Fig. 3.5). Although there is no unique way to do the coarse-graining, the coarse-graining procedure always leads to a reduction of the number of degrees of freedom and this decreases the computational work. The challenge is to establish systematic coarse-graining schemes that allow one to develop simplified model systems in terms of the information extracted from the underlying microscopic systems. Thus far, various approaches have been used to coarse-grain atomistic and molecular systems. For a review of systematic coarse-graining procedures, see the recent article by R. Faller [157].

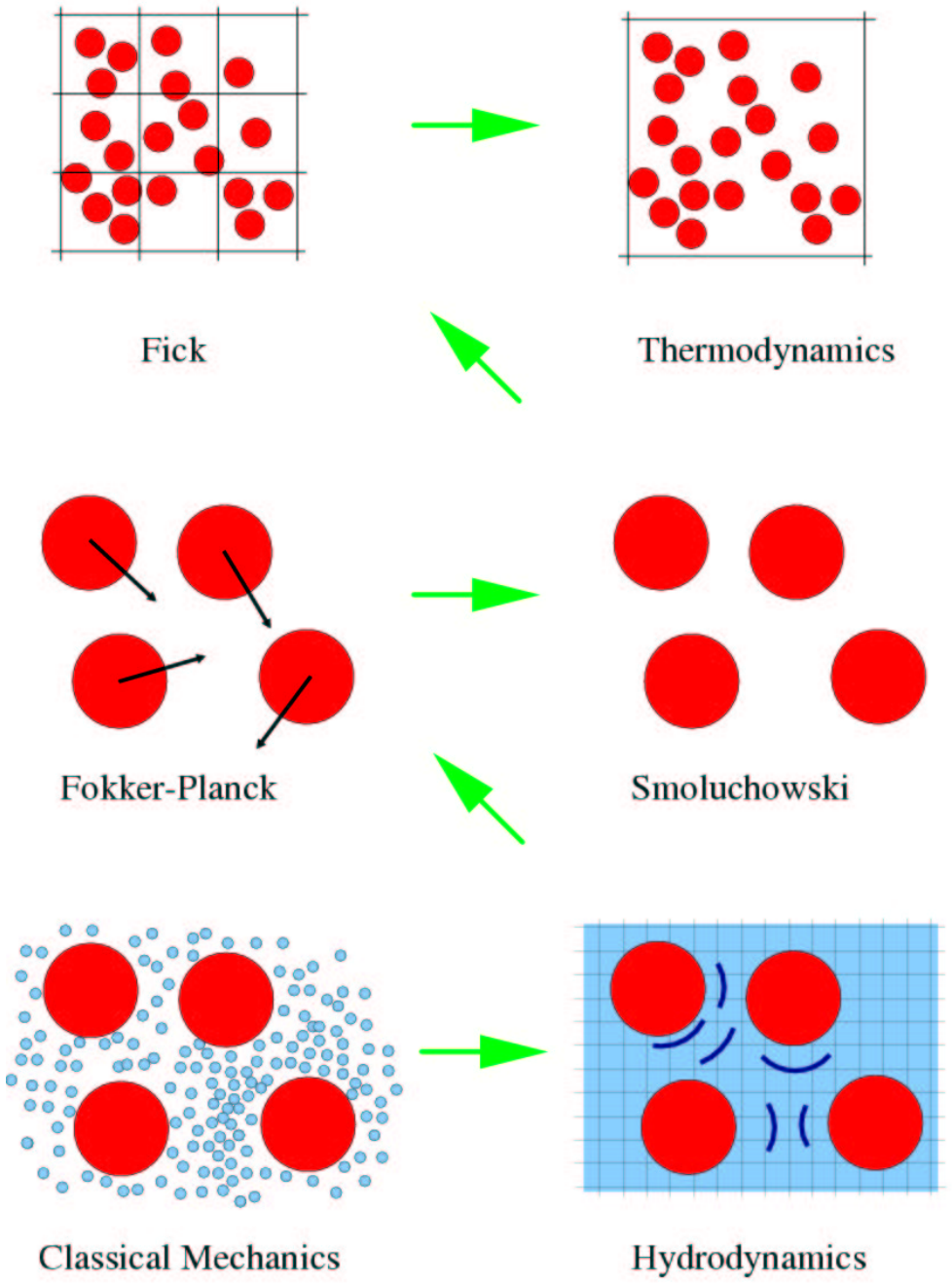

Figure 3.10: Different levels of description in a colloidal suspension. Arrows denote the direction of coarse graining from the classical mechanics level at the lower left hand corner to the level of thermodynamics at the top right hand corner. Figure taken from the article by P. Español [155].

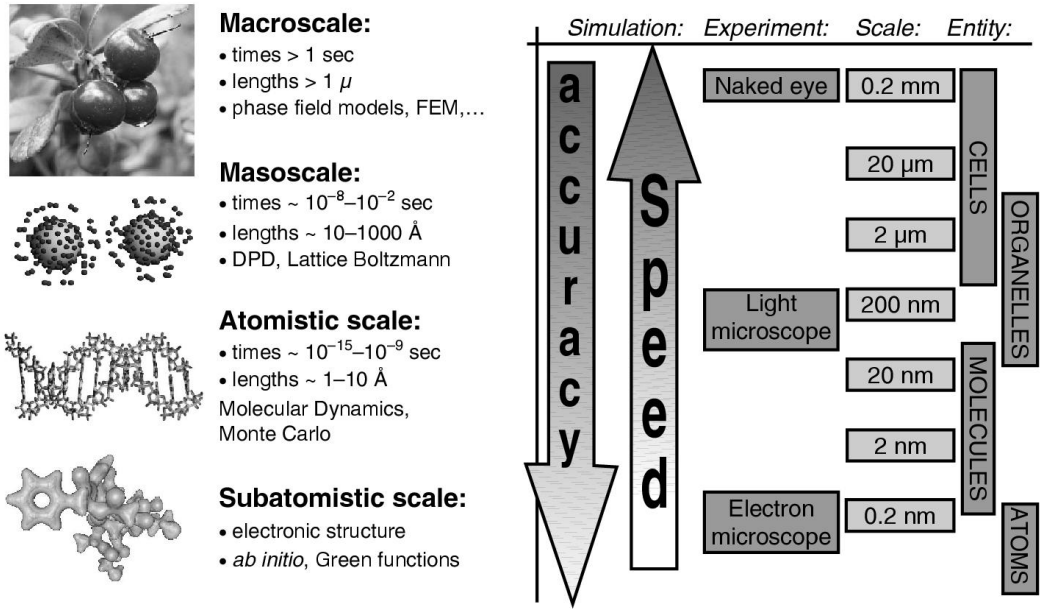

Figure 3.11: Different time and length scales, typical computational methods used to study them, and biological entities related to various length scales. Figure taken from the article by I. Vattulainen and M. Karttunen [158].

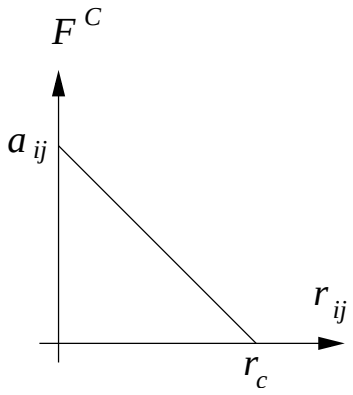

Figure 3.12: Conservative DPD force.

3.4.2 The DPD method

In the mesoscopic level, there are several methods available to simulate materials. The most popular of them are the lattice Boltzmann [159], stochastic rotation dynamics (or the Malevanets–Kapral method) [160], and the dissipative particle dynamics (DPD) [7,8]. The common factor in these methods is that they work with coarse-grained models and take hydrodynamics properly into account. Hydrodynamic effects are important in mesoscopic scales and become more and more important when approaching the continuum limit.

The DPD method describes a system in terms of N particles having masses m_i, positions $\vec{r}_i$, and velocities $\vec{v}_i$. As in molecular dynamics, the time evolution of particles is given by Newton's equations of motion [Eqs. (3.18) and (3.19)]. The total force acting on particle i is given as a sum of conservative, dissipative, and random forces, respectively, as

$$\vec{F}_i = \sum_{i \neq j} (\vec{F}_{ij}^C + \vec{F}_{ij}^D + \vec{F}_{ij}^R). \tag{3.28}$$

The conservative force $\vec{F}_{ij}^C$ is independent of the dissipative and random forces. Typically it takes the form (Fig. 3.12)

$$\vec{F}_{ij}^C = \begin{cases} a_{ij}(1 - r_{ij}/r_c)\vec{e}_{ij} & \text{if } r_{ij} < r_c; \\ 0 & \text{otherwise,} \end{cases} \tag{3.29}$$

with $\vec{r}_{ij} \equiv \vec{r}_i - \vec{r}_j$, $r_{ij} \equiv |\vec{r}_{ij}|$, and $\vec{e}_{ij} \equiv \vec{r}_{ij}/r_{ij}$. The variable a_{ij} describes the repulsion between particles i and j, and thus produces excluded volume interactions. The cutoff distance r_c sets the length scale for the model.

The dissipative force (Fig. 3.13) is expressed as

$$\vec{F}_{ij}^D = -\gamma \omega^D(r_{ij})(\vec{v}_{ij} \cdot \vec{e}_{ij})\vec{e}_{ij}, \tag{3.30}$$

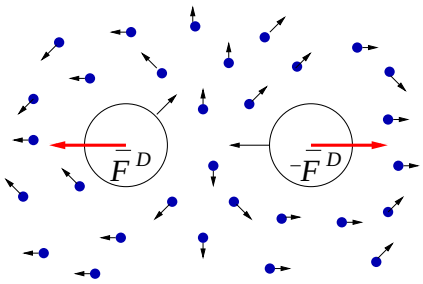

Figure 3.13: Dissipative force.

where γ is a friction parameter, $\omega^D(r_{ij})$ is a weight function for the dissipative force, and $\vec{v}_{ij} \equiv \vec{v}_i - \vec{v}_j$. The dissipative force slows down the particles by removing the kinetic energy from them.

This effect is balanced by the random force due to thermal fluctuations,

$$\vec{F}_{ij}^R = \sigma\omega^R(r_{ij})\zeta_{ij}\vec{e}_{ij}, \tag{3.31}$$

where σ is the amplitude of thermal noise, $\omega^R(r_{ij})$ is the weight function for the random force, and $\zeta_{ij}(t)$ are Gaussian random variables with

$$\langle\zeta_{ij}(t)\rangle = 0 \tag{3.32}$$

and

$$\langle\zeta_{ij}(t)\zeta_{kl}(t')\rangle = (\delta_{ik}\delta_{jl} + \delta_{il}\delta_{jk})\delta(t - t'). \tag{3.33}$$

The condition $\zeta_{ij}(t) = \zeta_{ji}(t)$ is required for momentum conservation. This is a necessary condition for the conservation of hydrodynamics.

The weight functions $\omega^D(r_{ij})$ and $\omega^R(r_{ij})$ cannot be chosen arbitrarily. P. Español and P. Warren [161] showed that the fluctuation-dissipation relations

$$\omega^D(r_{ij}) = [\omega^R(r_{ij})]^2 \tag{3.34}$$

and

$$\sigma^2 = 2\gamma k_B T \tag{3.35}$$

must be satisfied for the system to have a canonical equilibrium distribution (Appendix B). Here T is the temperature of the system and k_B is Boltzmann's constant. It is important to notice that the original DPD formulation by P. J. Hoogerbrugge and J. M. V. A. Koelman [112,113] does not obey the fluctuation-dissipation relations of Eqs. (3.34) and (3.35) and hence does not relax to the canonical distribution. Hence, the DPD formulation by P. Español and P. Warren [161] should be used.

The functional form of the weight functions is not defined by the DPD method but virtually all DPD studies use

$$\omega^D(r_{ij}) = [\omega^R(r_{ij})]^2 = \begin{cases} (1 - r_{ij}/r_c)^2 & \text{if } r_{ij} < r_c; \\ 0 & \text{otherwise.} \end{cases} \tag{3.36}$$

The random and dissipative parts of the DPD method can be thought of as a momentum conserving thermostat that allows one to study a system within the NVT ensemble with the correct canonical distribution. This DPD thermostat is by construction local and Galilean invariant [114] and therefore preserves hydrodynamics. Coarse-graining in the DPD method comes in through the soft conservative forces of Eq. (3.29). By "softness" we mean that the DPD force has a finite value at zero particle separation (Fig. 3.12), allowing particles to overlap. It was shown by B. M. Forrest and U. W. Suter [162] that coarse-graining indeed results in soft conservative forces like that of Fig. 3.12. Importantly, the conservative forces in DPD are independent of the random and dissipative ones, and thus the latter two can be used as a thermostat in any MD simulation.

The DPD technique was originally developed by P. J. Hoogerbrugge and J. M. V. A. Koelman to solve hydrodynamic flow problems in porous media. Since its introduction in 1992 [112, 113], the DPD technique has become the most used coarse-grained simulation technique in soft matter research, and several extensions and generalizations of DPD have been developed [163–169]. For example, E. G. Flekkøy et al. developed a systematic and rigorous DPD framework starting from a microscopic description [163, 164], P. Español, in turn, generalized the DPD technique to energy conserving systems [167]. The DPD technique has recently been used together with the MD method to coarse grain aqueous salt solutions [169] in which the effective interactions used in DPD simulations were obtained from MD simulations by the inverse Monte Carlo procedure [45].

Despite having its origin in porous media, DPD has gained most of its merits in simulations of polymers and surfactant systems [50, 170–172] and, very recently, also in simulations of biological systems [48, 49, 173–176]. To mention some examples, DPD has been applied to problems ranging from liquid–gas phase diagrams [177], to rupture of bacterial membranes [48], self-assembly in Huntington disease [176], and kinetics of microphase separation of diblock copolymers [170, 171]. The last 14 years have been very successful on both the analytical and the computational fronts—the theoretical basis of the DPD method is now well established, and the number of applications has increased at an accelerated pace.

There are still fundamental issues to be solved and clarified. One is the integration of the equations of motion. In the context of the MD method, the

present understanding of this issue is well developed. However, in the case of DPD simulations the situation is more problematic. The main difficulty arises from the dissipative forces, which depend on the relative velocities of the particles, while the velocities in turn depend on the dissipative forces. This difficulty is not present in MD simulations but leads to significant problems in DPD simulations, such as systematic error in temperature and artificial structures in the radial distribution function [4, 54, 55, 178, 179]. In overcome to these problems, a number of integration schemes [46, 51–57] for DPD simulations have been developed in the past few years. Self-consistent determination schemes exist on the one hand [53–55], but these are rather elaborate and may lead to undesired effects as well. Most of these algorithms have been tested in Refs. [54, 55], and in this work (Paper [4]) we have elaborated and detailed many of the outstanding issues.

Another problem of the DPD method is that it simulates fluids with comparable diffusion coefficient D and kinematic viscosity $\nu = \eta/\rho$, resulting in Schmidt numbers $\mathrm{Sc} = \nu/D$ close to 1. This value corresponds to a situation often found in gases, while in fluids the Schmidt number is of the order of 10^3 or even larger. Yet another problem relates to the soft conservative forces. These forces allow access to much larger length and time scales than the Lennard-Jones-type forces used in MD simulations. Of course, there is a price to pay: the softness of the conservative forces allows polymer chains to slide through each other thus strongly affecting the dynamics of the system. Indeed, the scaling laws obtained from DPD simulations of polymer melts [78, 79] are not able to describe entangled liquids. In this thesis (Paper [5]) we present and test a simple criterion that conservative forces should meet in order to give correct polymer dynamics.

3.4.3 Lowe–Andersen approach

Dissipative particle dynamics (DPD) technique described above can be thought of as a momentum conserving thermostat that allows one to study a system within the NVT ensemble with full hydrodynamics [4, 55]. The key features are therefore momentum and temperature conservation. As discussed above, momentum conservation arises naturally from the pairwise forces. Temperature conservation, in turn, arises from the random and dissipative forces that are chosen to satisfy the fluctuation-dissipation theorem.

An alternative approach to DPD was formulated by C. P. Lowe in 1999. This method, called the *Lowe–Andersen* thermostat [58], obeys the same conservation laws and is similar in spirit to DPD as it is aimed for studies of coarse-grained models in terms of soft interactions. In the Lowe–Andersen method, one first integrates Newton's equations of motion with a time step

Δt, and then thermalizes the system using the Andersen thermostat for pairs of particles. The algorithm proceeds as follows. For all pairs of particles for which $r_{ij} < r_c$, one decides with a probability $\Gamma\Delta t$ whether to take a new relative velocity from a Maxwell distribution. For each pair of particles whose velocities are to be thermalized, one works on the component of the velocity parallel to the line of centers and generates a relative velocity $\vec{v}_{ij}^{\,0} \cdot \vec{e}_{ij}$ from a distribution $\xi_{ij}^{(g)}(2k_BT/m)^{1/2}$. Here $\xi_{ij}^{(g)}$ are Gaussian random numbers with zero mean and unit variance. This approach has its origin in the Andersen thermostat [139], hence the name Lowe–Andersen method.

The key factor in the Lowe–Andersen method is the parameter $1/\Gamma$ which describes the decay time for relative velocities. Since the condition $0 < \Gamma\Delta t \leq 1$ is obvious, one finds that for $\Gamma\Delta t = 1$ the particle velocities are thermalized at every time step, while for $\Gamma\Delta t \approx 0$ the model system is only weakly coupled to the thermostat. The Lowe–Andersen method produces the canonical distribution and is by construction local and Galilean invariant. It therefore preserves hydrodynamics, just as the regular DPD method. Recently, L.-J. Chen *et al.* [180] have demonstrated that the Lowe–Andersen technique is able to reproduce certain "classical" DPD results published in Refs. [46, 78, 170].

The Lowe–Andersen approach is appealing for a number of reasons. First of all, since there are no dissipative forces we can assume that this method does not suffer from the same drawback as the DPD method: While the DPD method requires a self-consistent solution of the equations of motion, the Lowe–Andersen approach is easier to use and most likely performs well even with integration schemes that are commonly used in classical MD simulations. Nevertheless, the Lowe–Andersen thermostat also suffers from integration errors as is shown in this thesis (Paper [4]) and Refs. [178–180]. The second advantage is that the rate of how often the particle velocities are thermalized may be varied over a wide range, which implies that the dynamical properties of the system can be tuned in a controlled fashion. C. P. Lowe [58], and S. D. Stoyanov and R. D. Groot [181], have demonstrated this idea by showing how the Schmidt number Sc can be tuned to match values found in actual fluids. If compared to the regular DPD technique, the most significant disadvantage of the Lowe–Andersen thermostat is that it produces non-continuous phase space trajectories. This problem is resolved by E. A. J. F. Peters [182], who presented an improved version of the Lowe–Andersen thermostat. This scheme gives correct equilibrium statistics and reduces to the ordinary DPD equations in the limit of zero time step.

Chapter 4

Summary of publications and conclusions

As discussed in earlier chapters, computational methods provide a unique way to study physical problems. If compared to theories, computational methods are typically able to avoid the often necessary crude approximations that are sometimes unavoidable in building theories. If compared to experiments, computational methods can address questions that are beyond the limits and resolution of experimental techniques. Nevertheless, computational methods should not be considered as an alternative to theories or experiments, but these three approaches complement each other.

In this thesis, we have applied computational methods to two physical problems. First, we have studied the diffusion of atoms on solid surfaces. Second, we have considered methodological aspects of a simulation technique called the dissipative particle dynamics (DPD).

In the first part of this thesis (Papers [1–3]), we have studied the diffusion of atoms on solid surfaces. To this end, we have carried out Monte Carlo simulations for a lattice-gas model of O/W(110), first on clean surfaces and then on surfaces containing small concentrations of immobile, site-blocking impurities. In both cases, we have examined how non-equilibrium condition affects tracer diffusion and collective diffusion of atoms on a surface. In Paper [1], we used the Boltzmann–Matano method to determine the collective diffusion coefficient $D_C(\theta)$ as a function of coverage θ (surface density) from scaled coverage profiles. The coverage profiles were obtained from Monte Carlo simulations of a clean surface using a lattice-gas model of O/W(110). We focused on the temporal behavior of $D_C(\theta)$ as the system approaches equilibrium. We demonstrated that the effective $D_C(\theta)$ obtained in this fashion depends strongly on the time regime chosen for analysis of the density profiles, and thus may differ significantly from results obtained from equilibrium simula-

tions. The deviations from equilibrium are most pronounced within ordered phases and close to phase boundaries, where the non-equilibrium conditions lead to reduction of order. Based on our results, the non-equilibrium effects can be traced back to particle number fluctuations, which are significantly enhanced with respect to the equilibrium case.

In Paper [2], we continued this work and studied how the corresponding non-equilibrium effects in $D_C(\theta)$ depend on the initial density gradient and the initial state from which the spreading starts. To this end, we carried out extensive Monte Carlo simulations of a clean surface using the lattice-gas model of the O/W(110) system. Studies of submonolayer spreading from an initially ordered $p(2 \times 1)$ phase at $\theta = 1/2$ revealed that the spreading and diffusion rates in directions parallel and perpendicular to rows of oxygen atoms are significantly different within the ordered phase. Aside from this effect, we found that the degree of ordering in the initial phase has a relatively small impact on the overall behavior of $D_C(\theta)$. Also, although we found that non-equilibrium effects are clearly present in submonolayer spreading profiles, $D_C(\theta)$ determined from such data approaches its asymptotic equilibrium behavior much more rapidly than in case of full spreading. Nevertheless, in both cases there are noticeable deviations from equilibrium results that persist even at very long times. We note, however, that all quantities studied in this work eventually approach their equilibrium limits at very long times, as expected. The Boltzmann–Matano method therefore works well and yields the equilibrium behavior of $D_C(\theta)$ if one is only able to achieve the actual linear response regime of local equilibrium. To ensure this, particular care must be taken when profile spreading experiments are being carried out.

Non-equilibrium effects are one of the problems associated with interpreting the diffusion data, but not the only one. Namely, profile evolution experiments are usually made over macroscopic distances, which implies that the effects due to impurities and surface defects cannot be entirely eliminated. To address the significance of these effects, we studied, in Paper [3], how quenched (immobile) impurities affect the surface diffusion and ordering of strongly interacting adsorbate atoms on surfaces. To this end, we carried out Monte Carlo simulations for a lattice-gas model of O/W(110), including small concentrations of immobile impurities which block their adsorption sites. We examined the behavior of the diffusion coefficients and order parameters as a function of coverage at low temperatures. The effects of impurities were examined under both equilibrium and non-equilibrium conditions, and the results were compared to the studies on a completely clean surface. We found that even minute impurity concentrations affect the diffusion behavior considerably in equilibrium. The effects are strongest in ordered phases

and close to phase boundaries, where quenched impurities lead to a reduction of order. As the impurity concentration is increased to a level of a few percent of the total surface area, the reduction in order becomes particularly prominent. Further studies under non-equilibrium conditions revealed that non-equilibrium effects are strong in the absence of impurities, while for surfaces covered by impurities the non-equilibrium effects are relatively weaker.

In the second part of this thesis (Papers [4, 5]), we have considered methodological aspects of the dissipative particle dynamics (DPD) technique. The DPD technique is a relatively new simulation technique and is becoming very popular in studies of biologically motivated soft matter systems. First, in Paper [4] we addressed the question: "How to integrate the equations of motion in DPD simulations?" To this end, we tested and analyzed several novel DPD integration schemes on an equal footing through DPD simulations of three different model systems. By monitoring a number of physical observables including temperature, radial distribution function, radius of gyration for polymers, and tracer diffusion, we found that the methods by Lowe and Shardlow give the best overall performance and are superior also to the integrators tested in previous studies.

Second, we have studied the dynamics of polymer melts. In standard DPD, as well as in other coarse-grained soft-potential models, there is a problem that polymers can penetrate through themselves. This is a clear artifact, and has direct consequences on the polymer dynamics. To correct this problem, in Paper [5] we tuned the conservative forces within the polymer chain so strong that chains cannot cut through each other. We demonstrated that if a certain geometric criterion is met, it is impossible for polymer chains to cross. Through DPD simulations, we showed that our approach is able to reproduce Rouse-like dynamics for short polymer chains and reptational dynamics for longer chains. The results are in good agreement with polymer theories and experiments.

In the future, the role of computational physics will certainly keep on growing. The increase in the computing power and algorithmic development has enabled studies of more complicated and interesting systems than ever before. As a consequence, computational methods are nowadays the standard tools in almost every field of physics including particle physics, materials science, and cosmology. In surface science, computational methods have provided more understanding into surface properties of solid materials. This understanding is crucial in many technological applications such as semiconductor devices, catalysis, and coatings. The DPD technique, in turn, has been successfully applied to many soft matter systems, e.g., lipid bilayers, self-assembly, and the formation of polymer–surfactant complexes. The DPD

has also been useful as a thermostat for molecular dynamics simulations. The number of DPD applications is constantly increasing.

Although the computing power is constantly increasing, current methods are restricted to rather limited length and time scales. Therefore one cannot study everything from quarks to galaxies with a single method. To fill the gaps between different methods, various coarse-graining procedures have been introduced to link the methods. The further development of this methodology is important in the future.

Appendix A

Metropolis importance sampling

The Metropolis Monte Carlo method consists of generating a Markov chain of configurations with a required distribution. In a canonical ensemble, the probability distribution is given by

$$\pi_i = \frac{1}{Z} e^{-E_i/k_B T}, \tag{A.1}$$

where Z is the normalizing partition function, E_i is the energy of the microstate i, k_B is Boltzmann's constant, and T is temperature. Other commonly used distributions are the microcanonical and the grand canonical distributions.

The distribution π_i should be independent of the position within a Markov chain and independent of the initial configuration. Under certain conditions, a Markov chain yields indeed such an invariant distribution, at least for long times, as it needs some time to "forget" the chosen initial distribution. We shall not go into details, nor give proofs, but summarize these conditions—they are [105]: (i) every configuration in the ensemble should be accessible from every other configuration within a finite number of steps and (ii) there should be no periodicity.

Let us introduce the function $\pi_i(t)$ which gives us the probability of occurrence of configuration i at time step t. The time evolution of this function is governed by two processes: (i) going from a configuration i at time t to some other configuration j at time $t+1$, leading to decrease of $\pi_i(t)$, and (ii) going from some configuration j at time t to configuration i at time $t+1$, thus causing an increase in $\pi_i(t)$. These mechanisms can be summarized by the equation

$$\pi_i(t+1) - \pi_i(t) = -\sum_j \pi_i(t) P_{ij} + \sum_j \pi_j(t) P_{ji}, \tag{A.2}$$

where P_{ij} is the probability for a system to make a transition from configuration i to configuration j. This equation is called the *master equation*. We are trying to find the stationary distribution, which is found by requiring $\pi_i(t+1) = \pi_i(t)$, so that we have

$$\sum_j \pi_i(t) P_{ij} = \sum_j \pi_j(t) P_{ji}. \tag{A.3}$$

We omit the t-dependence of π from now on. It is difficult to find the general solution to this equation, but a particular solution is recognized immediately:

$$\pi_i P_{ij} = \pi_j P_{ji} \tag{A.4}$$

for all pairs of configurations i, j. This solution is called the *detailed balance* condition. It makes sure that transition rates between any pair of configurations i, j are balanced.

Let us reformulate the detailed balance condition such as to make it suitable for practical purposes. We write the transition probability in the form

$$P_{ij} = a_{ij} w_{ij} \tag{A.5}$$

where a_{ij} is a trial transition probability and w_{ij} is an acceptance probability. This means that the algorithm proceeds in two stages. In the first stage, given a configuration i, we propose a new configuration j with a probability a_{ij}. In the second stage, we accept the transition with a probability w_{ij}. In the Metropolis importance sampling, the matrix a_{ij} is symmetric:

$$a_{ij} = a_{ji}. \tag{A.6}$$

Substituting Eqs. (A.5) and (A.6) into Eq. (A.4) gives

$$\frac{w_{ij}}{w_{ji}} = \frac{\pi_j}{\pi_i}. \tag{A.7}$$

This requirement still leaves some ambiguity about the form of w_{ij}. A common choice is the *Metropolis form* $w_{ij} = \min(\pi_j/\pi_i, 1)$, which can be written as

$$w_{ij} = \begin{cases} e^{-(E_j - E_i)/k_B T} & \text{if } E_j - E_i > 0; \\ 1 & \text{otherwise,} \end{cases} \tag{A.8}$$

for the canonical ensemble. Other choices of w_{ij} are also possible [105].

In the studies of lattice-gas systems, a typical procedure is following. One particle is selected randomly and the other particles are kept fixed. The new position of the particle is then chosen randomly from its nearest neighbor lattice sites. If the nearest site chosen is full, no jump occurs. If it is empty a jump occurs with the probability given by Eq. (A.8). This updating scheme is called the *Kawasaki dynamics*. It is important to note that the Kawasaki scheme satisfies the detailed balance condition.

Appendix B

Fluctuation-dissipation relation for DPD

In this Appendix, we derive the fluctuation-dissipation relation [Eqs. (3.34) and (3.35)] for the dissipative particle dynamics (DPD) method. The fluctuation-dissipation relation was first derived by P. Español and P. Warren in 1995 [161] using a Fokker–Planck equation, which is at heart of the universally accepted DPD formulation.

The DPD interactions are composed of pairwise conservative, dissipative, and random forces exerted on particle i by particle j, respectively, and are given by

$$\begin{aligned} \vec{F}_{ij}^{C} &= F_{ij}^{(\mathrm{c})}(r_{ij})\vec{e}_{ij} \\ \vec{F}_{ij}^{D} &= -\gamma\omega^{D}(r_{ij})(\vec{v}_{ij}\cdot\vec{e}_{ij})\vec{e}_{ij} \\ \vec{F}_{ij}^{R} &= \sigma\omega^{R}(r_{ij})\zeta_{ij}\vec{e}_{ij}, \end{aligned} \tag{B.1}$$

where $\vec{r}_{ij}\equiv\vec{r}_i-\vec{r}_j$, $r_{ij}\equiv|\vec{r}_{ij}|$, $\vec{e}_{ij}\equiv\vec{r}_{ij}/r_{ij}$, and $\vec{v}_{ij}\equiv\vec{v}_i-\vec{v}_j$. By substituting these forces into Newton's equations of motion we obtain a set of Langevin equations. We write the resulting Langevin equations in the mathematically well-defined form of stochastic differential equations [183]

$$d\vec{r}_i = \frac{\vec{p}_i}{m_i}dt \tag{B.2}$$

$$\begin{aligned} d\vec{p}_i = &\left[\sum_{j\neq i}\vec{F}_{ij}^{C}(\vec{r}_{ij}) - \sum_{j\neq i}\gamma\omega^{D}(r_{ij})(\vec{v}_{ij}\cdot\vec{e}_{ij})\vec{e}_{ij}\right]dt + \\ &\sum_{j\neq i}\sigma\omega^{R}(r_{ij})\vec{e}_{ij}dW_{ij}, \end{aligned} \tag{B.3}$$

where $dW_{ij}=dW_{ji}$ are independent increments of the Wiener process. We will assume Itô interpretation which implies the Itô calculus rule

$$dW_{ij}dW_{kl} = (\delta_{ik}\delta_{jl}+\delta_{il}\delta_{jk})dt \tag{B.4}$$

i.e., $dW_{ij}(t)$ is an infinitesimal of order 1/2 [183].

Our next aim is to derive the Fokker–Planck equation that corresponds to the above stochastic differential equations. Following standard procedures [183], one considers the differential df of an arbitrary function f to second order and substitutes Eqs. (B.2) and (B.3). By using Eq. (B.4) and the fact that dW is an infinitesimal of order 1/2 one can obtain $\langle df/dt \rangle$ and extract the Fokker–Planck equation governing the temporal evolution of the distribution function $\rho(r, p; t)$ of the positions and momenta of all the particles [183]. The resulting Fokker–Planck equation takes the form

$$\partial_t \rho(r, p; t) = L_C \rho(r, p; t) + L_D \rho(r, p; t) \tag{B.5}$$

where we have defined the operators

$$L_C \rho(r, p; t) = -\left[\sum_i \frac{\vec{p}_i}{m} \frac{\partial}{\partial \vec{r}_i} + \sum_{i,j \neq i} \vec{F}_{ij}^C \frac{\partial}{\partial \vec{p}_i} \right] \rho(r, p; t) \tag{B.6}$$

$$\begin{aligned} L_D \rho(r, p; t) = & \sum_{i,j \neq i} \vec{e}_{ij} \frac{\partial}{\partial \vec{p}_i} \left[\gamma \omega^D(r_{ij}) (\vec{v}_{ij} \cdot \vec{e}_{ij}) + \right. \\ & \left. \frac{\sigma^2}{2} [\omega^R(r_{ij})]^2 \vec{e}_{ij} \left(\frac{\partial}{\partial \vec{p}_i} - \frac{\partial}{\partial \vec{p}_j} \right) \right] \rho(r, p; t) \end{aligned} \tag{B.7}$$

The operator L_C is the usual Liouville operator of a Hamiltonian system interacting with conservative forces $\vec{F}^C$. The operator L_D contains second derivatives and takes into account the effects of the dissipative and random forces.

The equilibrium distribution ρ^{eq} is given by the steady state solution of Eq. (B.5): $\partial_t \rho = 0$. We now consider the conditions under which the steady state solution is the canonical ensemble:

$$\rho^{\text{eq}}(r, p) = \frac{1}{Z} \exp\{-\mathcal{H}(r, p)/k_B T\} \tag{B.8}$$

$$= \frac{1}{Z} \exp\left\{ -\frac{1}{k_B T} \left[\sum_i \frac{p_i^2}{2m_i} + V(r) \right] \right\}, \tag{B.9}$$

where $\mathcal{H}$ is the Hamiltonian of the system, V is the potential function that gives rise to the conservative forces $\vec{F}^C$, k_B is Boltzmann's constant, T is the equilibrium temperature, and Z is the normalizing partition function. The canonical ensemble is the equilibrium solution for the conservative system, i.e., $L_C \rho^{\text{eq}} = 0$. In addition, we can satisfy $L_D \rho^{\text{eq}} = 0$ by requiring

$$\omega^D(r) = [\omega^R(r)]^2 \tag{B.10}$$

$$\sigma^2 = 2\gamma k_B T. \tag{B.11}$$

This is the fluctuation-dissipation theorem for the DPD method.

Bibliography

[1] P. Nikunen, I. Vattulainen, and T. Ala-Nissila, Surf. Sci. **447**, L162 (2000).

[2] P. Nikunen, I. Vattulainen, and T. Ala-Nissila, J. Chem. Phys. **114**, 6335 (2001).

[3] P. Nikunen, I. Vattulainen, and T. Ala-Nissila, J. Chem. Phys. **117**, 6757 (2002).

[4] P. Nikunen, M. Karttunen, and I. Vattulainen, Comp. Phys. Comm. **153**, 407 (2003).

[5] P. Nikunen, I. Vattulainen, and M. Karttunen, submitted to Phys. Rev. E (December, 2005); Helsinki Institute of Physics preprint HIP–2005–54/Th.

[6] M. Valtonen and H. Karttunen, *The Three-Body Problem* (Cambridge University Press, Cambridge, 2005).

[7] D. Frenkel and B. Smit, *Understanding molecular simulation: From algorithms to applications* (Academic Press, San Diego, 2002).

[8] R. Groot, in *Novel methods in soft matter simulations*, edited by M. Karttunen, I. Vattulainen, and A. Lukkarinen (Springer, Berlin, 2004).

[9] H. Lüth, *Surfaces and Interfaces of Solid Materials*, 3rd ed. (Springer, Berlin, 1998).

[10] *Surface Diffusion: Atomistic and Collective Processes*, edited by M. C. Tringides (Plenum, New York, 1997).

[11] J. V. Barth, Surf. Sci. Rep. **40**, 75 (2000).

[12] M. Giesen, Prog. Surf. Sci. **68**, 1 (2001).

[13] R. Gomer, Rep. Prog. Phys. **53**, 917 (1990).

[14] A. G. Naumovets and Y. S. Vedula, Surf. Sci. Rep. **4**, 365 (1985).

[15] G. L. Kellogg, Surf. Sci. Rep. **21**, 1 (1994).

[16] H. Brune, Surf. Sci. Rep. **31**, 125 (1998).

[17] T. R. Linderoth *et al.*, Phys. Rev. Lett. **82**, 1494 (1999).

[18] R. van Gastel *et al.*, Phys. Rev. Lett. **86**, 1562 (2001).

[19] T. Ala-Nissila, R. Ferrando, and S. C. Ying, Adv. Phys. **51**, 949 (2002).

[20] T. Ala-Nissila and S. C. Ying, Prog. Surf. Sci. **39**, 227 (1992).

[21] A. Danani, R. Ferrando, E. Scalas, and M. Torri, Int. J. Mod. Phys. B **11**, 2217 (1997).

[22] M. C. Tringides, in *The Chemical Physics of Solid Surfaces and Heterogeneous Catalysis: Phase Transitions and Adsorbate Restructuring of Metal Surfaces*, edited by D. A. King and D. P. Woodruff (Elsevier, Amsterdam, 1994), Vol. 7.

[23] M. C. Tringides, P. K. Wu, and M. G. Lagally, Phys. Rev. Lett. **59**, 315 (1987).

[24] P. K. Wu, M. C. Tringides, and M. G. Lagally, Phys. Rev. B **39**, 7595 (1989).

[25] M. C. Tringides and R. Gomer, Surf. Sci. **265**, 283 (1992).

[26] J. Haas, K. R. Roos, A. Jesina, and M. C. Tringides, Surf. Sci. **307**, 465 (1994).

[27] I. Vattulainen, J. Merikoski, T. Ala-Nissila, and S. C. Ying, Surf. Sci. **366**, L697 (1996).

[28] Z. Chvoj, J. Phys.: Condens. Matter **12**, 2135 (2000).

[29] M. A. Załuska-Kotur, S. Krukowski, Z. Romanowski, and Ł. A. Turski, Surf. Sci. **457**, 357 (2000).

[30] M. Šnábl *et al.*, J. Chem. Phys. **108**, 4212 (1998).

[31] A. T. Loburets, A. G. Naumovets, and Y. S. Vedula, Surf. Sci. **399**, 297 (1998).

[32] X.-D. Xiao *et al.*, Phys. Rev. Lett. **74**, 3860 (1995).

[33] X.-D. Xiao, Y. Xie, C. Jakobsen, and Y. R. Shen, Phys. Rev. B **56**, 12529 (1997).

[34] M. Kalff, G. Comsa, and T. Michely, Phys. Rev. Lett. **81**, 1255 (1998).

[35] S. Esch, M. Hohage, T. Michely, and G. Comsa, Phys. Rev. Lett. **72**, 518 (1994).

[36] B. Voigtländer, A. Zinner, T. Weber, and H. P. Bonzel, Phys. Rev. B **51**, 7583 (1995).

[37] C. H. Mak, J. L. Brand, A. A. Deckert, and S. M. George, J. Chem. Phys. **85**, 1676 (1986).

[38] J. L. Brand, A. A. Deckert, and S. M. George, Surf. Sci. **194**, 457 (1988).

[39] G. L. Kellogg, Phys. Rev. B **55**, 7206 (1997).

[40] J. Nara, T. Sasaki, and T. Ohno, Phys. Rev. Lett. **79**, 4421 (1997).

[41] S. Horch *et al.*, Nature **398**, 134 (1999).

[42] *Soft Matter Physics*, edited by M. Daoud and C. E. Williams (Springer, Berlin, 1999).

[43] *Nonequilibrium Dynamics, Metastability and Flow*, edited by M. E. Cates and M. R. Evans (Institute of Physics Publishing, Bristol, 2000).

[44] P.-G. de Gennes and J. Badoz, *Fragile Objects: Soft Matter, Hard Science, and the Thrill of Discovery* (Springer, New York, 1996).

[45] A. P. Lyubartsev and A. Laaksonen, Phys. Rev. E **52**, 3730 (1995).

[46] R. D. Groot and P. B. Warren, J. Chem. Phys. **107**, 4423 (1997).

[47] M. Venturoli and B. Smit, PhysChemComm **10**, (article 10) (1999).

[48] R. D. Groot and K. L. Rabone, Biophys. J. **81**, 725 (2001).

[49] S. Yamamoto, Y. Maruyama, and S. Hyodo, J. Chem. Phys. **116**, 5842 (2002).

[50] R. D. Groot, Langmuir **16**, 7493 (2000).

[51] K. E. Novik and P. V. Coveney, J. Chem. Phys. **109**, 7667 (1998).

[52] J. B. Gibson, K. Chen, and S. Chynoweth, Int. J. Mod. Phys. C **10**, 241 (1999).

[53] I. Pagonabarraga, M. H. J. Hagen, and D. Frenkel, Europhys. Lett. **42**, 377 (1998).

[54] G. Besold, I. Vattulainen, M. Karttunen, and J. M. Polson, Phys. Rev. E **62**, R7611 (2000).

[55] I. Vattulainen, M. Karttunen, G. Besold, and J. M. Polson, J. Chem. Phys. **116**, 3967 (2002).

[56] W. K. den Otter and J. H. R. Clarke, Europhys. Lett. **53**, 426 (2001).

[57] T. Shardlow, SIAM J. Sci. Comp. **24**, 1267 (2003).

[58] C. P. Lowe, Europhys. Lett. **47**, 145 (1999).

[59] S. F. Edwards, Proc. Phys. Soc. **92**, 9 (1967).

[60] P. G. de Gennes, J. Chem. Phys. **55**, 572 (1971).

[61] M. Doi and S. F. Edwards, *The theory of polymer dynamics* (Clarendon, Oxford, 1989).

[62] McLeish, Adv. Phys. **51**, 1379 (2002).

[63] R. Everaers *et al.*, Science **303**, 823 (2004).

[64] S. K. Sukumaran, G. S. Grest, K. Kremer, and R. Everaers, Polym. Sci. B **43**, 917 (2005).

[65] D. Richter *et al.*, Phys. Rev. Lett. **64**, 1389 (1990).

[66] J. Käs, H. Strey, and E. Sackmann, Nature **368**, 226 (1994).

[67] P. Schleger *et al.*, Phys. Rev. Lett. **81**, 124 (1998).

[68] K. Kremer, G. S. Grest, and I. Carmesin, Phys. Rev. Lett. **61**, 566 (1988).

[69] M. Pütz, K. Kremer, and G. S. Grest, Europhys. Lett. **49**, 735 (2000).

[70] W. Paul, K. Binder, D. W. Heermann, and K. Kremer, J. Chem. Phys. **95**, 7726 (1991).

[71] J. T. Padding and W. J. Briels, J. Chem. Phys. **115**, 2846 (2001).

[72] W. Paul and G. D. Smith, Rep. Prog. Phys. **67**, 1117 (2004).

[73] H. C. Öttinger, Non-Newtonian Fluid Mech. **120**, 207 (2004).

[74] K. Kremer, S. K. Sukumaran, R. Everaers, and G. S. Grest, Comp. Phys. Comm. **169**, 75 (2005).

[75] S. Förster and T. Plantenberg, Angew. Chem. Int. Ed. **41**, 688 (2002).

[76] S. Rastogi *et al.*, Nature Materials **4**, 635 (2005).

[77] P. E. Rouse, J. Chem. Phys. **21**, 1272 (1953).

[78] N. A. Spenley, Europhys. Lett. **49**, 534 (2000).

[79] X. Guerrault, B. Rousseau, and J. Farago, J. Chem. Phys. **121**, 6538 (2004).

[80] G. Pan and C. W. Manke, Int. J. Mod. Phys. B **17**, 231 (2003).

[81] L. D. Landau and E. M. Lifshitz, *Statistical physics, Part 1*, 3rd ed. (Butterworth–Heinemann, Oxford, 2000).

[82] R. K. Pathria, *Statistical mechanics* (Butterworth–Heinemann, Oxford, 1996).

[83] K. Huang, *Statistical mechanics* (Wiley, New York, 1987).

[84] S. R. de Groot and P. Mazur, *Non-equilibrium thermodynamics* (Dover, New York, 1984).

[85] N. W. Ashcroft and N. D. Mermin, *Solid state physics* (Saunders, Philadelphia, 1976).

[86] J. J. Binney, N. J. Dowrick, A. J. Fisher, and M. E. J. Newman, *The theory of critical phenomena: An introduction to the renormalization group* (Clarendon, Oxford, 1992).

[87] N. Goldenfeld, *Lectures on phase transitions and the renormalization group* (Addison–Wesley, Reading, 1992).

[88] P. M. Chaikin and T. C. Lubensky, *Principles of condensed matter physics* (Cambridge University Press, Cambridge, 1995).

[89] E. A. Guggenheim, J. Chem. Phys. **13**, 253 (1945).

[90] L. D. Landau and E. M. Lifshitz, *Fluid Mechanics*, 2nd ed. (Butterworth–Heinemann, Oxford, 2000).

[91] P. Wesseling, *Principles of computational fluid dynamics* (Springer, Berlin, 2001).

[92] J. P. Hansen and I. R. McDonald, *Theory of simple liquids*, 2nd ed. (Academic Press, London, 1986).

[93] S. C. Ying *et al.*, Phys. Rev. B **58**, 2170 (1998).

[94] C. Matano, Jpn. J. Phys. **8**, 109 (1933).

[95] M. Doi, *Introduction to polymer physics* (Clarendon, Oxford, 2001).

[96] A. Y. Grosberg and A. R. Khokhlov, *Giant molecules: here, there, and everywhere...* (Academic Press, San Diego, 1997).

[97] A. Y. Grosberg and A. R. Khokhlov, *Statistical Physics of Macromolecules* (AIP Press, New York, 1994).

[98] W. Kuhn, Kolloid Zeits. **68**, 2 (1934).

[99] P. J. Flory, J. Chem. Phys. **17**, 303 (1949).

[100] A. Pelissetto and E. Vicari, Phys. Rep. **368**, 549 (2002).

[101] P.-G. de Gennes, *Scaling concepts in polymer physics* (Cornell University Press, Ithaca, 1979).

[102] G. Beaucage, Polymer Physics: Dynamics, Lecture notes, `http://www.eng.uc.edu/~gbeaucag/Classes/Physics.html`.

[103] M. Doi, J. Polym. Sci., Polym. Lett. Ed. **19**, 265 (1981).

[104] M. P. Allen and D. J. Tildesley, *Computer simulation of liquids* (Oxford University Press, Oxford, 1989).

[105] J. M. Thijssen, *Computational physics* (Cambridge University Press, Cambridge, 1999).

[106] D. P. Landau and K. Binder, *A guide to Monte Carlo simulations in statistical physics* (Cambridge University Press, Cambridge, 2000).

[107] S. Duane, A. D. Kennedy, B. J. Pendleton, and D. Roweth, Phys. Lett. B **195**, 216 (1987).

[108] B. Mehlig, D. W. Heermann, and B. M. Forrest, Phys. Rev. B **45**, 679 (1992).

[109] J. A. Izaguirre and S. S. Hampton, J. Comp. Phys. **200**, 581 (2004).

[110] *The traveling salesman problem and its variations*, edited by G. Gutin and A. P. Punnen (Kluwer Academic, Dordrecht, 2002).

[111] W. H. Press, B. P. Flannery, S. A. Teukolsky, and W. T. Vetterling, *Numerical recipes in C++: The art of scientific computing* (Cambridge University Press, Cambridge, 2002).

[112] P. J. Hoogerbrugge and J. M. V. A. Koelman, Europhys. Lett. **19**, 155 (1992).

[113] J. M. V. A. Koelman and P. J. Hoogerbrugge, Europhys. Lett. **21**, 363 (1993).

[114] T. Soddemann, B. Dünweg, and K. Kremer, Phys. Rev. E **68**, 046702 (2003).

[115] D. R. Heine, G. S. Grest, and E. B. Webb III, Phys. Rev. E **68**, 061603 (2003).

[116] N. Metropolis *et al.*, J. Chem. Phys. **21**, 1087 (1953).

[117] A. Bunker and B. Dünweg, Phys. Rev. E **63**, 016701 (2001).

[118] W. Y. Ching, D. L. Huber, M. G. Lagally, and G.-C. Wang, Surf. Sci. **77**, 550 (1978).

[119] K. E. Johnson, R. J. Wilson, and S. Chiang, Phys. Rev. Lett. **71**, 1055 (1993).

[120] G.-C. Wang, T.-M. Lu, and M. G. Lagally, J. Chem. Phys. **69**, 479 (1978).

[121] P. Hahn, J. Clabes, and M. Henzler, J. Appl. Phys. **51**, 2079 (1980).

[122] G. Binnig, H. Rohrer, C. Gerber, and E. Weibel, Appl. Phys. Lett. **40**, 178 (1982).

[123] D. Sahu, S. C. Ying, and J. M. Kosterlitz, in *The Structure of Surfaces II*, edited by J. F. van der Veen and M. A. van Hove (Springer, Berlin, 1988).

[124] M. A. van Hove and S. Y. Tong, Phys. Rev. Lett. **35**, 1092 (1975).

[125] I. Vattulainen, J. Merikoski, T. Ala-Nissila, and S. C. Ying, Phys. Rev. B **57**, 1896 (1998).

[126] K. Binder and D. W. Heermann, *Monte Carlo simulation in statistical physics: An introduction* (Springer, Berlin, 1988).

[127] A. Zangwill, *Physics at surfaces* (Cambridge University Press, Cambridge, 1989).

[128] T. Ala-Nissila, J. Kjoll, and S. C. Ying, Phys. Rev. B **46**, 846 (1992).

[129] A. R. Leach, *Molecular modelling: principles and applications*, 2nd ed. (Prentice Hall, Harlow, 2001).

[130] T. Schlick, *Molecular Modeling: An Interdisciplinary Guide* (Springer, New York, 2002).

[131] J. W. Ponder and D. A. Case, Adv. Prot. Chem. **66**, 27 (2003).

[132] T. E. Cheatham III and M. A. Young, Biopolymers **56**, 232 (2001).

[133] B. R. Brooks *et al.*, J. Comp. Chem. **4**, 187 (1983).

[134] A. D. MacKerell Jr. *et al.*, in *Encyclopedia of Computational Chemistry*, edited by P. von Ragué Schleyer *et al.* (Wiley, Chichester, 1998), Vol. 1.

[135] W. L. Jorgensen and J. Tirado-Rives, J. Am. Chem. Soc. **110**, 1657 (1988).

[136] J. Hermans, H. J. C. Berendsen, W. F. van Gunsteren, and J. P. M. Postma, Biopolymers **23**, 1513 (1984).

[137] W. F. van Gunsteren, X. Daura, and A. E. Mark, in *Encyclopedia of Computational Chemistry*, edited by P. von Ragué Schleyer *et al.* (Wiley, New York, 1998), Vol. 2.

[138] H. J. C. Berendsen *et al.*, J. Chem. Phys. **81**, 3684 (1984).

[139] H. C. Andersen, J. Chem. Phys. **72**, 2384 (1980).

[140] J. A. Izaguirre, D. P. Catarello, J. M. Wozniak, and R. D. Skeel, J. Chem. Phys. **114**, 2090 (2001).

[141] S. Nosé, J. Chem. Phys. **81**, 511 (1984).

[142] W. G. Hoover, Phys. Rev. A **31**, 1695 (1985).

[143] G. S. Grest and K. Kremer, Phys. Rev. A **33**, 3628 (1986).

[144] K. Kremer and G. S. Grest, J. Chem. Phys. **92**, 5057 (1990).

[145] K. Kremer and G. S. Grest, J. Chem. Phys. **94**, 4103 (1991).

[146] D. R. Heine, G. S. Grest, and E. B. Webb III, Phys. Rev. E **70**, 011606 (2004).

[147] M. E. Tuckerman, Y. Liu, G. Ciccotti, and G. J. Martyna, J. Chem. Phys. **115**, 1678 (2001).

[148] G. Ciccotti and G. Kalibaeva, in *Novel methods in soft matter simulations*, edited by M. Karttunen, I. Vattulainen, and A. Lukkarinen (Springer, Berlin, 2004).

[149] G. J. Martyna, M. L. Klein, and M. Tuckerman, J. Chem. Phys. **97**, 2635 (1992).

[150] S. D. Bond, B. J. Leimkuhler, and B. B. Laird, J. Comp. Phys. **151**, 114 (1999).

[151] J.-P. Ryckaert, G. Ciccotti, and H. J. C. Berendsen, J. of Comp. Phys. **23**, 327 (1977).

[152] H. C. Andersen, J. Comp. Phys. **52**, 24 (1983).

[153] B. Hess, H. Bekker, H. J. C. Berendsen, and J. G. E. M. Fraaije, J. Comp. Chem. **18**, 1463 (1997).

[154] P. Niemelä, M. T. Hyvönen, and I. Vattulainen, Biophys. J. **87**, 2976 (2004).

[155] P. Español, in *Novel methods in soft matter simulations*, edited by M. Karttunen, I. Vattulainen, and A. Lukkarinen (Springer, Berlin, 2004).

[156] K. Kremer and F. Müller-Plathe, MRS Bull. **26**, 205 (2001).

[157] R. Faller, Polymer **45**, 3869 (2004).

[158] I. Vattulainen and M. Karttunen, in *Handbook of Theoretical and Computational Nanotechnology*, edited by M. Rieth and W. Schommers (American Scientific Publishers, Los Angeles, 2005).

[159] I. Pagonabarraga, in *Novel methods in soft matter simulations*, edited by M. Karttunen, I. Vattulainen, and A. Lukkarinen (Springer, Berlin, 2004).

[160] A. Malevanets and R. Kapral, in *Novel methods in soft matter simulations*, edited by M. Karttunen, I. Vattulainen, and A. Lukkarinen (Springer, Berlin, 2004).

[161] P. Español and P. Warren, Europhys. Lett. **30**, 191 (1995).

[162] B. M. Forrest and U. W. Suter, J. Chem. Phys. **102**, 7256 (1995).

[163] E. G. Flekkøy and P. V. Coveney, Phys. Rev. Lett. **83**, 1775 (1999).

[164] E. G. Flekkøy, P. V. Coveney, and G. De Fabritiis, Phys. Rev. E **62**, 2140 (2000).

[165] W. Dzwinel and D. A. Yuen, J. Colloid Interface Sci. **225**, 179 (2000).

[166] P. Español, Europhys. Lett. **39**, 605 (1997).

[167] P. Español, Europhys. Lett. **40**, 631 (1997).

[168] P. Español, M. Serrano, and I. Zuñiga, Int. J. Mod. Phys. C **8**, 899 (1997).

[169] A. P. Lyubartsev, M. Karttunen, I. Vattulainen, and A. Laaksonen, Soft Materials **1**, 121 (2003).

[170] R. D. Groot and T. J. Madden, J. Chem. Phys. **108**, 8713 (1998).

[171] R. D. Groot, T. J. Madden, and D. J. Tildesley, J. Chem. Phys. **110**, 9739 (1999).

[172] S. Jury *et al.*, Phys. Chem. Chem. Phys. **1**, 2051 (1999).

[173] S. Yamamoto and S. Hyodo, J. Chem. Phys. **118**, 7937 (2003).

[174] M. Kranenburg, M. Venturoli, and B. Smit, J. Phys. Chem. B **107**, 11491 (2003).

[175] M. Kranenburg, M. Venturoli, and B. Smit, Phys. Rev. E **67**, 060901(R) (2003).

[176] M. G. Burke, R. Woscholski, and S. N. Yaliraki, Proc. Natl. Acad. Sci. **100**, 13928 (2003).

[177] P. B. Warren, Phys. Rev. E **68**, 066702 (2003).

[178] B. Hafskjold, C. C. Liew, and W. Shinoda, Mol. Simul. **30**, 879 (2004).

[179] A. F. Jakobsen, O. G. Mouritsen, and G. Besold, J. Chem. Phys. **122**, 204901 (2005).

[180] L.-J. Chen *et al.*, J. Chem. Phys. **122**, 104907 (2005).

[181] S. D. Stoyanov and R. D. Groot, J. Chem. Phys. **122**, 114112 (2005).

[182] E. A. J. F. Peters, Europhys. Lett. **66**, 311 (2004).

[183] C. Gardiner, *Handbook of stochastic methods: For physics, chemistry and the natural sciences* (Springer, Berlin, 2003).